BIFURCATIONS OF EQUILIBRIA IN DNA ELASTICITY

BY YOAV Y. BITON

A dissertation submitted to the

Graduate School—New Brunswick

Rutgers, The State University of New Jersey

in partial fulfillment of the requirements

for the degree of

Doctor of Philosophy

Graduate Program in Mechanics

Written under the direction of

Bernard D. Coleman

and approved by

_____

_____

_____

_____

New Brunswick, New Jersey

October, 2007

ABSTRACT OF THE DISSERTATION

Bifurcations of equilibria in DNA elasticity

by Yoav Y. Biton

Dissertation Director: Bernard D. Coleman

DNA molecules in the familiar double helical B form are treated here as though they have rod-like structures obtained by stacking the nearly planar base pairs comprising them one on top of another with each rotated by approximately one-tenth of a full turn with respect to its immediate predecessor in the stack. As each base in a base pair is attached to the sugar-phosphate backbone chain of one of the two DNA strands that have come together to form the Watson-Crick structure, and each phosphate group in a backbone chain bears one electronic charge, two such charges are associated with each base pair. Thus, each base pair is subject to not only the elastic forces and moments exerted on it by its neighboring base pairs but also to remote electrostatic forces that, because they are only partially screened out by positively charged counter ions, can render the molecule's equilibrium configurations sensitive to changes in the concentration c of salt in the medium.

The observation that the step from one base pair to the next can be one of several distinct types, each having its own mechanical properties that depend on the nucleotide composition of the step, and the assumption that a base pair is rigid, led to the development of a theory of sequence dependent DNA elasticity [1]. The theory of

DNA molecules in aqueous solution developed here is based on but goes beyond that theory. It takes into account the intramolecular electrostatic interactions of the negatively charged phosphate groups in the molecule and the impenetrability of the DNA molecule for cases in which the electrostatic repulsive forces do not suffice to avoid self penetration. The theory permits one to calculate equilibrium configurations, to determine their stability , and to study the dependence of them on salt concentration and on all kinds of end conditions.

When the intramolecular electrostatic forces are taken into account, the equations of mechanical equilibrium for a DNA molecule with $N+1$ base pairs are a system of μN non-linear equations, where μ, the number of kinematical variables describing the relative displacement and orientation of adjacent base pairs is in general 6; it reduces to 3 when base-pair steps are assumed to be inextensible and non-shearable. An efficient numerically stable computational scheme is here presented for solving those equations and determining the mechanical stability of the calculated equilibrium configurations. That scheme is employed to compute and analyze bifurcation diagrams in which c is the bifurcation parameter and to show that, for an intrinsically curved molecule, small changes in c can have a strong effect on stable equilibrium configurations. Cases are presented in which self-contact must be taken into account even though the intramolecular electrostatic forces of repulsion are strong.

Acknowledgements

I have been fortunate to have Professor *Bernard D. Coleman* as my advisor. He has been my guide to the world of real science and has always led me to the right path. He showed me how to render my obscure thoughts transparent, and supported me in many ways in this period. Words are not enough to express my gratitude to him.

As my accomplishments would not have been possible without Professor *Reuven Segev*'s influence in my life and education, I herewith send him my most sincere thanks.

I want to thank my dissertation committee members, Professors *Ellis H. Dill*, *Alberto M. Cuitiño*, and *Richard S. Falk* for the time and advice they have given to me. I am thankful to Professor *Wilma K. Olson* for her guidance and encouragement through all the different phases of this work. I am grateful to Professor *David Swigon* for sharing with me his knowledge and experience in the stages of this research. Many thanks to professor *Irwin Tobias* for the fruitful discussions. I want to express my appreciation to the *National Science Foundation* for supporting the research.

I would like to express my deepest and warmest thanks to my family in Israel: My parents *Menahem* and *Aliza*, my brother *Avner*, and my sister *Michal*. They provided me with the persistence, courage, and belief which were necessary for such demanding research. They have been my stable and unconditional foundation from over the sea. Many thanks to my sister *Inbal* and my brother *Shalom* for forgiving me for such a long absence. I am grateful to my friends *David Dahan* (bet), *David Dahan* (shin), and my cousin *Eytan Turjeman* who helped me go through some difficult times.

A special thank to my warmhearted friend *Moises E. Smart* who was always there for me. I cannot imagine going through the past years without our true friendship.

Most of all, I am grateful to my wife, *Hila*, for her love, and continuous support and to my son, *Guy M.*, for filling my heart with infinite happiness.

Dedication

To my parents *Menahem* and *Aliza*

Table of Contents

List of Figures

Chapter 1

Introduction

There are in nature many examples of structures that have the characteristics of elastic rods: cross-sectional diameter significantly smaller than length, and elastic resistance to bending, twisting, shearing, and stretching. Perhaps the most important example of such rod-like structure is a duplex DNA molecule, but other macroscopic examples are botanical filaments and human hairs. [1] Although the work presented here provides methods of computing, and analyzing the stability of, equilibrium configurations of DNA molecules in solution with intramolecular electrostatic interactions taken into account, the general mathematical theory developed is expected to be applicable to a broad class of naturally discrete rod-like structures and to provide effective discretization procedures for continuous rods.

A duplex DNA molecule is comprised of two polymeric strands whose units, called nucleotides, contain a negatively charged phosphate group and a sugar that is covalently attached to a nearly planar nucleotide base. Each nucleotide is covalently bound to its adjacent neighbor in the same strand in such a way that the strand has directionality. There are four different types of nucleotide bases: Adenine (A), Thymine (T), Cytosine (C), and Guanine (G), with (A) complementary to (T) and (C) complementary to (G). The two strands, oriented with opposite directionality, form the Watson-Crick double helical structure [4] in which each base in one strand is joined to its compliment in the other strand to form an approximately planar *base pair*, with two hydrogen

---

[1]Goriely and Tabor [2] treated climbing plants as continuous elastic rods with intrinsic curvature. Zandi et. al. [3] suggested that their model of electrostatically charged elastic rod (originally proposed to model nano-tubes) is appropriate to the analysis of the stiffening of human hairs as a result of electrostatic repulsion.

bonds in a base pair A-T and three in G-C. Although displacements and rotations of one base relative to its complimentary base in the base pair are possible, such deformations are expected to be relatively small, and it is here assumed that the base pairs in a DNA molecule are planar and rigid objects that are stacked one on top of another with each rotated by approximately one-tenth of a full turn with respect to its immediate predecessor in the stack. [2] This assumption enables the definition of kinematical variables for the description of a DNA configuration. [3] Following such definitions one can relate the six numbers that determine the translation and orientation of a base pair relative to its predecessor to a set of cartesian coordinates for the positions in space of the atoms in the two adjacent base pairs that comprise a base-pair step. Thus, one obtains a description of the molecule as a structure with 6 degrees of freedom at each step. The six kinematical variables employed here for each base-pair step were introduced by El Hassan and Calldine [8]. The precise definitions are given in the Appendix and in [9]. The six numbers, $\theta_1^n, \theta_2^n, \theta_3^n, \rho_1^n, \rho_2^n, \rho_3^n$ that characterize the orientation and displacement of the $(n+1)$-th base pair relative to the n-th are called tilt, roll, twist, shift, slide, and rise. Such variables were proposed in early paper of Zhurkin, Lysov, and Ivanov [6]. The currently used requirements and nomenclature for these variables, ("the Cambridge accord") are summarized in [10]. As shown in Figure 1.1, tilt, roll, and slide describe rotations, shift and slide describe displacements associated with shearing motion, and rise describes displacements associated with extension (i.e., stretching).

As a phosphate group bears one (negative) electronic charge, two such charges are associated with one base pair. Two base pairs exert on each other an electrostatic force of repulsion, the strength of which depends on both the distance between charged sites and the concentration c of salt in the aqueous solution of DNA. The dependence on c results from the fact that salt ions of positive charge form a dense cloud around a

---

[2]For a detailed description see for example the book by Calladine, Drew, Luisi, and Travers [5].

[3]See e.g., [6], [7], [8]
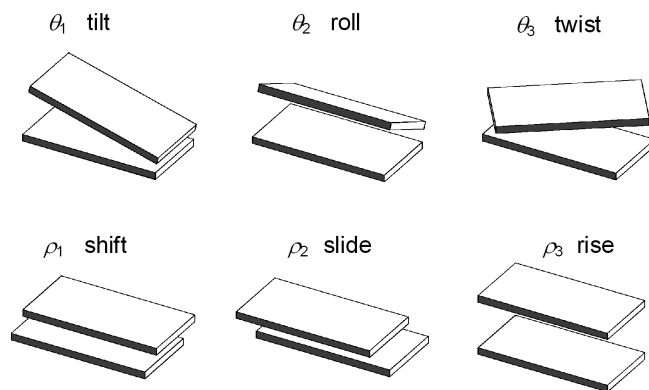
Figure 1.1: Schematic representations of the kinematical variables that describe the relative orientation and displacement of consecutive base pairs: θ_1 and θ_2 are angles of rotation about two perpendicular lines that lie in the midplane between the base pairs; θ_3 is an angle of rotation about a line l perpendicular to the midplane; ρ_1 and ρ_2 are mutually perpendicular displacements in directions parallel to the midplane; and ρ_3 is a displacement along l. Each drawing illustrates one of the kinematical variables for the (artificial) case in which that variable has a positive value and the others (with the exception of ρ_3) are set equal to zero.

negatively charged site on the DNA and in so doing partially screen out the electrostatic interaction of the site with other sites. As a consequence, an increase in c decreases the repulsion of nonadjacent base pairs and weakens the tendency of electrostatic forces to straighten DNA molecules.

Chapter 2

The equations of mechanical equilibrium

In the work presented here a configuration of a DNA molecule is specified, up to a rigid body motion, by $6N$ numbers. As shown below, when a DNA molecule is in a mechanical equilibrium, these numbers can be determined for a given set of end conditions, and external forces and moments exerted on the DNA molecule (including the repulsive electrostatic forces generated by the charges along the molecule). A DNA molecule is said to be in its *intrinsic configuration* when it is relaxed, i.e., being in a stress-free state when no external forces and moments are exerted on it. Cases are presented here in which for each base-pair step, only μ of the 6 kinematical numbers are unknown, and referred to as kinematical variables, while the remaining $(6-\mu)$ are constants and have their intrinsic values, i.e., values that comprise the intrinsic configuration. Here the value of μ will be 6 in the most general case and 3 in the case in which ρ_1^n, ρ_2^n, and ρ_3^n are preassigned. The theory presented here is applicable to the cases in which $\mu = 4$ or $\mu = 5$ (i.e., in which one or two of the parameters ρ_i are fixed), but will not be discussed at present.

2.1   Kinematical relations

Let $\mathbf{x}^n$ be the spatial position of the barycenter of the n-th base-pair in a DNA molecule with $N+1$ base pairs, and let the right handed orthonormal triad $(\mathbf{d}_1^n, \mathbf{d}_2^n, \mathbf{d}_3^n)$ be embedded in the n-th base pair and such that $\mathbf{d}_1^n$ and $\mathbf{d}_2^n$ span the plan associated with it. The vector $\mathbf{r}^n = \mathbf{x}^{n+1} - \mathbf{x}^n$ joins the barycenters of the n-th and the $(n+1)$-th base pairs, and its components $r_k^n = \mathbf{r}^n \cdot \mathbf{d}_k^n$ with respect to $(\mathbf{d}_1^n, \mathbf{d}_2^n, \mathbf{d}_3^n)$ are related to the
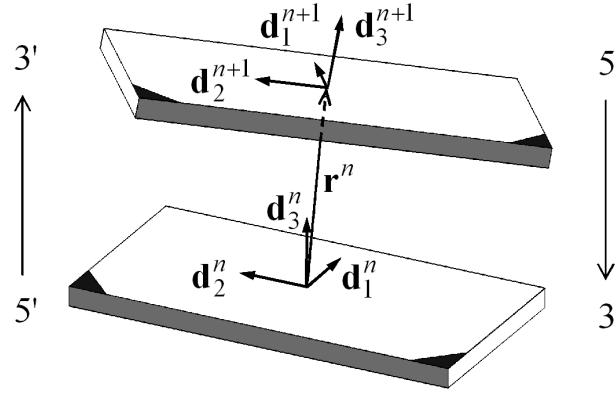
Figure 2.1: A schematic drawing of the n-th base-pair step showing the vectors $\mathbf{r}^n$, $\mathbf{d}_i^n$, and $\mathbf{d}_i^{n+1}$. Each nucleotide base in the n-th base pair lies mainly on one side of the plane spanned by $\mathbf{d}_1^n$ and $\mathbf{d}_3^n$ and is covalently bonded at its darkened corner to one of the two sugar phosphate chains. The direction of that oriented chain is indicated by a light-face arrow; the chain itself is not shown. The gray-shaded long edges are in the minor groove of the DNA.

local shift, slide, and rise by the orthogonal transformation [1]

$$r_k^n = R_{jk}^n \rho_j^n. \tag{2.1}$$

The shift, slide, and rise are the components $\rho_j^n = \mathbf{r}^n \cdot \mathbf{d}_j^{n+\frac{1}{2}}$ of $\mathbf{r}^n$ with respect to the middle frame triad [2] $(\mathbf{d}_1^{n+\frac{1}{2}}, \mathbf{d}_2^{n+\frac{1}{2}}, \mathbf{d}_3^{n+\frac{1}{2}})$. In equation (2.1) the components $R_{ij}^n = \mathbf{d}_i^{n+\frac{1}{2}} \cdot \mathbf{d}_j^n = \tilde{R}_{ij}(\theta_1^n, \theta_2^n, \theta_3^n)$ are functions of the local tilt, roll and twist that are given explicitly in the Appendix. A schematic drawing of a base-pair step and the vectors associated with it is shown in Figure 2.1.

A configuration of a DNA molecule is determined by the set of points $\{\mathbf{x}^1, \mathbf{x}^2, ..., \mathbf{x}^{N+1}\}$ characterizing the piecewise linear *axial curve*, $\mathcal{C}$, of the molecule's configuration, and the set of triads associated with each of the base pairs, $\{(\mathbf{d}_1^1, \mathbf{d}_2^1, \mathbf{d}_3^1), (\mathbf{d}_1^2, \mathbf{d}_2^2, \mathbf{d}_3^2), ...(\mathbf{d}_1^{N+1}, \mathbf{d}_2^{N+1}, \mathbf{d}_3^{N+1})\}$. The choice of the direction in which n is increasing along the molecule is arbitrary; for that choice, the unit vectors $\mathbf{d}_3^n$, for $n = 1, 2, ..., N+1$, must be such that the scalar products $\mathbf{r}^n \cdot \mathbf{d}_3^n$ are positive. [3] A

---

[1] The Einstein summation convention is used for double subscripts that indicate components or basis vectors in $\mathbb{R}^3$. For such subscripts only the letters i, j, k, l, and t were used. The summation symbol is used explicitly when a summation is performed over a higher dimension.

[2] For a precise definition of the middle frame triad, see [8] and the Appendix.

[3] For an open molecule the choice of the direction of increasing n is a consequence of the choice of

change in the choice of the direction of increasing n leaves the roll, twist, slide, and rise ($\theta_2^n, \theta_3^n, \rho_2^n$, and ρ_3^n) invariant but changes the sign of the tilt (θ_1^n), and the shift (ρ_1^n) [8]. [4]

For a given vector $\mathbf{x}^1$ and a given basis $(\mathbf{d}_1^1, \mathbf{d}_2^1, \mathbf{d}_3^1)$ the vectors $\mathbf{x}^n$ and the triads $(\mathbf{d}_1^n, \mathbf{d}_2^n, \mathbf{d}_3^n)$, for $n = 2, 3, ..., N+1$, are related to the $6N$ numbers $\{(\theta_1^m, \theta_2^m, \theta_3^m \rho_1^m, \rho_2^m, \rho_3^m)\}$, with $m = 1, 2, ...N$, by the relations,

$$\mathbf{x}^n = \mathbf{x}^1 + \sum_{p=1}^{n-1} \mathbf{d}_j^p R_{ij}^p \rho_i^p, \quad n = 2, 3, ..., N+1, \tag{2.2}$$

$$\mathbf{d}_i^n = Q_{ji}^n \mathbf{d}_j^1, \tag{2.3}$$

where the components, Q_{ji}^n, of the orthogonal transformation $\mathbf{Q}^n$ that relates the components of a vector with respect to $(\mathbf{d}_1^n, \mathbf{d}_2^n, \mathbf{d}_3^n)$ to its components with respect to $(\mathbf{d}_1^1, \mathbf{d}_2^1, \mathbf{d}_3^1)$, can be written in the form

$$Q_{ij}^n = \tilde{Q}_{ij}^n(\theta_1^1, \theta_2^1, \theta_3^1, \theta_1^2, ..., \theta_1^{n-1}, \theta_2^{n-1}, \theta_3^{n-1}) = D_{ik_1}^1 D_{k_1 k_2}^2 ... D_{k_{n-2}j}^{n-1} = \mathbf{d}_i^1 \cdot \mathbf{d}_j^n. \tag{2.4}$$

The numbers

$$D_{ij}^n = \mathbf{d}_i^n \cdot \mathbf{d}_j^{n+1} = \tilde{D}_{ij}(\theta_1^n, \theta_2^n, \theta_3^n) \tag{2.5}$$

are the components of the orthogonal transformation that takes $(\mathbf{d}_1^{n+1}, \mathbf{d}_2^{n+1}, \mathbf{d}_3^{n+1})$ into $(\mathbf{d}_1^n, \mathbf{d}_2^n, \mathbf{d}_3^n)$, and are explicitly given (see the Appendix) as functions of the local tilt, roll, and twist.

Equations (2.2), (2.3), (2.4), and (2.5), permit one to identify a configuration, up to a rigid body motion, with the vector $^6\boldsymbol{\alpha} \in \mathbb{R}^{6N}$ whose components are the set of $6N$ numbers, $\{(\theta_1^n, \theta_2^n, \theta_3^n, \rho_1^n, \rho_2^n, \rho_3^n)\}$, $n = 1, 2, ..., N$, ordered such that

$$^6\alpha_{\underline{n}} = \theta_a^n, \quad \text{for } a = 1, 2, 3, \tag{2.6a}$$

$$^6\alpha_{\underline{n}} = \rho_{a-3}^n, \quad \text{for } a = 4, 5, 6. \tag{2.6b}$$

---

the end base pair for which $n = 1$, however, in the case of a closed DNA molecule both the direction and the base pair with $n = 1$ can be chosen arbitrarily.

[4] A discussion on implications of this statement is given in [1], and later in this work.

The number $\underline{n}$ is defined to be $\underline{n}=a+(n-1)6$. However, as throughout this work attention is given also to the case for which the three numbers ρ_1^n, ρ_2^n, and ρ_3^n characterizing each of the base-pair steps are held fixed, a subset ${}^3\boldsymbol{\alpha}$ of ${}^6\boldsymbol{\alpha}$ is defined so that its components are given by

$$ {}^3\alpha_{\underline{n}} = \theta_k^n, \quad \text{for } k= 1, 2, 3 , \tag{2.7} $$

where the number $\underline{n}$ is now given by the relation $\underline{n}=k+(n-1)3$. This definition of the vector ${}^3\boldsymbol{\alpha}$ is vital to put emphasis on the subset of ${}^6\boldsymbol{\alpha}$ that contains only (and all of) the kinematical variables which are not constant in the discussed problem.

The assumption under which a base pair is rigid, restricts any variation of the vectors $(\mathbf{d}_1^n, \mathbf{d}_2^n, \mathbf{d}_3^n)$ to a variation that preserves their orthonormality and right-handedness. A variation of that kind is characterized by the relation

$$ \delta \mathbf{d}_i^n = \boldsymbol{\gamma}^n \times \mathbf{d}_i^n. \tag{2.8} $$

The equations (2.5) and (2.8) imply that

$$ D_{kj}^n \frac{\partial \tilde{D}_{ij}}{\partial \theta_l^n} \delta\theta_l^n = \epsilon_{kij} \mathbf{d}_j^n \cdot (\boldsymbol{\gamma}^{n+1} - \boldsymbol{\gamma}^n), \tag{2.9} $$

where ϵ_{kij} is the permutation symbol of Levi-Civita. As was discussed in [1], making use of the fact that the matrices $D_{kj}^n \frac{\partial \tilde{D}_{ij}}{\partial \theta_l^n}$ are skew, i.e.,

$$ D_{kj}^n \frac{\partial \tilde{D}_{ij}}{\partial \theta_l^n} = -D_{ij}^n \frac{\partial \tilde{D}_{kj}}{\partial \theta_l^n}, \quad l = 1, 2, 3, \tag{2.10} $$

permits one to write equation (2.9) in the form

$$ \Xi_{il}^n \delta\theta_l^n = \mathbf{d}_i^n \cdot (\boldsymbol{\gamma}^{n+1} - \boldsymbol{\gamma}^n), \tag{2.11} $$

where the components of the matrix $\boldsymbol{\Xi}^n$ are given by

$$ \Xi_{1l}^n = D_{2j}^n \frac{\partial \tilde{D}_{3j}}{\partial \theta_l^n}, \quad \Xi_{2l}^n = D_{3j}^n \frac{\partial \tilde{D}_{1j}}{\partial \theta_l^n}, \quad \Xi_{3l}^n = D_{1j}^n \frac{\partial \tilde{D}_{2j}}{\partial \theta_l^n}. \tag{2.12} $$

As was stated in reference [1] the matrix $\boldsymbol{\Xi}^n = \tilde{\boldsymbol{\Xi}}(\theta_1, \theta_2, \theta_3)$ is invertible for the domain of $(\theta_1^n, \theta_2^n, \theta_3^n)$ that is proper for the models and the problems discussed here, and hence the solution of (2.11) is

$$ \delta\theta_l^n = \Gamma_{il}^n \mathbf{d}_i^n \cdot (\boldsymbol{\gamma}^{n+1} - \boldsymbol{\gamma}^n), \tag{2.13} $$

where the numbers $\Gamma_{ik}^n = \tilde{\Gamma}_{ik}(\theta_1^n, \theta_2^n, \theta_3^n)$ are the components of the transpose of $(\mathbf{\Xi}^n)^{-1}$ i.e., [1]

$$\left(\mathbf{\Gamma}^n\right)^T = (\mathbf{\Xi}^n)^{-1}. \tag{2.14}$$

Using the functions $\tilde{D}_{ij}$ defined by equation (2.5) one can construct a triplet $(\zeta_1, \zeta_2, \zeta_3)$ of angles that characterize the orientation of the $(N+1)$-th base pair relative to the 1-st in the same way that $(\theta_1^n, \theta_2^n, \theta_3^n)$ relates the orientation of the $(n+1)$-th base pair to the n-th. That triplet is by definition the solution of the equation

$$\tilde{D}_{ij}(\zeta_1, \zeta_2, \zeta_3) = Q_{ij}^{N+1} = \mathbf{d}_i^1 \cdot \mathbf{d}_j^{N+1}. \tag{2.15}$$

The variations of the angles $(\zeta_1, \zeta_2, \zeta_3)$ have a form analogous to that seen in equation (2.13),

$$\delta\zeta_l = \tilde{\Gamma}_{il}(\zeta_1, \zeta_2, \zeta_3)\mathbf{d}_i^1 \cdot (\boldsymbol{\gamma}^{N+1} - \boldsymbol{\gamma}^1). \tag{2.16}$$

The functions $\tilde{\Gamma}_{ik}$ in equation (2.16) are the same as those seen in equation (2.14).

In terms of the components $x_k^n = \mathbf{x}^n \cdot \mathbf{d}_k^1$ of $\mathbf{x}^n$ with respect to $\mathbf{d}_k^1$, equation (2.2) has the form

$$x_k^n = x_k^1 + \sum_{p=1}^{n-1} Q_{kj}^p R_{ij}^p \rho_i^p, \qquad n = 2, 3, ..., N+1. \tag{2.17}$$

Equation (2.8) allows one to write for a variation of $Q_{kj}^p = \mathbf{d}_k^1 \cdot \mathbf{d}_j^p$ the relation

$$\delta Q_{kj}^p = (\mathbf{d}_k^1 \times \mathbf{d}_j^p) \cdot (\boldsymbol{\gamma}^1 - \boldsymbol{\gamma}^p). \tag{2.18}$$

On the other hand, as the middle frame triad $(\mathbf{d}_1^{n+\frac{1}{2}}, \mathbf{d}_2^{n+\frac{1}{2}}, \mathbf{d}_3^{n+\frac{1}{2}})$, is determined by the relative orientation between the $(n+1)$-th and the n-th triads, for the variation of R_{ij}^p one can use equation (2.13) to write

$$\delta R_{ij}^p = \frac{\partial \tilde{R}_{ij}^p}{\partial \theta_l^p} \Gamma_{kl}^p \mathbf{d}_k^p \cdot (\boldsymbol{\gamma}^{p+1} - \boldsymbol{\gamma}^p). \tag{2.19}$$

Thus, as follows from equations (2.1), (2.17), (2.18), and (2.19), a variation δx_k^n takes

the form

$$\delta x_k^n = \delta x_k^1 + \sum_{p=1}^{n-1} \left((\mathbf{d}_k^1 \times \mathbf{r}^p) \cdot (\boldsymbol{\gamma}^1 - \boldsymbol{\gamma}^p) + \right.$$

$$\left. Q_{kj}^p \rho_i^p \frac{\partial \tilde{R}_{ij}^p}{\partial \theta_l^p} \Gamma_{tl}^p \mathbf{d}_t^p \cdot (\boldsymbol{\gamma}^{p+1} - \boldsymbol{\gamma}^p) + Q_{kj}^p R_{ij}^p \delta \rho_i^p, \quad (2.20)$$

for $n = 2, 3, ..., N + 1$. As will be shown later, the relation (2.20) is of a great importance for the derivation of the *equations of mechanical equilibrium* as it relates a variation of the spatial position to variations of the triads and the local displacements.

2.2   The energy of a DNA molecule

In analogous to the continuous elastic rod model, the main hypothesis taken here is that the elastic energy, Ψ, of a DNA molecule in a specified configuration is given by the sum over m of the local energies of interaction, ψ^m, associated with the m-th base-pair step,

$$\Psi = \sum_{m=1}^{N} \psi^m. \quad (2.21)$$

The local energy ψ^m, depends upon the nucleotide bases in the m-th and the $(m+1)$-th base pairs and the relative displacement and orientation between the $(m+1)$-th and the m-th base pairs, and has to be in accord with the principle of frame indifference, e.g., invariance under any rigid body motion. Consequently, one can write,

$$\psi^n = \check{\psi}^n(\theta_1^n, \theta_2^n, \theta_3^n, \rho_1^n, \rho_2^n, \rho_3^n). \quad (2.22)$$

Any scheme that defines the kinematical numbers and any form of the functions $\check{\psi}^n$ have to be such that the energy $\check{\psi}^n(\theta_1^n, \theta_2^n, \theta_3^n, \rho_1^n, \rho_2^n, \rho_3^n)$ is independent of the direction of increasing n along the molecule.

As an approximation, it is further assumed here that the two negative charges associated with each base pair are located at the barycenter of that base pair [11]. According to this assumption, the associated electrostatic forces yield no resultant moments.

Thus, the electrostatic energy, $\Phi = \check{\Phi}(\mathbf{x}^1, \mathbf{x}^2, ..., \mathbf{x}^{N+1})$, of a configuration has the form

$$\Phi = \frac{1}{2} \sum_{n=1}^{N+1} \phi^n, \tag{2.23}$$

where $\phi^n = \check{\phi}^n(\mathbf{x}^1, \mathbf{x}^2, ..., \mathbf{x}^{N+1})$, is the electrostatic energy associated with the n-th base pair, and can be written in the form

$$\phi^n = \sum_{m=1}^{N+1} \varphi^{nm}, \qquad \varphi^{nn} \equiv 0, \tag{2.24}$$

in which $\varphi^{nm} = \varphi^{mn}$, the potential energy of electrostatic interaction between the charges on the n-th and the m-th base pairs, is a function of the distance,

$$x^{nm} = |\mathbf{x}^n - \mathbf{x}^m|, \tag{2.25}$$

between the two base pairs, i.e., $\varphi^{nm} = \check{\varphi}(x^{nm})$. For the model considered throughout the present work, it is supposed that the elastic energy of interaction between two adjacent base pairs includes in its form the electrostatic energy associated with that base-pair step, and consequently

$$\varphi^{n(n+1)} = 0, \qquad \text{for} \quad n = 1, 2, ..., N. \tag{2.26}$$

The total energy U of a DNA molecule is taken to be the sum of its elastic energy Ψ and its electrostatic energy Φ

$$U = \Psi + \Phi. \tag{2.27}$$

2.3 Variational statement I: the first variation of the energy

A configuration of a DNA molecule is said to be in a *mechanical equilibrium* if its total energy possesses a local extremum, under a given set of end conditions. A configuration at that state is referred to as an *equilibrium configuration*. Although the end conditions can in general take the form of (i) kinematical constraints for which the relative orientation and displacement of the base pairs at the two ends are preassigned,

(ii) mechanical constraints for which given set of external moments and forces exerted on the molecule's ends are preassigned or (iii) any combination of the two types, for a derivation of the equations of mechanical equilibrium it is sufficient to discuss the first case. In that case, the relative orientation of the two end base pairs (base pair 1 and base pair $(N+1)$) is set to be characterized by the three preassigned rotational parameters, $(_o\zeta_1, _o\zeta_2, _o\zeta_3)$, and the relative displacement between the two ends of the molecule is given by the three translational parameters, $_o\ell_1, _o\ell_2, _o\ell_3$, such that the six scalar equations expressing the constraints are

$$\zeta_i - _o\zeta_i = 0, \quad i = 1, 2, 3, \tag{2.28a}$$

$$\ell_k - _o\ell_k = 0, \quad k = 1, 2, 3, \tag{2.28b}$$

where ℓ_k are the components of the end-to-end vector $\boldsymbol{\ell} = (\mathbf{x}^{N+1} - \mathbf{x}^1)$ with respect to the basis vectors $\mathbf{d}_k^1$, i.e.,

$$\ell_k = (\mathbf{x}^{N+1} - \mathbf{x}^1) \cdot \mathbf{d}_k^1. \tag{2.29}$$

The form of the constrained variational problem can be transformed to that of a constraint-free problem by the introduction of the modified energy

$$U^* = \tilde{U}^*(^\mu\boldsymbol{\alpha}, \tau_1, \tau_2, \tau_3, P_1, P_2, P_3) = U + \tau_i\zeta_i + P_k\ell_k \tag{2.30}$$

in which the numbers τ_1, τ_2, τ_3, and P_1, P_2, P_3, are Lagrange multipliers, the physical meaning of which will be discussed later. The definition of a contact free [5] equilibrium configuration can now be restated: A DNA molecule's configuration under the imposed constraints of equations (2.28) is an equilibrium configuration if for it the first variation of the modified energy U^* vanishes,

$$\delta U^* = \delta U + \tau_i\delta\zeta_i + P_k\delta\ell_k = 0, \tag{2.31}$$

for any variation in the position and orientation of the molecule's base pairs.

---

[5]The special case of equilibrium configurations with self contact is discussed in a subsequent section.

2.4 The equations of mechanical equilibrium

In this section a detailed derivation of the equations of mechanical equilibrium originated from equation (2.31) is given. The equations are derived for the general case, $\mu=6$, in which none of the kinematical numbers is frozen. The first term in the right hand side of equation (2.31), δU, is given by

$$\delta U = \sum_{n=1}^{N} \frac{\partial \check{\psi}^n}{\partial \theta_l^n} \delta \theta_l^n + \sum_{n=1}^{N} \frac{\partial \check{\psi}^n}{\partial \rho_l^n} \delta \rho_l^n - \sum_{n=1}^{N+1} g_k^n \delta x_k^n, \tag{2.32}$$

where g_k^n are the components with respect to $\mathbf{d}_k^1$ of the electrostatic force, $\mathbf{g}^m$, acting on the n-th base pair, and are given by

$$g_k^n = -\frac{\partial \check{\Phi}}{\partial x_k^n} = -\sum_{m=1}^{N+1} \frac{\partial \check{\varphi}^{nm}}{\partial x_k^n}. \tag{2.33}$$

The electrostatic force $\mathbf{g}^n$ is the sum of the repulsive electrostatic forces that non-adjacent (to base pair n) base pairs exert on the n-th base pair,

$$\mathbf{g}^n = \sum_{m=1}^{N+1} \mathbf{G}^{nm}, \quad \mathbf{G}^{nn} \equiv 0, \tag{2.34}$$

with

$$\mathbf{G}^{nm} = -\mathbf{G}^{mn} = -\left(\partial \check{\varphi}(x^{nm})/\partial x_k^n\right)\mathbf{d}_k^1, \tag{2.35}$$

the repulsive force that the m-th base pair exerts on the n-th, and which is acting along the straight line connecting their barycenters. Because of this mutuality of the electrostatic force the two relations given below are obeyed independently of the configuration,

$$\sum_{m=1}^{N+1} \mathbf{g}^m = \mathbf{0}, \tag{2.36}$$

$$\sum_{n=2}^{N+1} \mathbf{g}^n \times \sum_{p=1}^{n-1} \mathbf{r}^p = -\sum_{p=1}^{N} \mathbf{r}^p \times \sum_{n=p+1}^{N+1} \mathbf{g}^n = \mathbf{0}. \tag{2.37}$$

By making use of equations (2.13),(2.16), (2.20), and rewriting equation (2.32) in terms of configurational variations that are characterized by γ^n and $\delta \rho_i^n$, one can write

δU^* in the form

$$\delta U^* = \sum_{n=1}^{N} \frac{\partial \check{\psi}^n}{\partial \theta_l^n} \Gamma_{il}^n \mathbf{d}_i^n \cdot (\boldsymbol{\gamma}^{n+1} - \boldsymbol{\gamma}^n) + \tau_k \tilde{\Gamma}_{ik}(\zeta_1, \zeta_2, \zeta_3) \mathbf{d}_i^1 \cdot (\boldsymbol{\gamma}^{N+1} - \boldsymbol{\gamma}^1)$$

$$+ \sum_{p=1}^{N} \mathbf{r}^p \times \left(\sum_{n=p+1}^{N+1} \mathbf{g}^n - \mathbf{P} \right) \cdot (\boldsymbol{\gamma}^1 - \boldsymbol{\gamma}^p)$$

$$- \sum_{p=1}^{N} \left(Q_{kj}^p \rho_i^p \frac{\partial \tilde{R}_{ij}^p}{\partial \theta_l^p} \Gamma_{tl}^p \mathbf{d}_t^p \left(\sum_{n=p+1}^{N+1} g_k^n - P_k \right) \right) \cdot (\boldsymbol{\gamma}^{p+1} - \boldsymbol{\gamma}^p)) \qquad (2.38)$$

$$- \sum_{p=1}^{N} Q_{kj}^p R_{ij}^p \left(\sum_{n=p+1}^{N+1} g_k^n - P_k \right) \delta \rho_i^p$$

$$+ \sum_{n=1}^{N} \frac{\partial \check{\psi}^n}{\partial \rho_i^n} \delta \rho_i^n - \sum_{n=1}^{N+1} g_k^n \delta x_k^1,$$

where $\mathbf{P} = P_k \mathbf{d}_k^1$. Furthermore, by defining the following vectors

$$\mathbf{h}^n = \sum_{m=n+1}^{N+1} \mathbf{g}^m - \mathbf{P} = - \sum_{m=1}^{n} \mathbf{g}^m - \mathbf{P}, \qquad \mathbf{h}^n = h_j^n \mathbf{d}_j^n = \bar{h}_j^n \mathbf{d}_j^1, \qquad (2.39a)$$

$$\mathbf{m}^n = \Gamma_{tl}^n \left(\frac{\partial \check{\psi}^n}{\partial \theta_l^n} - \rho_i^n \frac{\partial \tilde{R}_{ij}^n}{\partial \theta_l^n} h_j^n \right) \mathbf{d}_t^n, \qquad \mathbf{m}^n = m_j^n \mathbf{d}_j^n = \bar{m}_j^n \mathbf{d}_j^1, \qquad (2.39b)$$

$$\mathbf{T} = \tau_k \tilde{\Gamma}_{ik}(\zeta_1, \zeta_2, \zeta_3) \mathbf{d}_i^1, \qquad (2.39c)$$

$$\mathbf{f}^n = \frac{\partial \check{\psi}^n}{\partial \rho_i^n} \mathbf{d}_i^{n+\frac{1}{2}}, \qquad \mathbf{f}^n = f_j^n \mathbf{d}_j^n = \bar{f}_j^n \mathbf{d}_j^1, \qquad (2.39d)$$

$$\delta \mathbf{r}^n = \delta \rho_i^n \mathbf{d}_i^{n+\frac{1}{2}}, \qquad (2.39e)$$

and properly recollecting terms in equation (2.38), one can finally write, with the use of equations (2.36) and (2.37), the first variation of the modified energy U^* in a form from which the equations of equilibrium can be deduced:

$$\delta U^* = - \left(\mathbf{m}^1 + \mathbf{r}^1 \times \mathbf{h}^1 + \mathbf{T} + \boldsymbol{\ell} \times \mathbf{P} \right) \cdot \boldsymbol{\gamma}^1$$

$$- \sum_{n=2}^{N} \left(\mathbf{m}^n - \mathbf{m}^{n-1} + \mathbf{r}^n \times \mathbf{h}^n \right) \cdot \boldsymbol{\gamma}^n$$

$$+ \left(\mathbf{m}^N + \mathbf{T} \right) \cdot \boldsymbol{\gamma}^{N+1} \qquad (2.40)$$

$$- \sum_{n=1}^{N} \left(\mathbf{h}^n - \mathbf{f}^n \right) \cdot \delta \mathbf{r}^n - \sum_{n=1}^{N+1} g_k^n \delta x_k^1 .$$

When none of the $3N$ kinematical variables, ρ_i^n, is frozen, i.e., when $\mu = 6$, a config-uration ${}^6\alpha$ is an equilibrium configuration if the first variation of the modified energy δU^* vanishes for any choice of: (a) δx_k^1, with $k = 1, 2, 3$, (b) $\delta \mathbf{r}^n$, with $n = 1, 2, ..., N$, and (c) $\boldsymbol{\gamma}^m$, with $m = 1, 2, ..., N+1$. Part (a) of the above condition is automatically satisfied as equation (2.36) is valid independently of the configuration, namely the sum of all the electrostatic forces acting on a molecule is identically zero. A satisfaction of part (b) is obtained if and only if the following equations are obeyed

$$\mathbf{F}^n = \mathbf{h}^n - \mathbf{f}^n = \mathbf{0}, \quad n = 1, 2, ..., N. \tag{2.41}$$

If one substitutes the n-th equation of the set of N vectorial equations (2.41) with the equation obtained by subtracting the $(n-1)$-th equation from the n-th equation, i.e., with the equation $\mathbf{F}^n - \mathbf{F}^{n-1} = \mathbf{0}$, for $n = 2, 3, ...N$, one gets the following set of $N+1$ vectorial equations, i.e., $3N + 3$ equations ($3N$ of which are independent),

$$\mathbf{f}^1 + \mathbf{g}^1 + \mathbf{P} = \mathbf{0}, \tag{2.42a}$$

$$\mathbf{f}^n - \mathbf{f}^{n-1} + \mathbf{g}^n = \mathbf{0}, \quad n = 2, 3, ..., N, \tag{2.42b}$$

$$-\mathbf{f}^N + \mathbf{g}^{N+1} - \mathbf{P} = \mathbf{0}. \tag{2.42c}$$

A necessary and sufficient condition under which part (c) of the statement for the van-ishing of the first variation is satisfied, is that the $N+1$ vectorial equations,

$$\mathbf{M}^1 = \mathbf{m}^1 + \mathbf{r}^1 \times \mathbf{h}^1 + \mathbf{T} + \boldsymbol{\ell} \times \mathbf{P} = \mathbf{0}, \tag{2.43a}$$

$$\mathbf{M}^n = \mathbf{m}^n - \mathbf{m}^{n-1} + \mathbf{r}^n \times \mathbf{h}^n = \mathbf{0}, \quad n = 2, 3, ..., N, \tag{2.43b}$$

$$\mathbf{M}^{N+1} = -\mathbf{m}^N - \mathbf{T} = \mathbf{0}, \tag{2.43c}$$

N (or $3N$ scalar equations) of which are independent, are obeyed. The derivation of the equations (2.42) from the equations (2.41) makes it clear that the equations (2.42a) and (2.42b) imply (2.42c). Furthermore, using the relations (2.35), (2.36), and (2.37), one can show that the equations (2.43a) and (2.43b) imply (2.43c).

The equations (2.41) or equivalently (2.42) together with the equations (2.43) are

here referred to as the *equations of mechanical equilibrium*, and form the discrete analog of the differential equations expressing the balance of forces and moments in Kirchhoff's theory of elastic rods [12], [13], [14], [15], [16]. The vectors $\mathbf{f}^n$ and $\mathbf{m}^n$ are interpreted as the force and moment exerted on the n-th base pair by the $(n+1)$-th base pair. The vector $-\mathbf{h}^n$ is the sum of all the external forces [6] exerted on the subsegment that includes the base pairs $1, 2, ..., n$, and hence, the vector $-\mathbf{F}^n$ is the sum of all the forces exerted on that subsegment. The vector $\mathbf{M}^n$ denotes the sum of moments exerted on the n-th base pair. The vectors $\mathbf{P}$ and $\mathbf{T}$ represent the force and moment exerted on base pair 1 by the external world (or equivalently by the base pair $N+1$), and are the result of confining the two ends of the molecule to the kinematical constraints given in equations (2.28).

For the clarity of the discussions next to be presented, it is convenient to define the vectors, $^\mu\mathbf{\Omega} \in \mathbb{R}^{\mu N}$, where μ equals 6 or 3, to be the vectors with the μN components, for $n = 1, 2, ..., N$,

$$^6\Omega_{\underline{n}} = -\mathbf{M}^n \cdot \mathbf{d}_a^1, \ \text{ for } \ a = 1, 2, 3 \, , \qquad ^6\Omega_{\underline{n}} = -\mathbf{F}^n \cdot \mathbf{d}_{a-3}^1, \ \text{ for } \ a = 4, 5, 6 \, , \quad (2.44a)$$

$$^3\Omega_{\underline{n}} = -\mathbf{M}^n \cdot \mathbf{d}_a^1, \ \text{ for } \ a = 1, 2, 3 \, , \tag{2.44b}$$

where the number $\underline{n} = a + (n-1)\mu$. In the case in which the end conditions are given by kinematical constraints, an equilibrium configuration is calculated by solving a system of $\mu N + 6$ nonlinear equations for the set of μN kinematical variables that defines a configuration $^\mu\boldsymbol{\alpha}$, together with the six Lagrange multipliers τ_1, τ_2, τ_3, and P_1, P_2, P_3. [7] This system of equations includes the μN equations of mechanical equilibrium, which, following the definitions (2.44), can shortly be written in the form

$$^\mu\Omega_{\underline{n}} = \, ^\mu\tilde{\Omega}_{\underline{n}}(^\mu\boldsymbol{\alpha}) = 0, \ \text{ for } \ \underline{n} = 1, ..., \mu N \, , \tag{2.45}$$

---

[6]It is assumed here that the only forces are those that originated by the intramolecular electrostatic interaction and the end conditions, a more general case in which contact forces are present will be discussed in the subsequent section.

[7]In the case in which the molecule is not free of self contact an additional unknown is associated with each contact point. The case of self contact is discussed in details in the following section.

and the 6 constraints given by equations (2.28). It is important to note, that when $\mu = 6$, the computation of an equilibrium configuration does not necessitate the calculation of the vectors $\mathbf{h}^n$ directly from the relation (2.39a), but instead one can use equations (2.41) to replace $\mathbf{h}^n$ by $\mathbf{f}^n$, and use the constitutive relations (2.39d) for the components of $\mathbf{f}^n$. In the case of end conditions that are given by mechanical constraints of the form,

$$\mathbf{T} = \mathbf{T}^0, \quad \mathbf{P} = \mathbf{P}^0, \tag{2.46}$$

i.e., by which the vectors $\mathbf{P}$ and $\mathbf{T}$ are preassigned, the number of unknowns reduces to μN, and clearly no use should be made with the 6 equations (2.28).

2.5 The equations of equilibrium when self contact is taken into account

Although in cases for which the *distance of closest approach*, [8] $\mathcal{D}_{\mathrm{ca}}$, is in the order of magnitude of the effective diameter, $\mathcal{D}_{\mathrm{o}} = 20\text{Å}$, of the DNA molecule the electrostatic energy serves as a natural "penalty function", in the sense that the total energy increases significantly as $\mathcal{D}_{\mathrm{ca}}$ approaches $\mathcal{D}_{\mathrm{o}}$ (from above), there are examples for which the end conditions are such that the repulsive electrostatic forces as were taken in the present theory [9] are not sufficient to avoid self penetration of the DNA molecule . Such is the case for equilibria of a closed supercoiled DNA molecule, a molecule that was pretwisted and closed to form a circular molecule. (See e.g., the experiments reported

---

[8]The distance of closest approach is here taken as the minimal distance over the set of pairs of points on the axial curve, $\mathcal{C}$, that are separated by more than 20 base-pair steps, i.e., the DNA subsegment between the two points consist of more than 20 base pairs. It is assumed here that a DNA subsegment of less than 20 base pairs cannot have self contact as such cases require values of curvature that are significantly higher than the maximal admissible values.

[9]There are theoretical evidences [17], supported by computer simulations [18], [19], by which when the distance of closest approach is small relative to the Debye length (see the discussion on the electrostatic energy) there may be attractive forces between the two subsegments that are in proximity. This possibility is not considered here.
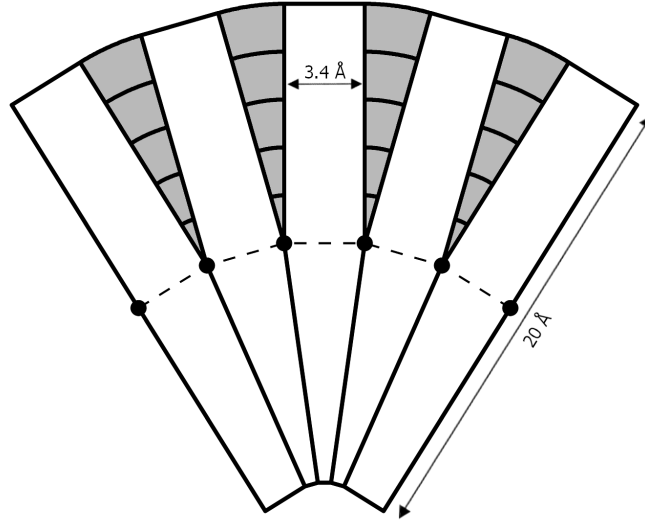
Figure 2.2: A schematic drawing of the assumed impenetrable surface of the DNA. The dashed line represent the piecewise linear axial curve of the DNA. Each rectangle represents a rigid cylinder with a diameter of 20Å. A cylinder is associated with each base-pair step such that its axis coincides with the line connecting the barycenters of the corresponding adjacent base pairs. The small circles represent the barycenters of the base pairs. The grey patches represent spherical sections, the centers of which coincide with the barycenters of the corresponding base pairs, that fill the gaps (as a result of the local curvature) between each two adjacent cylinders.

in [20]). To calculate equilibrium configurations that satisfy the impenetrability condition,

$$\mathcal{D}_{\mathrm{ca}} >= \mathcal{D}_{\mathrm{o}}, \tag{2.47}$$

one must account for self-contact, in a way analogous to the theory of elastic rods with self contact [21], [22], [23].

For that purpose, the impenetrable surface of a DNA molecule is assumed to be the boundary of the union of the N cylinders $\mathcal{T}^n$ of diameter $\mathcal{D}_{\mathrm{o}}$, with $n = 1, 2, ...,N$, such that a point $\mathbf{x}$ is on $\mathcal{T}^n$ if and only if

$$\left|\mathbf{x} - \mathbf{x}^n - \frac{(\mathbf{x} - \mathbf{x}^n) \cdot \mathbf{r}^n}{\mathbf{r}^n \cdot \mathbf{r}^n}\mathbf{r}^n\right| = \frac{\mathcal{D}_{\mathrm{o}}}{2} \quad \text{and} \quad 0 \leq (\mathbf{x} - \mathbf{x}^n) \cdot \frac{\mathbf{r}^n}{|\mathbf{r}^n|} \leq |\mathbf{r}^n|, \tag{2.48}$$

and the $N+1$ spheres $\mathcal{B}^m$ of diameter $\mathcal{D}_{\mathrm{o}}$, that are centered at $\mathbf{x}^m$, with $m = 2, ...,N$. A two dimensional schematic description of the assumed impenetrable surface is given in Figure 2.2.

Accordingly, two base-pair steps, $m_\imath$ and $n_\imath$, with $n_\imath \geq m_\imath+20$, are said to be in contact if and only if

$$\mathcal{D}^{m_\imath n_\imath} = \min \hat{\mathcal{D}}^{m_\imath n_\imath}(s_{m_\imath}, s_{n_\imath}) = \hat{\mathcal{D}}^{m_\imath n_\imath}({}_*s_{m_\imath}, {}_*s_{n_\imath}) = \mathcal{D}_{\mathrm{o}},$$
$$0 \leq s_{m_\imath} < 1, \quad 0 \leq s_{n_\imath} < 1, \tag{2.49}$$

where $\mathcal{D}^{m_\imath n_\imath}$ is the minimum value of the function $\hat{\mathcal{D}}^{m_\imath n_\imath}$, that gives the distance,

$$\hat{\mathcal{D}}^{m_\imath n_\imath}(s_{m_\imath}, s_{n_\imath}) = |\mathbf{p}^{n_\imath}(s_{n_\imath}) - \mathbf{p}^{m_\imath}(s_{m_\imath})|, \tag{2.50}$$

between two points,

$$\mathbf{p}^{m_\imath}(s_{m_\imath}) = \mathbf{x}^{m_\imath} + s_{m_\imath}\mathbf{r}^{m_\imath} \qquad \text{and} \qquad \mathbf{p}^{n_\imath}(s_{n_\imath}) = \mathbf{x}^{n_\imath} + s_{n_\imath}\mathbf{r}^{n_\imath}, \tag{2.51}$$

on the line intervals associated with the two base-pair steps. In other words, the function $\hat{\mathcal{D}}^{m_\imath n_\imath}$ gives the distance between a point on the linear interval connecting $\mathbf{x}^{m_\imath}$ and $\mathbf{x}^{m_\imath+1}$ and a point on the interval connecting $\mathbf{x}^{n_\imath}$ and $\mathbf{x}^{n_\imath+1}$. The minimal value of $\hat{\mathcal{D}}^{m_\imath n_\imath}$ (in the domain of the two linear segments) is generally a function of the position of the four barycenters of the $m_\imath$-th, $(m_\imath+1)$-th, $n_\imath$-th, and the $(n_\imath+1)$-th base pairs, i.e., $\mathcal{D}^{m_\imath n_\imath} = \tilde{\mathcal{D}}(\mathbf{x}^{m_\imath}, \mathbf{x}^{m_\imath+1}, \mathbf{x}^{n_\imath}, \mathbf{x}^{n_\imath+1})$. There are four possible cases of self contact (for which $\mathcal{D}^{m_\imath n_\imath} = \mathcal{D}_{\mathrm{o}}$) between a couple of base-pair steps $m_\imath$ and $n_\imath$: (I) a contact between the spheres, $\mathcal{B}^{m_\imath}$ and $\mathcal{B}^{n_\imath}$, i.e., the case in which equation (2.49) is satisfied with ${}_*s_{m_\imath} = 0$ and ${}_*s_{n_\imath} = 0$, (II) a contact between the sphere $\mathcal{B}^{m_\imath}$ and the cylinder $\mathcal{T}^{n_\imath}$, i.e., the case in which equation (2.49) is satisfied with ${}_*s_{m_\imath} = 0$ and $0 < {}_*s_{n_\imath} < 1$, (III) a contact between the cylinder $\mathcal{T}^{m_\imath}$ and the sphere $\mathcal{B}^{n_\imath}$, i.e., the case in which equation (2.49) is satisfied with $0 < {}_*s_{m_\imath} < 1$ and ${}_*s_{n_\imath} = 0$, and (IV) a contact between the two cylinders $\mathcal{T}^{m_\imath}$ and $\mathcal{T}^{n_\imath}$, i.e., the case in which equation (2.49) is satisfied with $0 < {}_*s_{m_\imath} < 1$ and $0 < {}_*s_{n_\imath} < 1$. Hence, the minimum distance $\mathcal{D}^{m_\imath n_\imath}$ can be written for each possible case[10] as follows:

---

[10]The case for which $\mathbf{r}^{m_\imath}$ and $\mathbf{r}^{n_\imath}$ are exactly parallel when the two associated base-pair steps are in contact is extremely rare in problems of supercoiled DNA or any other rod-like structure with self contact. In such a case one of the two functions given for cases II and III can be used for case IV.

I II & III IV
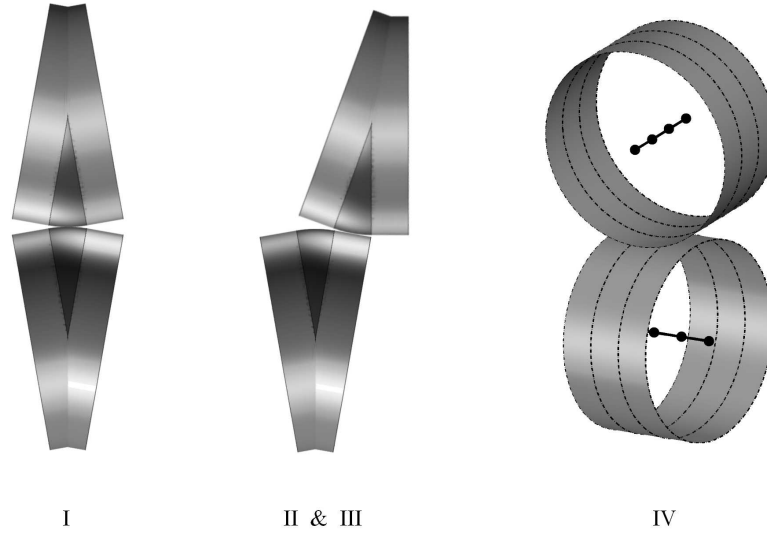
Figure 2.3: A schematic drawing of the different types of contact. The figure on the left hand side illustrates a contact between two spheres (case I). The center figure shows the case of contact between a sphere and a cylinder (cases II and III). The right hand side figure illustrates a case of contact between two cylinders (case IV). The subsegments of the piecewise-linear axial curve which determines the position and orientation of the cylinders are depicted as lines connecting the barycenters of the base pairs (black circles).

$$
\mathcal{D}^{m_\imath n_\imath} = \begin{cases} \left| \mathbf{x}^{n_\imath} - \mathbf{x}^{m_\imath} \right|, & \text{for case (I),} \\[2ex] \left| \mathbf{x}^{m_\imath} - \mathbf{x}^{n_\imath} - \dfrac{\left(\mathbf{x}^{m_\imath} - \mathbf{x}^{n_\imath}\right) \cdot \mathbf{r}^{n_\imath}}{\mathbf{r}^{n_\imath} \cdot \mathbf{r}^{n_\imath}} \mathbf{r}^{n_\imath} \right|, & \text{for case (II),} \\[3ex] \left| \mathbf{x}^{n_\imath} - \mathbf{x}^{m_\imath} - \dfrac{\left(\mathbf{x}^{n_\imath} - \mathbf{x}^{m_\imath}\right) \cdot \mathbf{r}^{m_\imath}}{\mathbf{r}^{m_\imath} \cdot \mathbf{r}^{m_\imath}} \mathbf{r}^{m_\imath} \right|, & \text{for case (III),} \\[3ex] \left| \dfrac{\left(\mathbf{x}^{n_\imath} - \mathbf{x}^{m_\imath}\right) \cdot \left(\mathbf{r}^{n_\imath} \times \mathbf{r}^{m_\imath}\right)}{\left| \mathbf{r}^{n_\imath} \times \mathbf{r}^{m_\imath} \right|} \right|, & \text{for case (IV).} \end{cases}
\tag{2.52}
$$

The different cases of contact are illustrated in Figure 2.3.

Therefore, by pursuing an $\acute{a}$ priori conjecture in which only the pairs of base-pair steps $\{m_\imath, n_\imath\}$ with $n_\imath > m_\imath + 20$, $\imath = 1, 2, ..., N_\mathrm{c}$, can possibly be in contact, one can convert the inequality constraints for the impenetrability of a molecule,

$$
\mathcal{D}^{m_\imath n_\imath} >= \mathcal{D}_\mathrm{o}, \quad \imath = 1, 2, ..., N_\mathrm{c},
\tag{2.53}
$$

into constraints that are given by the equations,

$$
\mathcal{D}^{m_\imath n_\imath} - \mathcal{D}_\mathrm{o} - v_\imath^2 = 0,
\tag{2.54}
$$

in which the numbers $v_1, v_2, ..., v_{N_c}$ are "slack" variables that assure the satisfaction of the inequality constraints (2.53). [11]

The arguments just described permits the introduction of a modified energy,

$$U^{**} = \tilde{U}^{**}(^\mu\boldsymbol{\alpha}, \tau_1, \tau_2, \tau_3, P_1, P_2, P_3, \chi_1, \chi_2, ..., \chi_{N_c}, v_1, v_2, ..., v_{N_c}) =$$
$$U^* - \sum_{i=1}^{N_c} \chi_i \left(\mathcal{D}^{m_i n_i} - \mathcal{D}_o + v_i^2 \right), \quad (2.55)$$

where the numbers, $\chi_1, \chi_2, ..., \chi_{N_c}$ are the Lagrange multipliers associated with the constraints (2.54). Each number χ_i indicates the change in the total energy due to a change in the distance between the base-pair steps associated with it. As a result, when the constraint associated with χ_i is active, i.e., $\chi_i \neq 0$, it can be interpreted as the *contact force* which, for a contact of case (I), acts along a line connecting the barycenters of the two base pairs in contact; for cases (II) or (III), acts along a line that goes through the barycenter of the base pair in contact and is perpendicular to the base-pair step (in the other side of the molecule); and for case (IV), acts along a line perpendicular to both base-pair steps in contact. A positive value of χ_i indicates a force of repulsion as must be the case for contact forces. As a negative value of χ_i indicates an attractive force, this case is not physical for the problems discussed here.

The definition of an equilibrium configuration, as was discussed in the end of Section (2.3), is valid only for the special case in which the molecule is free of self contact. In the more general case, discussed in the present section, a configuration is said to be in equilibrium if:

i. it satisfies the end conditions (2.28) or (2.46), the constraints (2.54), and for any pair of base pairs for which $v_i = 0$ equation (2.49) is strictly obeyed, i.e., the contact point is such that $0 \leq {}_* s_{m_i} < 1, \quad 0 \leq {}_* s_{n_i} < 1$;

---

[11] The purpose of introducing these variables is mainly for the derivation of the conditions for equilibrium. See e.g., the book on nonlinear programming by D. M. Simmoms [24]. A Practical use of the slack variables is very rare, and has not been made in this work.

ii. for it the first variation of U^{**}, vanishes for any variation of the orientation and position of the base pairs and for any variation of the slack variables, $v_\imath$ i.e.,

$$\delta U^{**} = 0 = \delta U^* - \sum_{\imath=1}^{N_c} \chi_\imath \, \delta \mathcal{D}^{m_\imath n_\imath}, \tag{2.56}$$

where $\delta \mathcal{D}^{m_\imath n_\imath}$, the variation of $\mathcal{D}^{m_\imath n_\imath}$, is given by

$$\delta \mathcal{D}^{m_\imath n_\imath} = \frac{\partial \tilde{\mathcal{D}}}{\partial x_k^{m_\imath}} \delta x_k^{m_\imath} + \frac{\partial \tilde{\mathcal{D}}}{\partial x_k^{m_\imath+1}} \delta x_k^{m_\imath+1} + \frac{\partial \tilde{\mathcal{D}}}{\partial x_k^{n_\imath}} \delta x_k^{n_\imath} + \frac{\partial \tilde{\mathcal{D}}}{\partial x_k^{n_\imath+1}} \delta x_k^{n^\imath+1}, \tag{2.57}$$

and $\partial U^{**} / \partial v_\imath = 0$ which when combined with (2.54) yields

$$\chi_\imath (\mathcal{D}^{m_\imath n_\imath} - \mathcal{D}) = 0, \qquad \imath = 1, 2, ..., N_c; \tag{2.58}$$

iii. the lagrange multipliers, $\chi_\imath$, associated with it (by satisfying equation (2.56)) are non-negative,

$$\chi_\imath \geq 0, \quad \imath = 1, 2, ..., N_c; \tag{2.59}$$

iv. for any pair of base-pair steps, $\{m, n\}$, that is not in the list $\{m_\imath, n_\imath\}$, $\imath = 1, 2, ..., N_c$, and for which $n \geq m+20$ the inequality constraint $\mathcal{D}^{mn} > \mathcal{D}_o$ is obeyed.

Equations (2.56), (2.58), and (2.59) comprise the "Kuhn-Tucker necessary conditions" [12] as are applied to the present problem. Hence, in accord with their theory [26], at a configuration $^\mu \alpha$ which gives an extremum value to the total energy, U, under the given constraints, there must exist lagrange multipliers, $\tau_1, \tau_2, \tau_3, P_1, P_2, P_3$, and $\chi_1, \chi_2, ..., \chi_{N_c}$, such that the equations (2.56), (2.58), and (2.59) are satisfied.

In the reminder of this section, the equations of mechanical equilibrium for DNA molecules with self contact are derived from equation (2.56). As the equations of mechanical equilibrium for DNA molecules that are free of self contact were derived (from the first variation of U^*) in Section (2.4), it is sufficient to address the second part of equation (2.56) by expressing the variations of the distances $\mathcal{D}^{m_\imath n_\imath}$ in terms of

---

[12]See e.g., [24], [25].

variations of the μN kinematical variables. This is done by expressing the quantities $\delta x_k^{m_i}, \delta x_k^{m_i+1}, \delta x_k^{n_i}, \delta x_k^{n_i+1}$ in terms of the explicit formula given by equation (2.20), and recollecting the terms in a similar way to that shown in details in the previous section. If one follows these steps one finds that the following revision should be made to the constitutive equation (2.39a) [13] when the pairs of base-pair steps $\{m_i, n_i\}$ are in contact:

$$\mathbf{h}^n = -\sum_{m=1}^{N} \mathbf{g}^m - \mathbf{P} + \sum_{i=1}^{N_c} (u_{m_i}^n \mathbf{V}^{m_i} + u_{m_i+1}^n \mathbf{V}^{m_i+1} + u_{n_i}^n \mathbf{V}^{n_i} + u_{n_i+1}^n \mathbf{V}^{n_i+1}), \quad (2.60)$$

where the discrete step function, u_m^n, is defined here by,

$$u_m^n = \begin{cases} 1 & \text{if } n < m \\ 0 & \text{if } n \geq m, \end{cases} \quad (2.61)$$

and the resultant contact forces $\mathbf{V}^{m_i}, \mathbf{V}^{m_i+1}, \mathbf{V}^{n_i}$, and $\mathbf{V}^{n_i+1}$ exerted on base pairs m_i, m_i+1, n_i, and n_i+1 respectively are given by

$$\mathbf{V}^{m_i} = \chi_i \frac{\partial \tilde{\mathcal{D}}}{\partial x_k^{m_i}} \mathbf{d}_k^1, \qquad \mathbf{V}^{m_i+1} = \chi_i \frac{\partial \tilde{\mathcal{D}}}{\partial x_k^{m_i+1}} \mathbf{d}_k^1,$$
$$\mathbf{V}^{n_i} = \chi_i \frac{\partial \tilde{\mathcal{D}}}{\partial x_k^{n_i}} \mathbf{d}_k^1, \qquad \mathbf{V}^{n_i+1} = \chi_i \frac{\partial \tilde{\mathcal{D}}}{\partial x_k^{n_i+1}} \mathbf{d}_k^1. \quad (2.62)$$

Equations (2.60) and (2.61) imply the important relation,

$$\mathbf{h}^n - \mathbf{h}^{n-1} = -\mathbf{g}^n - \sum_{i=1}^{N_c} (\delta_{m_i}^n \mathbf{V}^{m_i} + \delta_{m_i+1}^n \mathbf{V}^{m_i+1} + \delta_{n_i}^n \mathbf{V}^{n_i} + \delta_{n_i+1}^n \mathbf{V}^{n_i+1}), \quad (2.63)$$

in which δ_m^n is a generalized kronecker delta defined by

$$\delta_m^n = \begin{cases} 1 & \text{if } n = m, \\ 0 & \text{if } n \neq m. \end{cases} \quad (2.64)$$

Thus as follows from equations (2.41), equation (2.63) permits one to rewrite the equations of balance of forces (2.42) for the more general case in which contact forces are

---

[13]Notice that the revised constitutive relation affects equation (2.39b).

taken into account,

$$\mathbf{f}^1 + \mathbf{g}^1 + \mathbf{P} + \delta^1_{m_\iota} \mathbf{V}^{m_\iota} = \mathbf{0} \tag{2.65a}$$

$$\mathbf{f}^n - \mathbf{f}^{n-1} + \mathbf{g}^n + \sum_{\iota=1}^{N_c} (\delta^n_{m_\iota} \mathbf{V}^{m_\iota} + \delta^n_{m_{\iota+1}} \mathbf{V}^{m_{\iota+1}} +$$

$$\delta^n_{n_\iota} \mathbf{V}^{n_\iota} + \delta^n_{n_{\iota+1}} \mathbf{V}^{n_{\iota+1}}) = \mathbf{0}, \quad n = 2, 3, ..., N, \tag{2.65b}$$

$$-\mathbf{f}^N + \mathbf{g}^{N+1} - \mathbf{P} + \delta^{N+1}_{n_\iota+1} \mathbf{V}^{n_\iota+1} = \mathbf{0}. \tag{2.65c}$$

For the derivation of the constitutive relation (2.60), two relations, which are valid as identities for any configuration, were used,

$$\mathbf{V}^{m_\iota} + \mathbf{V}^{m_{\iota+1}} + \mathbf{V}^{n_\iota} + \mathbf{V}^{n_{\iota+1}} = \mathbf{0}, \tag{2.66}$$

and

$$\mathbf{x}^{m_\iota} \times \mathbf{V}^{m_\iota} + \mathbf{x}^{m_{\iota+1}} \times \mathbf{V}^{m_{\iota+1}} + \mathbf{x}^{n_\iota} \times \mathbf{V}^{n_\iota} + \mathbf{x}^{n_{\iota+1}} \times \mathbf{V}^{n_{\iota+1}} = \mathbf{0}. \tag{2.67}$$

As analogous to the electrostatic energy function, $\check{\Phi}$, which yields the identities (2.36) and (2.37), the above identities are consequence of the properties of the function $\hat{\mathcal{D}}$ and are valid for each of the cases given in equation (2.52) .

Chapter 3

The computation of equilibrium configurations

In this chapter a detailed description of the computational procedure that was used to calculate equilibrium configurations is outlined. The procedure cannot be presented precisely without stating explicitly the energy functions that has been used throughout this work. In Section 3.1, an explicit formulation of the elastic and electrostatic energy is given. However, the theory that is discussed throughout this work is applicable for any other choice of the form of the total energy, as long as it is in accord with Section 2.2. In Section 3.2 the numerical scheme for the computation of equilibrium configurations is described.

3.1 The assumed energy functions

The elastic energy is assumed to be a quadratic form in the excess tilt $\Delta\theta_1^n$, the excess roll $\Delta\theta_2^n$, the excess twist $\Delta\theta_3^n$, and, for the most general case in which $\mu = 6$, also in the excess shift $\Delta\rho_1^n$, the excess slide $\Delta\rho_2^n$, and the excess rise $\Delta\rho_3^n$. These quantities are defined so that

$$\theta_i^n = {}_{\rm o}\theta_i^n + \Delta\theta_i^n, \qquad \rho_{\rm i}^{\rm n} = {}_{\rm o}\rho_i^n + \Delta\rho_i^n, \tag{3.1}$$

where ${}_{\rm o}\theta_i^n$ and ${}_{\rm o}\rho_i^n$ are intrinsic values, i.e., values appropriate to a stress free state of the n-th base-pair step. Therefore, when none of the 6 kinematical numbers is fixed ($\mu = 6$),

$$\psi^n = \frac{1}{2}F_{ij}^n\Delta\theta_i^n\Delta\theta_j^n + G_{ij}^n\Delta\theta_i^n\Delta\rho_j^n + \frac{1}{2}H_{ij}^n\Delta\rho_i^n\Delta\rho_j^n, \tag{3.2}$$

and when the three displacement parameters $\rho_1^n, \rho_2^n, \rho_3^n$ are fixed ($\mu = 3$),

$$\psi^n = \frac{1}{2} F_{ij}^n \Delta\theta_i^n \Delta\theta_j^n. \tag{3.3}$$

The elastic moduli, $F_{ij}^n = F_{ji}^n$, G_{ij}^n, and $H_{ij}^n = H_{ji}^n$, and the intrinsic parameters are constants that depend on the nucleotide composition of the n-th and $(n+1)$-th base pairs.[1] In the theory of elasticity the moduli F_{11}^n and F_{22}^n are commonly referred to as the local coefficients of rigidity for bending and the modulus F_{33}^n as the corresponding coefficient for twisting. In the same manner, the modulus H_{33}^n is associated with the (Young's) tensile modulus, where the moduli H_{11}^n and H_{22}^n are associated with the elastic shear modulus. All other 15 moduli are associated with the coupling of the 6 modes of deformation which here are consequences of variations of the tilt, roll, twist, shift, slide, and rise.

Under the assumption that the elastic energy associated with a base-pair step depends solely on the relative orientation and displacement of the two base pairs comprising it, a Taylor expansion of the local energy in the vicinity of the stress-free state of a base-pair step, at which the first variation of the (local) elastic energy vanishes, yields a quadratic energy function of the form (3.2) that is valid for small values of $\Delta\theta_i^n$, and $\Delta\rho_i^n$.

The observation (made in Section 2.1) to the essence of a change in the choice of the direction of increasing n, which leaves θ_2^n, θ_3^n, ρ_2^n, and ρ_3^n invariant but changes the sign of θ_1^n and ρ_1^n here places restrictions only on the moduli associated with coupling tilt or shift with roll, twist, slide and rise, namely, F_{12}^n, F_{13}^n, G_{12}^n, G_{13}^n, G_{21}^n, G_{31}^n, H_{12}^n, and H_{13}^n. A thorough discussion on that effect is given in [1]. Implications of cases of coupling are presented in [27].

For the electrostatic energy calculation, a form of Manning's theory of charge condensation [28], which is in accord with equations (2.23) and (2.24), is employed. The

---

[1]In the present work it is assumed that the elastic moduli and intrinsic parameters are completely determined by the nucleotide composition of the n-th base pair, and hence are independent of the composition of other base pairs. However, the general theory and computational procedure discussed here do not require such an assumption.

energy resulting from the electrostatic interaction between the charge associated with the n-th base pair and the charge associated with the m-th base pair is taken to be, [2]

$$\varphi^{nm} = \frac{q^2}{4\pi\epsilon_0\epsilon_{\mathrm{w}}} e^{-\kappa x^{nm}} / x^{nm}, \qquad (3.4)$$

where x^{nm} is as in (2.25), ϵ_0 the permittivity of free space, and ϵ_{w} the dielectric constant of water. In accord with Manning's theory [28] [29], q is set equal to 24% of the charge of the two phosphate groups associated with each base pair, i.e., $q = 2 \times 0.24\mathrm{e}^-$, where e^- is the charge of an electron. It is further assumed that (2.26) holds, i.e., nearest neighbors are omitted when employing (2.23) for the calculation of ϕ^n. An insertion of the equation (3.4) to (2.35) and (2.34) yields the following expression for $\mathbf{g}^n$, the total electrostatic force acting on the n-th base pair,

$$\mathbf{g}^n = \sum_{\substack{m \neq n \\ m \neq n \pm 1}} \varphi^{nm} \left(\frac{1}{x^{nm}} + \kappa \right) \frac{\mathbf{x}^n - \mathbf{x}^m}{x^{nm}}. \qquad (3.5)$$

As for the cases discussed in the present work the DNA is assumed to be in a solution of water and monovalent salt (e.g., Nacl) of concentration c, the Debye screening parameter κ is given by the formula

$$\kappa = 0.329\sqrt{c}, \qquad (3.6)$$

in which c is measured in units of moles per liter and κ in units of $\mathring{\mathrm{A}}^{-1}$.

As was remarked in [9], the electrostatic energy as taken in the present work rest upon the assumption that the two negative charges associated with each base pair are located at the barycenter of that base pair. In fact, each negative charge belongs to a phosphate group that is, in general, at the surface of the DNA double helix and not at its center. Nevertheless, according to Manning's charge condensation theory, it is reasonable to expect that the net charge is not localized at definite site but, as a result of rapid fluctuations of counter ions in a cylindrical region around the molecule, it is

---

[2]See also the discussion of Westcott et al. [11]

distributed along the molecule such that this assumption does not introduce a serious error.

Throughout the rest of this work an emphasis is given to the influence of the salt concentration c on equilibrium configurations. As indicated by equations (3.6), (3.4), and (3.5) high values of c (greater than 1M) give rise to an almost vanishing intramolecular repulsive forces, while relatively low values of c result significant intramolecular forces, which, in general, bring the molecule's equilibrium configuration to a more extended shape, with a higher value of the distance of closest approach, $\mathcal{D}_{\mathrm{ca}}$.

3.2   The numerical scheme

The sensitivity of equilibrium configurations to c will be investigated thoroughly by calculating equilibrium configurations for a large range of values of c. An equilibrium configuration, $^{\mu}\boldsymbol{\alpha}$, is a solution of the system (2.45), in which the force vectors $\mathbf{h}^{n}$ are in accord with equation (2.39a) when the molecule is free of contact or with equation (2.60) when the molecule is subject to self contact forces, and which obeys 6 end conditions together with the impenetrability condition (2.47). Thus, for a given c, for given kinematical end conditions of the form (2.28), and for a general case of N_{c} (possible) contact points, the system $\mathcal{S}$ can be written as:

$$
\underline{\boldsymbol{\Omega}} = \underline{\tilde{\boldsymbol{\Omega}}}(^{\mu}\underline{\boldsymbol{\alpha}}) =
\begin{bmatrix}
^{\mu}\boldsymbol{\Omega} \\
\boldsymbol{\Upsilon} \\
\boldsymbol{\Lambda}
\end{bmatrix}
= \mathbf{0},
\tag{3.7}
$$

where the (column) vector $^{\mu}\underline{\boldsymbol{\alpha}}$ includes all the unknown variables, i.e.,

$$
^{\mu}\underline{\boldsymbol{\alpha}} = \left[^{\mu}\boldsymbol{\alpha}, \tau_1, \tau_2, \tau_3, P_1, P_2, P_3, \chi_1, \chi_2, ..., \chi_{N_{\mathrm{c}}} \right]^{T},
\tag{3.8}
$$

and the components of $\mathbf{\Upsilon}$ and $\mathbf{\Lambda}$ describe quantities which, when vanishing, yield satisfaction of (2.28) and (2.58), i.e.,

$$\Upsilon_a = \begin{cases} \zeta_a - {}_0\zeta_a, & a = 1, 2, 3, \\ \ell_k - {}_0\ell_k, & k = a - 3, \quad a = 4, 5, 6, \end{cases} \tag{3.9}$$

and

$$\Lambda_\imath = \chi_\imath(\mathcal{D}^{m_\imath n_\imath} - \mathcal{D}), \quad \imath = 1, 2, ..., N_{\mathrm{c}}. \tag{3.10}$$

The system, $\mathcal{S}$, of the $\mu N + 6 + N_{\mathrm{c}}$ (scalar) nonlinear equations given in (3.7), would clearly be reduced in its size when the molecule is assumed to be free of self contact, in which case $N_{\mathrm{c}} = 0$, and the vector $\mathbf{\Lambda}$ must be omitted from (3.7). The vector ${}^\mu\underline{\alpha}$ must also be reduced in its size accordingly, as no Lagrange multiplier associated with contact points needs to be determined. Furthermore, in the case of mechanical end conditions given in the form of equations (2.46), the vector $\mathbf{\Upsilon}$ must be omitted from (3.7), and as the external force $\mathbf{P}$ and the external moment $\mathbf{T}$ are pre-specified, the list of (now known) variables $(\tau_1, \tau_2, \tau_3, P_1, P_2, P_3)$ should be excluded from the list comprising ${}^\mu\underline{\alpha}$. In the following discussions, it should be clear that the vector $\underline{\mathbf{\Omega}}$, the vector ${}^\mu\underline{\alpha}$, and the equations (3.7) have a form appropriate to the specific end conditions and to the ($\acute{a}$ priori) assumption with regard to the (possible) existence of self contact. To keep the discussion as general as possible, the number of equations (and unknowns) is taken to be $\mu N + N_{\mathrm{e}} + N_{\mathrm{c}}$ with $N_{\mathrm{e}} = 6$ when the kinematical end conditions are applied and $N_{\mathrm{e}} = 0$ when the external moment and force are prespecified.

Suppose one seeks a solution in the vicinity of an initial guess, ${}_*^\mu\underline{\alpha}$, as, for example, is the case when a solution ${}_*\underline{\alpha}$ of (3.7) was calculated for a specified value of ${}_*c$, and a solution of (3.7) at a salt concentration c close to ${}_*c$ is sought. A Taylor expansion of the system $\mathcal{S}$ (of the nonlinear equations (3.7)) about ${}_*^\mu\underline{\alpha}$ yields [3]

$$\mathbf{0} = \tilde{\underline{\mathbf{\Omega}}}({}^\mu\underline{\alpha}) = \tilde{\underline{\mathbf{\Omega}}}({}_*^\mu\underline{\alpha} + \hat{\Delta}{}^\mu\underline{\alpha}) = \tilde{\underline{\mathbf{\Omega}}}({}_*^\mu\underline{\alpha}) + \nabla\tilde{\underline{\mathbf{\Omega}}}({}_*^\mu\underline{\alpha})[\hat{\Delta}{}^\mu\underline{\alpha}] + \mathrm{O}(\|\hat{\Delta}{}^\mu\underline{\alpha}\|^2), \tag{3.11}$$

---

[3]The configuration ${}_*^\mu\underline{\alpha}$ is no longer a solution of the system (3.7) as the system of equations should be solved for the value c of the salt concentration and not for ${}_*c$.

where $\nabla\tilde{\underline{\Omega}}(_*^\mu\underline{\alpha})$ is the gradient of the function $\underline{\tilde{\Omega}}(\cdot)$ evaluated at $_*^\mu\underline{\alpha}$ for a salt concentration c. The vector [4] $\hat{\Delta}^\mu\underline{\alpha}$ is the difference between the solution of the linearized problem and $_*^\mu\underline{\alpha}$, i.e., $\hat{\Delta}^\mu\underline{\alpha} = {}^\mu\underline{\alpha} - {}_*^\mu\underline{\alpha}$, and its norm is here taken to be the ∞-norm i.e.,

$$\|\hat{\Delta}^\mu\underline{\alpha}\| = \max_{\substack{\underline{n}=1,...,\mu N \\ j,k=1,2,3 \\ \imath=1,...,N_c}}(|{}^\mu\alpha_{\underline{n}} - {}_*^\mu\alpha_{\underline{n}}|, |\tau_j - {}_*\tau_j|, |P_k - {}_*P_k|, |\chi_\imath - {}_*\chi_\imath|). \tag{3.12}$$

The gradient of the system $\mathcal{S}$ is characterized by the $(\mu N+N_e+N_c)\times(\mu N+N_e+N_c)$ Jacobian matrix $\mathbf{J}$, with $N_e = 6$ in the case of kinematical end conditions and $N_e = 0$ in the case of mechanical end conditions. The matrix $\mathbf{J}$ is in general full as a consequence of the intramoleculr electrostatic interactions, and its entries are defined as follows:

$$J_{\underline{n}\,\underline{m}} = \frac{\partial\,{}^\mu\Omega_{\underline{n}}}{\partial\,{}^\mu\alpha_{\underline{m}}}, \quad \text{for } \underline{n}, \underline{m}= 1, ..., \mu N , \tag{3.13a}$$

$$J_{\underline{n}\,(\mu N+k)} = \frac{\partial\,{}^\mu\Omega_{\underline{n}}}{\partial\tau_k}, \quad \text{for } \underline{n}= 1, ..., \mu N, \quad k = 1, 2, 3, \tag{3.13b}$$

$$J_{\underline{n}\,(\mu N+3+k)} = \frac{\partial\,{}^\mu\Omega_{\underline{n}}}{\partial P_k}, \quad \text{for } \underline{n}= 1, ..., \mu N, \quad k = 1, 2, 3, \tag{3.13c}$$

$$J_{\underline{n}\,(\mu N+6+\imath)} = \frac{\partial\,{}^\mu\Omega_{\underline{n}}}{\partial\chi_\imath}, \quad \text{for } \underline{n}= 1, ..., \mu N, \quad \imath = 1, ..., N_c, \tag{3.13d}$$

$$J_{(\mu N+a)\,\underline{m}} = \frac{\partial\Upsilon_a}{\partial\,{}^\mu\alpha_{\underline{m}}}, \quad \text{for } \underline{m}= 1, ..., \mu N , \quad a = 1, ..., N_e, \tag{3.13e}$$

$$J_{(\mu N+a+\imath)\underline{m}} = \frac{\partial\Lambda_\imath}{\partial\,{}^\mu\alpha_{\underline{m}}}, \quad \text{for } \underline{m}= 1, ..., \mu N , \quad \imath = 1, ..., N_c, \tag{3.13f}$$

$$J_{(\mu N+N_e+\imath)(\mu N+N_e+\imath)} = \frac{\partial\Lambda_\imath}{\partial\chi_\imath}, \quad \text{for } \imath = 1, ..., N_c . \tag{3.13g}$$

$$J_{\underline{p}\,\underline{q}} = 0, \quad \text{for all other entries.} \tag{3.13h}$$

As the functions $\tilde{R}_{ij}$, $\tilde{D}_{ij}$, and $\tilde{\Gamma}_{ik}$ are available (see the Appendix), an explicit analytical expression of all the components of $\underline{\Omega}$ and $\mathbf{J}$ can be evaluated with the aid of the equations (2.1), (2.4), (2.17), (2.21), (2.23), (2.24), (2.39), (2.44), (2.52), (2.60), (3.1), (3.2), (3.4), (3.5), and (3.6). As such expressions are extremely long and complex, a computer code that collects the large number of algebraic terms in each functional

---

[4]The symbol $\hat{\Delta}$ in place of Δ is used to distinguish the components of $\hat{\Delta}^\mu\underline{\alpha}$ from the quantities $\Delta\theta_i^n$ in equation (3.1) that measure the departure of the kinematical variables form their intrinsic values.

component of $\underline{\mathbf{\Omega}}$ and $\mathbf{J}$ is used to efficiently compute an exact value of each of these components as a function of (the known) $_*^{\mu}\underline{\boldsymbol{\alpha}}$.

Thus, a numerical approximation for the computation of $\mathbf{J}$ is avoided, and a numerically stable Newton-Raphson scheme in which the following linear system, derived from equation (3.11) by an omission of the term $\mathrm{O}(\|\hat{\Delta}^{\mu}\underline{\boldsymbol{\alpha}}\|^2)$, is solved for $\hat{\Delta}^{\mu}\underline{\boldsymbol{\alpha}}$ in each iteration:

$$\hat{\Delta}^{\mu}\underline{\boldsymbol{\alpha}} = -\mathbf{J}^{-1}\tilde{\underline{\mathbf{\Omega}}}(_*^{\mu}\underline{\boldsymbol{\alpha}})\,. \tag{3.14}$$

In that efficient scheme the vector $_*^{\mu}\underline{\boldsymbol{\alpha}}$ is updated in each iteration in accord with,

$$_*^{\mu}\underline{\boldsymbol{\alpha}}^{\mathrm{new}} \;=\; _*^{\mu}\underline{\boldsymbol{\alpha}}^{\mathrm{old}} + \hat{\Delta}^{\mu}\underline{\boldsymbol{\alpha}}\,. \tag{3.15}$$

The iterative scheme is terminated when for the calculated $_*^{\mu}\underline{\boldsymbol{\alpha}}$ each of the components of $\tilde{\underline{\mathbf{\Omega}}}(_*^{\mu}\underline{\boldsymbol{\alpha}})$ has an absolute value less than ϵ. [5]

A procedure for generating an initial guess, $_*^{\mu}\underline{\boldsymbol{\alpha}}$ is commonly referred to as a *predictor*, and the procedure that uses the that initial guess as a starting point in an iterative scheme that yields a solution to the system $\mathcal{S}$ is called the *corrector*, see e.g., [30]. In accord with this terminology the Newton-Raphson scheme described in equations (3.14) and (3.15) is referred to as the corrector procedure, and it is used for all the examples that are given in this work.

---

[5]For all the calculations reported here, it was found that ϵ is within machine accuracy.

Chapter 4

Stability of equilibria

An equilibrium configuration, $^\mu\boldsymbol{\alpha}$, obeying the system $\mathcal{S}$ is here defined as *stable* if , for it, the second variation of the total energy is strictly positive for any admissible[1] non-zero variation (which is not associated with a rigid body motion) in the triads $\{(\mathbf{d}_1^1, \mathbf{d}_2^1, \mathbf{d}_3^1), (\mathbf{d}_1^2, \mathbf{d}_2^2, \mathbf{d}_3^2), ... (\mathbf{d}_1^{N+1}, \mathbf{d}_2^{N+1}, \mathbf{d}_3^{N+1})\}$, and, in the relative displacements of the base pairs, ρ_i^n. As will be discussed later in this chapter, in applications of the present theory, there are cases in which equilibrium configurations of DNA molecules have symmetries implying the existence of variations with neutral directions. When such variations are present they are excluded when the stability criterion is employed.

4.1   Variational statement II: the second variation of the energy

A variation, $^\mu\boldsymbol{\beta} \in \mathbb{R}^{\mu N+3}$, in the triads $(\mathbf{d}_1^m, \mathbf{d}_2^m, \mathbf{d}_3^m)$ and, for $\mu = 6$, in the relative displacements $(\rho_1^n, \rho_2^n, \rho_3^n)$, is defined here such that its components are given by,

$$^6\beta_{\underline{n}} = \boldsymbol{\gamma}^n \cdot \mathbf{d}_a^1, \quad \text{for } a= 1, 2, 3\,, \qquad ^6\beta_{\underline{n}} = \delta\bar\rho_{a-3}^n, \quad \text{for } a= 4, 5, 6\,, \quad (4.1a)$$

$$^3\beta_{\underline{n}} = \boldsymbol{\gamma}^n \cdot \mathbf{d}_a^1, \quad \text{for } a= 1, 2, 3\,, \qquad\qquad\qquad (4.1b)$$

$$^\mu\beta_{\mu N+k} = \boldsymbol{\gamma}^{N+1} \cdot \mathbf{d}_k^1, \quad \text{for } k= 1, 2, 3\,, \qquad\qquad (4.1c)$$

where $\underline{n} = a+(n-1)\mu$, $n = 1, ..., N$, and $\delta\bar\rho_k^n$ are the components of $\delta\mathbf{r}^n$ (see equation 2.39e) with respect to $(\mathbf{d}_1^1, \mathbf{d}_2^1, \mathbf{d}_3^1)$, i.e.,

$$\delta\bar\rho_k^n = Q_{kj}^n R_{ij}^n \delta\rho_i^n. \qquad\qquad (4.2)$$

---

[1]In the sense that the variation must not violate the end conditions and the impenetrability constraints, and be such that when $\mu < 6$, the $6 - \mu$ constant kinematical numbers associated with each base-pair step along the molecule would not be changed when employed.

Equations (2.40) in which the force vectors $\mathbf{h}^n$ are chosen in accord with the (á priori) assumption with regard to the (possible) existence of self contact, and the relation (4.1), permit one to write the first variation of the (modified) energy in the following form, [2]

$$\delta U^{\#} = \sum_{\underline{n}=1}^{\mu N+3} {}^{\mu}\Omega_{\underline{n}} \, {}^{\mu}\beta_{\underline{n}}, \tag{4.3}$$

where, for $k = 1, 2, 3$,

$$ {}^{\mu}\Omega_{\mu N+k} = -\mathbf{M}^{N+1} \cdot \mathbf{d}_k^1. \tag{4.4}$$

If one defines a $(\mu N + 3) \times (\mu N)$ matrix $\mathbf{J}^{\#}$ to be such that (i) its upper $(\mu N) \times (\mu N)$ sub-matrix has its entries as in equation (3.13a), i.e.,

$$J^{\#}_{\underline{n}\,\underline{m}} = J_{\underline{n}\,\underline{m}}, \quad \text{for } \underline{n}, \underline{m} = 1, ..., \mu N, \tag{4.5}$$

and (ii) its $3 \times \mu N$ lower sub-matrix has entries given by,

$$J^{\#}_{(\mu N+k)\underline{m}} = \frac{\partial \, {}^{\mu}\Omega_{\mu N+k}}{\partial \, {}^{\mu}\alpha_{\underline{m}}}, \quad \text{for } \underline{m} = 1, ..., \mu N, \quad k = 1, 2, 3, \tag{4.6}$$

one can write for the second variation of the modified energy in equilibrium (obeying equations (3.7)),

$$\delta^2 U^{\#} = \sum_{\underline{n}=1}^{\mu N+3} \sum_{\underline{m}=1}^{\mu N} J^{\#}_{\underline{n}\,\underline{m}} \delta^{\mu}\alpha_{\underline{m}} \, {}^{\mu}\beta_{\underline{n}} = {}^{\mu}\boldsymbol{\beta}^T \mathbf{J}^{\#} \delta^{\mu}\boldsymbol{\alpha}, \tag{4.7}$$

where the components of $\delta^{\mu}\boldsymbol{\alpha}$ are variations in the kinematical variables, i.e., for $\mu = 6$, $(\delta^{\mu}\alpha_1 = \delta\theta_1^1, \, \delta^{\mu}\alpha_2 = \delta\theta_2^1, \, \delta^{\mu}\alpha_3 = \delta\theta_3^1, \, \delta^{\mu}\alpha_4 = \delta\rho_1^1, \, ..., \delta^{\mu}\alpha_{6N} = \delta\rho_3^N)$, and, for $\mu = 3$, $(\delta^{\mu}\alpha_1 = \delta\theta_1^1, \, \delta^{\mu}\alpha_2 = \delta\theta_2^1, \, \delta^{\mu}\alpha_3 = \delta\theta_3^1, \, \delta^{\mu}\alpha_4 = \delta\theta_1^2, \, ..., \delta^{\mu}\alpha_{3N} = \delta\theta_3^N)$.

The relation (2.13) between a variation in the triads $(\mathbf{d}_1^{n+1}, \mathbf{d}_2^{n+1}, \mathbf{d}_3^{n+1})$ and $(\mathbf{d}_1^n, \mathbf{d}_2^n, \mathbf{d}_3^n)$ and a variation in the kinematical variables $(\theta_1^n, \theta_2^n, \theta_3^n)$ and the relation (4.2) can be used to construct a linear transformation, ${}^{\mu}\mathbf{V} : \mathbb{R}^{\mu N+3} \to \mathbb{R}^{\mu N}$ that takes the vector ${}^{\mu}\boldsymbol{\beta}$ into the vector $\delta^{\mu}\boldsymbol{\alpha}$, i.e.,

$$\delta^{\mu}\boldsymbol{\alpha} = {}^{\mu}\mathbf{V} \, {}^{\mu}\boldsymbol{\beta}. \tag{4.8}$$

---

[2]The symbol "#" should be replaced by "**" if self contact occurs or by "*" if the molecule is free of self contact.

This transformation is essential for the expression of $\delta U^{\#}$ as a quadratic form characterized by a symmetric matrix. For the case in which $\mu = 6$ the $(6N) \times (6N + 3)$ matrix $^{6}\mathbf{V}$ has the following structure:

$$
\begin{bmatrix}
-\mathbf{\Gamma}^{1^T}\mathbf{Q}^{1^T} & \mathbf{O} & \mathbf{\Gamma}^{1^T}\mathbf{Q}^{1^T} & \mathbf{O} & \mathbf{O} & \cdots & \mathbf{O} & \mathbf{O} & \mathbf{O} \\
\mathbf{O} & \bar{\mathbf{I}}^{1} & \mathbf{O} & \mathbf{O} & \mathbf{O} & \cdots & \mathbf{O} & \mathbf{O} & \mathbf{O} \\
\mathbf{O} & \mathbf{O} & -\mathbf{\Gamma}^{2^T}\mathbf{Q}^{2^T} & \mathbf{O} & \mathbf{\Gamma}^{2^T}\mathbf{Q}^{2^T} & \cdots & \mathbf{O} & \mathbf{O} & \mathbf{O} \\
\mathbf{O} & \mathbf{O} & \mathbf{O} & \bar{\mathbf{I}}^{2} & \mathbf{O} & \cdots & \mathbf{O} & \mathbf{O} & \mathbf{O} \\
\vdots & & & & \ddots & & & & \vdots \\
\mathbf{O} & \mathbf{O} & \cdots & & & \mathbf{O} & -\mathbf{\Gamma}^{N^T}\mathbf{Q}^{N^T} & \mathbf{O} & \mathbf{\Gamma}^{N^T}\mathbf{Q}^{N^T} \\
\mathbf{O} & \mathbf{O} & \cdots & & & & \mathbf{O} & \bar{\mathbf{I}}^{N} & \mathbf{O}
\end{bmatrix}
\tag{4.9}
$$

For the case in which $\mu = 3$ the $3N \times (3N + 3)$ matrix $^{3}\mathbf{V}$ is constructed as follows:

$$
\begin{bmatrix}
-\mathbf{\Gamma}^{1^T}\mathbf{Q}^{1^T} & \mathbf{\Gamma}^{1^T}\mathbf{Q}^{1^T} & \mathbf{O} & \mathbf{O} & \cdots & \mathbf{O} \\
\mathbf{O} & -\mathbf{\Gamma}^{2^T}\mathbf{Q}^{2^T} & \mathbf{\Gamma}^{2^T}\mathbf{Q}^{2^T} & \mathbf{O} & \cdots & \mathbf{O} \\
\vdots & & \ddots & \ddots & & \vdots \\
\mathbf{O} & \mathbf{O} & \cdots & \mathbf{O} & -\mathbf{\Gamma}^{N^T}\mathbf{Q}^{N^T} & \mathbf{\Gamma}^{N^T}\mathbf{Q}^{N^T}
\end{bmatrix}
\tag{4.10}
$$

Each entry in the above matrices is a 3×3 matrix. The components of the (orthogonal transformation) matrix $\bar{\mathbf{I}}^{n}$ are given by

$$
\bar{I}_{ki}^{n} = R_{kp}^{n} Q_{ip}^{n},
\tag{4.11}
$$

$\mathbf{O}$ is a matrix which all of its components are zero, and the matrices $\mathbf{\Gamma}^{n}$ and $\mathbf{Q}^{n}$ are as in (2.14) and (2.4). The second variation $\delta^{2} U^{\#}$ can now be written as a quadratic form in $^{\mu}\boldsymbol{\beta}$, i.e.,

$$
\delta^{2} U^{\#} = {}^{\mu}\boldsymbol{\beta}^{T} \mathbf{S} \, {}^{\mu}\boldsymbol{\beta},
\tag{4.12}
$$

which is characterized by the $(\mu N + 3) \times (\mu N + 3)$ symmetric matrix,

$$
\mathbf{S} = \mathbf{J}^{\#} \, {}^{\mu}\mathbf{V}.
\tag{4.13}
$$

The calculation of the matrices $\mathbf{J}^\#$ and $^\mu\mathbf{V}$ is not a computationally expensive matter, as their entries are calculated when applying the computational scheme described in Section (3), see e.g., equation (4.5). Thus, the numerical scheme that is employed here for the calculation of an equilibrium configuration, provides all the necessary data for the stability analysis of the calculated equilibrium configuration.

Equation (4.12) describes the change in energy as a result of any free variation $^\mu\boldsymbol{\beta}$ from an equilibrium configuration. However, an equilibrium configuration is stable if, for it, $\delta^2 U^\#$ is positive for any admissible variation. Hence, when (4.12) is employed, only variations for which the end conditions and the impenetrability condition are obeyed should be considered. The matrix $\mathbf{S}$ is appropriate for stability analysis when the mechanical end conditions (2.46) are imposed, and the molecule is free of self contact, because such end conditions do not impose restrictions on variations from equilibrium.

4.2   Filtering non-admissible variations

In this section a modification of the symmetric matrix $\mathbf{S}$, characterizing the second variation $\delta^2 U^\#$ is discussed. The objective is to derive a linear transformation $\mathbb{R}^{\mu N+3} \to \mathbb{R}^{\mu N+3}$ which takes any variation to its projection on the hyperplane spanned by all admissible variations, and which can be calculated with small computational cost.

The theory is specified for the general case in which the equilibrium configuration has contact points and obeys the $N_\mathrm{e} = 6$ kinematical end conditions (2.28). As mentioned above, if the equilibrium configuration is free of self contact, and the end conditions are in accord with (2.46), no modification of the symmetric matrix $\mathbf{S}$ is necessary. To keep the discussion general, suppose that the equilibrium configuration that was calculated has N_d points of contact, between the pairs of base-pair step $\{m_\jmath, n_\jmath\}$, $\jmath = 1, 2, ..., N_\mathrm{d}$, such that

$$\mathcal{D}^{m_\jmath n_\jmath} = \mathcal{D}_\mathrm{o}, \quad \jmath = 1, ..., N_\mathrm{d} \,. \tag{4.14}$$

In the present work an admissible variation is defined to be such that, for it, equation (4.14) must hold, and the end conditions are obeyed. This definition is adequate as, because $\chi_{J} > 0$ for $J = 1, ..., N_{\mathrm{d}}$, variations which result an increase in the value of the distance between pairs of base-pair steps, that are in contact when the configuration is in equilibrium, yield an increase in U^* and therefore can be excluded when stability is examined. Accordingly, an admissible configuration must obey the relations,

$$\delta \Upsilon_a = \sum_{\underline{m}=1}^{\mu N} \frac{\partial \Upsilon_a}{\partial \,^{\mu}\alpha_{\underline{m}}} \delta^{\mu}\alpha_{\underline{m}} = \mathbf{W}_a \, \delta^{\mu}\boldsymbol{\alpha} = 0, \quad \text{for} \ \ a = 1, ..., N_{\mathrm{e}}, \tag{4.15a}$$

$$\delta \mathcal{D}^{m_J n_J} = \sum_{\underline{m}=1}^{\mu N} \frac{\partial \mathcal{D}^{m_J n_J}}{\partial \,^{\mu}\alpha_{\underline{m}}} \delta^{\mu}\alpha_{\underline{m}} = \mathbf{W}_{J+N_{\mathrm{e}}} \, \delta^{\mu}\boldsymbol{\alpha} = 0, \quad \text{for} \ \ J = 1, ..., N_{\mathrm{d}}. \tag{4.15b}$$

By setting the $(N_{\mathrm{e}}+N_{\mathrm{d}}) \times \mu N$ matrix [3] $\mathbf{W}$ to be of the form,

$$\mathbf{W} = \begin{bmatrix} \mathbf{W}_1 \\ \mathbf{W}_2 \\ \vdots \\ \mathbf{W}_{N_{\mathrm{e}}+N_{\mathrm{d}}} \end{bmatrix}, \tag{4.16}$$

and using the relations (4.8), equations (4.15) can be written in the form,

$$\mathbf{W} \,^{\mu}\mathbf{V} \,^{\mu}\boldsymbol{\beta} = 0. \tag{4.17}$$

Equation (4.17) implies that the rows of the $(N_{\mathrm{d}}+N_{\mathrm{e}}) \times \mu N+3$ matrix $\mathbf{W} \,^{\mu}\mathbf{V}$ span a space which is orthogonal to every admissible variation. Suppose now that the $(N_{\mathrm{d}}+N_{\mathrm{e}}) \times (\mu N+3)$ matrix $\hat{\mathbf{W}}$ has rows that constitute an orthonormal basis to that space. [4] With such a matrix in hand, a general variation $^{\mu}\bar{\boldsymbol{\beta}}$ can be transformed into an admissible variation, $^{\mu}\boldsymbol{\beta}$, by subtracting from it its projection onto the space spanned by the row vectors of $\hat{\mathbf{W}}$, i.e.,

$$^{\mu}\boldsymbol{\beta} = (\bar{\mathbf{I}} - \hat{\mathbf{W}}^T \hat{\mathbf{W}})^{\mu}\bar{\boldsymbol{\beta}}, \tag{4.18}$$

---

[3] As was mentioned previously $N_{\mathrm{e}} = 6$ for the kinematical end conditions (2.28) and $N_{\mathrm{e}} = 0$ for the mechanical end conditions (2.46).

[4] Such orthogonalization can be performed numerically by using the familiar Modified Gram-Schmidt algorithm. See e.g., [31].

where $\bar{\mathbf{I}}$ is the $(\mu N + 3) \times (\mu N + 3)$ identity matrix. A substitution of equation (4.18) into equation (4.12) yields,

$$\delta^2 U^\# = {}^\mu \vec{\boldsymbol{\beta}}^T \, \bar{\mathbf{S}} \, {}^\mu \bar{\boldsymbol{\beta}}, \tag{4.19}$$

where the $(\mu N + 3) \times (\mu N + 3)$ modified symmetric matrix $\bar{\mathbf{S}}$ is given by,

$$\bar{\mathbf{S}} = (\bar{\mathbf{I}} - \hat{\mathbf{W}}^T \hat{\mathbf{W}}) \, \mathbf{S} \, (\bar{\mathbf{I}} - \hat{\mathbf{W}}^T \hat{\mathbf{W}}). \tag{4.20}$$

4.3 Stability criterion

The matrix $\bar{\mathbf{S}}$ characterizes the second variation of the energy, $\delta^2 U^\#$, with no restriction on the choice of variation. Its rank is smaller than the rank of $\mathbf{S}$ by the dimension of $\hat{\mathbf{W}}$, which is equal to the number of active constraints. For the case in which the equilibrium configuration has N_d points of contact,

$$\text{rank}(\bar{\mathbf{S}}) = \text{rank}(\mathbf{S}) - N_e - N_d. \tag{4.21}$$

A non-zero variation of the configuration, when expressed in terms of the components of ${}^\mu \boldsymbol{\beta} \in \mathbb{R}^{\mu N + 3}$, can result a pure rigid body rotation.[5] As the total energy of the molecule is invariant under rigid body motion, the symmetric matrix $\mathbf{S}$ must have 3 proper numbers that are always zero. Moreover, equation (4.21) implies that $\bar{\mathbf{S}}$ has additional $N_e + N_d$ zero proper numbers. Thus, when the proper numbers of $\bar{\mathbf{S}}$ which are not identically zero are placed in a sequence $(\lambda_1, \lambda_2, ..., \lambda_{\mu N - N_e - N_d})$ with $\lambda_1 \leq \lambda_2 \leq ... \leq \lambda_{\mu N - N_e - N_d}$, the equilibrium configuration under consideration is stable if and only if λ_1 is strictly positive .

Although the number of non-identically zero proper numbers is, in general, $\mu N - N_e - N_d$, it can be reduced when the configuration has symmetries that yield neutral variations. For example, when the DNA molecule is assumed to be intrinsically straight and transversely isotropic, and it is closed to form a ring, an eversion mode of

---

[5]When a variation is expressed in terms of ${}^\mu \boldsymbol{\alpha} \in \mathbb{R}^{\mu N}$, a pure rigid body rotation can be described only by a zero variation.

motion, in which every base pair is rotated about the vector $\mathbf{d}_3^n$, that is normal to it, such that θ_3^n and $\sqrt{(\theta_1^n)^2 + (\theta_2^n)^2}$, for $n = 1, ..., N$, remain constant, is associated with a neutral variation as it preserves the total energy.

4.4   Continuation methods

The numerical scheme that was introduced in Section 3.2 permits one to calculate equilibrium configurations as the parameter c is varying along an equilibrium path. In that scheme the predictor procedure is simply the use of a known solution of $\mathcal{S}$ at a salt concentration $_*c$ as the initial guess for the calculation of a solution of $\mathcal{S}$ at c close to $_*c$. A method in which a predictor procedure is followed by a corrector procedure to generate solutions on a branch of equilibrium configurations is often called a *continuation* method.

While using a continuation method to follow a branch of equilibria one may reach a configuration $_s^\mu\boldsymbol{\alpha}$ at which the matrix $\bar{\mathbf{S}}$ has at least one (non-identically zero) proper number that is vanishing. The vanishing of one (or more) of the proper numbers of $\bar{\mathbf{S}}$ is a consequence of a local singularity of the Jacobian matrix $\mathbf{J}$ (see equations (3.13) and (3.14)) at a singular point. Such a singular point is either a *turning point* of a *fold* or a *bifurcation point*. The local singularity violets the uniqueness of solution of (3.14) and, as will be shown in the next chapters, yields (symmetry-breaking) pitchfork bifurcations or folds.

Along an equilibrium path, with c the independent variable, an admissible (non-zero) variation $\delta^\mu\boldsymbol{\alpha} = {}^\mu\mathbf{V}\,{}^\mu\boldsymbol{\beta}$ from $({}^\mu\boldsymbol{\alpha}, c)$ to $({}^\mu\boldsymbol{\alpha} + \delta^\mu\boldsymbol{\alpha}, c + \delta c)$ for which $\underline{\tilde{\Omega}}({}^\mu\boldsymbol{\alpha}) = \underline{\tilde{\Omega}}({}^\mu\boldsymbol{\alpha} + \delta^\mu\boldsymbol{\alpha}) = 0$ obeys, to a first order approximation, the relation [6]

$$\mathbf{S}\,{}^\mu\boldsymbol{\beta} + {}^\mu\mathbf{V}^T\,\mathbf{W}^T\,\delta\boldsymbol{\nu} + {}^\mu\boldsymbol{\omega}\delta c = \mathbf{0}, \tag{4.22}$$

---

[6]The first term on the left side of equation (4.22) is implied by equations (4.8) and (4.13). The second term on the left is implied by equations (4.15) and (4.16).

where the components of the vector ${}^{\mu}\boldsymbol{\omega}$ in $\mathbb{R}^{\mu N+3}$ are given by,

$$
{}^{\mu}\omega_{\underline{n}} = \frac{\partial^{\mu}\tilde{\Omega}_{\underline{n}}}{\partial c}, \qquad n = 1, ..., \mu N+3, \tag{4.23}
$$

and the components of $\delta\boldsymbol{\nu}$ are the variations of the Lagrange multipliers associated with the (active) constraints, i.e., $(\delta\nu_1 = \delta\tau_1, \delta\nu_2 = \delta\tau_2, \delta\nu_3 = \delta\tau_3, \delta\nu_4 = \delta P_1, \delta\nu_5 = \delta P_2,$ $\delta\nu_6 = \delta P_3, \delta\nu_7 = \delta\chi_1, ..., \delta\nu_{N_e+N_d} = \delta\chi_{N_e})$.

As was discussed in the previous section, the columns of the matrix ${}^{\mu}\mathbf{V}^{T}\,\mathbf{W}^{T}$ span the space of non-admissible variations. With this in mind, the following relation that is based on (4.22) is implied by equations (4.8), (4.18), and (4.20):

$$
\bar{\mathbf{S}}\,{}^{\mu}\boldsymbol{\beta} + (\bar{\mathbf{I}} - \hat{\mathbf{W}}^{T}\hat{\mathbf{W}})\,{}^{\mu}\boldsymbol{\omega}\delta c = \mathbf{0}. \tag{4.24}
$$

Suppose $({}^{\mu}_{s}\boldsymbol{\alpha}, {}_{s}c)$ is a singular point and the proper numbers of $\bar{\mathbf{S}}$ at $({}^{\mu}_{s}\boldsymbol{\alpha}, {}_{s}c)$ are $(\lambda_1^{R}, \lambda_2^{R}, \lambda_3^{R}, \lambda_1^{c}, ..., \lambda_{N_e+N_d}^{c}, \lambda_1, \lambda_2, ..., \lambda_{\mu N-N_e-N_d})$, where $\lambda_i^{R} \equiv 0$ for $i = 1, 2, 3$, are the proper numbers associated with rigid body rotation, and $\lambda_z^{c} \equiv 0$, for $z = 1, ..., N_e+N_d$, are the proper numbers associated with the active constraints. As at a singular point at least one of the non-identically zero proper numbers is vanishing, it is further assumed that $\lambda_{\underline{q}}$ is the only non-identically zero proper number that is vanishing at $({}^{\mu}_{s}\boldsymbol{\alpha}, {}_{s}c)$.[7] The orthonormal characteristic vectors associated with each of the $\mu N+3$ proper numbers of $\bar{\mathbf{S}}$ are given in the following list, $(\mathbf{y}_1^{R}, \mathbf{y}_2^{R}, \mathbf{y}_3^{R}, \mathbf{y}_1^{c}, ..., \mathbf{y}_{N_e+N_d}^{c}, \mathbf{y}_1, \mathbf{y}_2, ..., \mathbf{y}_{\mu N-3-N_e-N_d})$.

The vectors ${}^{\mu}\boldsymbol{\beta}$ and ${}^{\mu}\boldsymbol{\omega}$ can be expressed as linear combinations of the characteristic vectors, i.e.,

$$
{}^{\mu}\boldsymbol{\beta} = \sum_{\underline{p}=1}^{\mu N-N_e-N_d} b_{\underline{p}}\mathbf{y}_{\underline{p}}, \tag{4.25}
$$

and

$$
{}^{\mu}\boldsymbol{\omega} = \sum_{i=1}^{3} a_i^{R}\mathbf{y}_i^{R} + \sum_{z=1}^{N_e+N_d} a_z^{c}\mathbf{y}_z^{c} + \sum_{\underline{p}=1}^{\mu N-N_e-N_d} a_{\underline{p}}\mathbf{y}_{\underline{p}}, \tag{4.26}
$$

---

[7]For simplicity, in the present discussion, it is assumed that the characteristic space of $\bar{\mathbf{S}}$ corresponding to a vanishing proper number $\lambda_{\underline{q}}$ is unidimensional, however the same arguments hold for the case in which the vanishing proper numbers are degenerate.

The determination of the type of a singular point $({}^{\mu}_{s}\boldsymbol{\alpha}, {}_{s}c)$ relies on the subspace containing the vector ${}^{\mu}\boldsymbol{\omega}$. If in equation (4.26) the components $a_{\underline{p}}$ are such that,

$$a_{\underline{p}} = 0, \ \text{for} \ \underline{p} \neq \underline{q}, \tag{4.27}$$

i.e., ${}^{\mu}\boldsymbol{\omega} \in \text{Null}(\bar{\mathbf{S}})$, then any possible solution of equation (4.24) is of the form,

$$ {}^{\mu}\boldsymbol{\beta} = b_{\underline{q}}\mathbf{y}_{\underline{q}}, \qquad \delta c = 0, \tag{4.28}$$

that represents the turning point of a fold.[8] If, on the other hand, the components $a_{\underline{p}}$ of ${}^{\mu}$ with respect to the characteristic vectors are such that

$$a_{\underline{q}} = 0, \qquad (\text{with} \ \lambda_{\underline{q}} = 0), \tag{4.29}$$

then the components $a_{\underline{p}}$ of a solutions of (4.24) are given by,

$$b_{\underline{p}} = a_{\underline{p}}\delta c/\lambda_{\underline{p}}, \ \text{for} \ \underline{p} \neq \underline{q}, \tag{4.30}$$

and with $b_{\underline{q}}$ undetermined. In this case the choice of $b_{\underline{q}} = 0$ is associated with a variation along the original branch, while a nonzero value of $b_{\underline{q}}$ is associated with a branch that either originates at the bifurcation point or crosses the original branch. In a similar way, the variations of the Lagrange multipliers, i.e., the components of $\delta\boldsymbol{\nu}$, can be determined from the components $a_{\underline{z}}^{c}$ of ${}^{\mu}\boldsymbol{\omega}$ with respect to the characteristic vectors $\mathbf{y}_{\underline{z}}^{c}$ (that are associated with non-admissible variations) using equation (4.22).

Thus, an initial guess that may yield a solution point $({}^{\mu}\boldsymbol{\alpha}, c)$ on the issuing branch is taken to be,

$$ {}^{\mu}_{\text{p}}\boldsymbol{\alpha} = {}^{\mu}_{\#}\boldsymbol{\alpha} + {}^{\mu}\mathbf{V}[b_{\#} \, \mathbf{y}_{\underline{q}}], \tag{4.31}$$

where the solution point in the original branch $({}^{\mu}_{\#}\boldsymbol{\alpha}, c)$ is in a close neighborhood to the bifurcation point $({}^{\mu}_{s}\boldsymbol{\alpha}, {}_{s}c)$. A reasonable value of $b_{\#}$ can be generated by successive adjustments, such that a solution point on the issuing branch would be the result of the corrector procedure described in chapter 3 with ${}^{\mu}_{\text{p}}\boldsymbol{\alpha}$ as the initial guess.

---

[8]A discussion on the determination and calculation of turning points is given in [32]

Clearly in the vicinity of a turning point of a fold one cannot set a step in c and calculate for it the equilibrium configuration as described in chapter 3. A more elaborated predictor procedure must be used so that both the initial guess, and the value of c will be estimated in a way that would allow to follow the folding branch. A numerical procedure that was developed specifically for the work presented here makes use of three previously calculated equilibrium configurations, ${}^{\mu}\boldsymbol{\alpha}_0$, ${}^{\mu}\boldsymbol{\alpha}_1$, ${}^{\mu}\boldsymbol{\alpha}_2$, at salt concentration values, c_0, c_1, c_2, for the calculation of the next initial guess ${}^{\mu}_{p}\boldsymbol{\alpha}$ and the next salt concentration c_3. [9] At first an arc-length parameter, σ, is calculated for each of the three equilibrium configurations such that,

$$\sigma_{\rm o} = 0, \qquad \sigma_1 = \|{}^{\mu}\boldsymbol{\alpha}_1 - {}^{\mu}\boldsymbol{\alpha}_0\|^{1/2}, \qquad \sigma_2 = \|{}^{\mu}\boldsymbol{\alpha}_2 - {}^{\mu}\boldsymbol{\alpha}_1\|^{1/2}, \tag{4.32}$$

where the norm is taken to be the (Euclidian) L^2-norm in $\mathbb{R}^{\mu N}$. The parameter σ is then treated as the independent variable, and the salt concentration, $c_3 = c_2 + \Delta c$, for the next configuration in the branch is calculated at $\sigma_3 = \sigma_2 + \Delta \sigma$, as a second order extrapolation,

$$c_3 = \tilde{a}_1(c_0, c_1, c_2) \left(\frac{\sigma_3}{\sigma_2}\right)^2 + \tilde{a}_2(c_0, c_1, c_2)\frac{\sigma_3}{\sigma_2} + \tilde{a}_3(c_0), \tag{4.33}$$

where the functions $\tilde{a}_1$, $\tilde{a}_2$, and $\tilde{a}_3$ for the coefficients of the quadratic polynomial are given by the relations, [10]

$$\tilde{a}_1(b_0, b_1, b_2) = \frac{b_0(1 - \vartheta) - b_1 + b_2\vartheta}{(1 - \vartheta)\vartheta}, \tag{4.34a}$$

$$\tilde{a}_2(b_0, b_1, b_2) = \frac{-b_0(1 - \vartheta^2) + b_1 + b_2\vartheta^2}{(1 - \vartheta)\vartheta}, \tag{4.34b}$$

$$\tilde{a}_3(b_0) = b_0, \tag{4.34c}$$

with $\vartheta = \sigma_1/\sigma_2$. In the same way each of the kinematical variables, ${}^{\mu}_{p}\alpha_{\underline{n}}$, in the (initial guess) configuration ${}^{\mu}_{p}\boldsymbol{\alpha}$ (and each of the unknown Lagrange multipliers) is extrapolated

---

[9]The method relies on the theory behind pseudo-arclength continuation methods, see e.g., [30].

[10]The variables b_0, b_1, and b_2, are used here only to show the form of the functions $\tilde{a}_1$, $\tilde{a}_2$, and $\tilde{a}_3$. They should be distinguished from similar variables that were used along the present work.

by substituting the corresponding component of ${}^{\mu}\underline{\boldsymbol{\alpha}}_0$, ${}^{\mu}\underline{\boldsymbol{\alpha}}_1$, ${}^{\mu}\underline{\boldsymbol{\alpha}}_2$, in place of c_0, c_1, and c_2 in equation (4.33). The step-length $\Delta\sigma$ is readjusted in accord with the local behavior of the branch.

Chapter 5

The dependence of equilibrium configurations of open DNA molecules on the salt concentration

In this chapter computational results illustrating the strong dependence on c of open equilibrium configurations of three *open molecules* are thoroughly reported. An open molecule is defined here as a molecule with an axial curve that is not a closed curve and with its two ends free of external moments and forces. Accordingly, the end conditions for an open molecule are,

$$\mathbf{T=0}, \qquad \mathbf{P=0}. \tag{5.1}$$

All three molecules are assumed to be transversely isotropic in the sense that: (a) their intrinsic shift and slide are zero, and their rise is 3.4Å,

$$_o\rho_1^n = 0, \quad _o\rho_2^n = 0, \quad _o\rho_3^n = 3.4\text{Å}, \tag{5.2}$$

for $n = 1, ..., N$; and (b) the moduli F_{11}^n and F_{22}^n, for tilt and roll (as in equation (3.2) or (3.3)) are equal, and there is no coupling between any pair of different modes of deformation, i.e.,

$$F_{11}^n = F_{22}^n, \quad F_{12}^n = F_{13}^n = F_{23}^n = H_{12}^n = H_{13}^n = F_{23}^n = 0, \text{ and } \quad G_{ij}^n = 0, \tag{5.3}$$

for $n = 1, ..., N$.

A DNA molecule with intrinsic twist close to that of a DNA, which approximately forms a circle in its stress free configuration, cannot be constructed with the intrinsic kinematical parameters the same at each base-pair step, as in such case the (constant) twist and bend will yield a helical shape and not a circle. However, a molecule with

a constant twist $_o\theta_3^n = 2\pi L_k/N_o$, with L_k its *linking number*, [1] and intrinsic curvature such that N_o base pairs form a perfect and complete circle [2] can be constructed by introducing the angles ξ^n and ω^n such that, [3]

$$\xi^n = \sqrt{(\theta_1^n)^2 + (\theta_2^n)^2}, \qquad \theta_1^n = \xi^n \cos(\omega^n), \qquad \theta_2^n = \xi^n \sin(\omega^n), \qquad (5.4)$$

and setting the molecule's intrinsic values $_o\xi^n$ and $_o\omega^n$ to be,

$$_o\xi^n = \frac{2\pi}{N_o}, \qquad _o\omega^n = \frac{2\pi}{N_o} L_k(n - 1/2), \qquad \text{for } n = 1, ..., N. \qquad (5.5)$$

In other words, the intrinsic kinematical parameters for such a molecule are given by,

$$_o\theta_1^n = \frac{2\pi}{N_o} \sin(\frac{2\pi L_k}{N_o}(n - 1/2)), \quad _o\theta_2^n = \frac{2\pi}{N_o} \cos(\frac{2\pi L_k}{N_o}(n - 1/2)), \qquad (5.6)$$

with $n = 1, ..., N$, and (5.2).

A molecule for which the relations (5.6), and (5.2) are obeyed would be perfectly planar in its intrinsic configuration, but would also have a strong dependence of $_o\theta_1^n$ and $_o\theta_2^n$ on n with both parameters attaining positive and negative values, which is not in accord with the presently estimated values.[4] A theoretic construction of a more realistic intrinsically curved molecule was suggested in reference [1]. The molecule treated there was composed of repetitions of 10 base pair segments in which 5 base-pairs form a homogeneous, intrinsically straight subsegment and the remaining 5 form a homogeneous, intrinsically curved subsegment. By an appropriate adjustment of $_o\theta_2^n$ (or $_o\theta_1^n$) and $_o\theta_3^n$ of the curved subsegments one can control the intrinsic curvature and the number of base pairs that would give a closed, circular, stress-free configuration.

---

[1]The linking number is a topologically invariant quantity which is an integer. In applications of closed DNA its value equals to the number of times the two strands of the molecule are linked together. For a precise mathematical definition see [33] and [34].

[2]For a complete circle the 1-st and (N+1)-th base pairs coincide. A configuration is said to be a perfect circle or a ring if for it the barycenters of the base pairs lie on a circle, i.e., its piecewise linear axial curve, $\mathcal{C}$, is a planar polygon of N equal sides.

[3]The geometric meaning of the angles ξ^n and ω^n is described in details in the Appendix. See also the reference [8] in which these angles were introduced.

[4]Statistical analysis of X-ray structure data [35] indicates that, in general, $_o\theta_1^n$ is approximately zero and $_o\theta_2^n$ is not negative.

5.1 Intrinsically curved molecules with 300 base pairs

As a first example a study was performed on the dependence of equilibrium configurations of two DNA molecules with 300 base pairs (i.e., $N = 299$) on the salt concentration c. The intrinsic curvature was taken to be such that 150 base pairs subsegment would form a complete circle when stress-free (i.e., in its intrinsic configuration). In a stress-free state the DNA molecules under consideration would have an axial curve made of a doubly wound (planar) circle, however, because the molecule cannot penetrate itself, that stress-free configuration is not physically attainable. A homogeneous molecule labeled $\mathcal{H}300$ and a periodic molecule labeled $\mathcal{P}300$ were considered. For both molecules the transverse isotropy conditions (a) and (b) are met. A transversely isotropic molecule obeying the relations (5.6) has equilibrium configurations with axial curve and mechanical behavior identical to those of a homogenous molecule with

$$_o\theta_1^n = 0, \quad _o\theta_2^n = \frac{2\pi}{N_o}, \quad _o\theta_3^n = 0, \qquad n = 1, ..., N, \tag{5.7}$$

and hence the simple case of a homogenous molecule $\mathcal{H}300$ that has parameters as in (5.7) with $_o\theta_2^n = 2.4^o$ ($N_o = 150$) and $N = 299$ was investigated.

The molecule $\mathcal{P}300$, treated here, is made of 30 repetitions of 10 base-pair subsegments. As in reference [1] for the first 5 base-pair steps in each subsegment,

$$_o\theta_1^n = 0, \qquad _o\theta_2^n = 0, \qquad _o\theta_3^n = 36^o, \tag{5.8a}$$

and for the remaining 5

$$_o\theta_1^n = 0, \qquad _o\theta_2^n = 7.413^o, \qquad _o\theta_3^n = 35.568^o. \tag{5.8b}$$

For the molecule $\mathcal{H}300$ the translational parameters are assumed to be fixed ($\mu = 3$), while for $\mathcal{P}300$ they are variable and do not necessarily remain at their intrinsic values ($\mu = 6$). The intrinsic translational parameters for both molecules are taken to be as in (5.2). The elastic moduli for both molecules are as in (5.3), and with

$$F_{11}^n = F_{22}^n = 0.0427 \, k_B \, T/\deg^2, \quad F_{33}^n = 1.05 F_{11}^n, \tag{5.9}$$

for $n = 1, ..., N$. In equation (5.9) k_B is the Boltzmann constant, and T is the temperature which for all cases studied in the present work was taken to be $300\,\mathrm{K}$. It was further assumed that the elastic moduli associated with the displacement variables for the molecule $\mathcal{P}300$, (with ($\mu = 6$)) are sufficiently large to suppress significant departures from the intrinsic values of the parameters $({}_\mathrm{o}\rho_1^n,\ {}_\mathrm{o}\rho_2^n,\ {}_\mathrm{o}\rho_3^n)$. Thus,

$$H_{11}^n = H_{22}^n = H_{33}^n = 50\,k_\mathrm{B}\,T/\mathrm{\AA}^2. \tag{5.10}$$

It is worthwhile to mention that, for a given value of c, the total energy, U, associated with a configuration, ${}^3\alpha_\mathrm{tw}$, of a molecule with a constant non-zero intrinsic twist constructed as in (5.6) with all its other properties identical to those of $\mathcal{H}300$, is equal to the energy of $\mathcal{H}300$ in a configuration ${}^3\alpha$, whenever ${}^3\alpha_\mathrm{tw}$ is related to ${}^3\alpha$ by the transformation,

$$\theta_1^n \mapsto ({}_\mathrm{o}\xi^n + \Delta\xi^n)\sin({}_\mathrm{o}\omega^n + \Delta\omega^n),$$
$$\theta_2^n \mapsto ({}_\mathrm{o}\xi^n + \Delta\xi^n)\cos({}_\mathrm{o}\omega^n + \Delta\omega^n), \tag{5.11}$$
$$\theta_3^n \mapsto \theta_3^n + \Delta\theta^n,$$

where $\Delta\xi^n$, $\Delta\omega^n$, and $\Delta\theta^n$ are the excess values of the configuration ${}^3\alpha$ of $\mathcal{H}300$ (with its intrinsic configuration in accord with (5.7)), and where the values of ${}_\mathrm{o}\xi^n$ and ${}_\mathrm{o}\omega^n$ are as in (5.5). This assertion permits one to first calculate equilibrium configuration of homogeneous molecule that is in accord with (5.7), (5.2), and (5.3), and then, with a use of the transformation (5.11), calculate the equilibrium configuration for a molecule obeying (5.6).

There are two qualitative differences between the molecules $\mathcal{H}300$ and $\mathcal{P}300$: (I) A 150 base pair subsegment of $\mathcal{H}300$ has, when it is stress-free and closed, a perfectly circular configuration, while a 150 subsegment of $\mathcal{P}300$ has a circular configuration which is nearly, but not perfectly, planar when it is closed and, as a consequence of the way the curved subsegments are constructed, has a chiral structure.[5] (II) As oppose to

---

[5]The chirality of a closed curve is frequently measured in term of the writhe, $\mathcal{W}$. A precise definition of $\mathcal{W}$ is given in [36]. For the axial curve of a closed 150 base pair subsegment of $\mathcal{P}300$, $\mathcal{W} = 0.078$.

the homogenous molecule $\mathcal{H}300$ the molecule $\mathcal{P}300$ has a directionality: the 5 base-pair subsegment at one of its ends is intrinsically curved while that at the other end is straight.

As follows from equations (2.2) and (2.6), the axial curve $\mathcal{C}$ is a function of $^6\alpha$. A configuration with an axial curve, $\mathcal{C}'$, which is a mirror image of $\mathcal{C}$ can be constructed by employing the following transformation for $n = 1, ..., N$,

$$(\theta_1^n, \theta_2^n, \theta_3^n, \rho_1^n, \rho_2^n, \rho_3^n) \mapsto (-\theta_1^n, \theta_2^n, -\theta_3^n, \rho_1^n, -\rho_2^n, \rho_3^n). \qquad (5.12)$$

As was mentioned earlier[6] the choice of the end of an open molecule for which $n = 1$ is arbitrary. The two choices yield two configurations that are related by the transformation,

$$\begin{aligned}(\theta_1^n, \theta_2^n, \theta_3^n, \rho_1^n, \rho_2^n, \rho_3^n) \mapsto (&-\theta_1^{N-n+1}, \theta_2^{N-n+1}, \theta_3^{N-n+1}, \\ &-\rho_1^{N-n+1}, \rho_2^{N-n+1}, \rho_3^{N-n+1}).\end{aligned} \qquad (5.13)$$

Two configurations that are related by one of the transformations (5.12) and (5.13), or by any composition of the two, yield axial curves that can be mapped to each other by a length preserving unitary transformation, i.e., rotation and reflection transforation. As a result, (at a given c) the electrostatic energy, Φ, associated with a configuration remains unaltered when the configuration is transformed by (5.12) or (5.13). However, in general, as in the case of a periodic molecule, this assertion in not true for the elastic energy, Ψ, as when applying such transformations on a configuration of a molecule the excess values of the kinematical variables may be altered. Nevertheless, the value of the elastic energy of any configuration of a homogenous molecule that was constructed in accord with (5.3), (5.7), and (5.2) is indifference to such transformations. As a result, an equilibrium configuration, $^3\alpha$, of the molecule $\mathcal{H}300$ at a given c may represent a group of 1,2, or 4 equilibrium configurations that are congruent in the sense that they can be mapped to each other by (5.12) or (5.13).[7] For a molecule with these symmetries

---

[6]see the paragraph below Figure 2.1

[7]A configuration that is mapped into itself by these transformations is counted once as it is represented by a single point in $\mathbb{R}^{\mu N}$.

the system $\mathcal{S}$ of the equations (3.7) is said to be perfect [8] and as shown in Figure (5.1) yield pitchfork bifurcations from which new equilibrium paths are issuing as a result of symmetry breaking.

5.1.1 Bifurcations of equilibria of the molecule $\mathcal{H}300$

A bifurcation diagram in which each point represents an equilibrium configuration of $\mathcal{H}300$ is shown in Figure 5.1. The smallest proper number, λ_1, of the matrix $\mathbf{S}$, is plotted as a function of c. At least one configuration on each branch is depicted next to its branch as a cylindrical tube of diameter $\mathcal{D}_o= 20\,\text{Å}$. For the range of c in Figure 5.1 equilibrium configurations of $\mathcal{H}300$ at 8 different values of c are shown in Figures 5.2, 5.3, 5.4, 5.5, 5.6, and 5.7. The configurations are labeled by their branch labels with numbers indicating the values of c in which these equilibria were calculated and are denoted by circles on the bifurcation diagram. As shown in the top of the figure the number 1 stands for $c= 1\,\text{M}$, the number 2 for $c= 5\times 10^{-1}\,\text{M}$ and so fourth. Each bifurcation point is denoted by the symbol "✘". The values of λ_1 in each of the branches in the diagram correspond to equilibrium configurations that were calculated under the assumption that the impenetrability constraint (2.47) is satisfied with no points of self contact. However, for each of the branches there exists a critical value c_c such that for $c>c_c$ self-contact forces must be taken into account for a satisfaction of (2.47). As a result of the discrete nature of the DNA under the present model, for the range of $c>c_c$, the graph of λ_1 versus c suffers severe discontinuities when self-contact is taken into account, and although equilibrium configurations with self contact were calculated at values of $c>c_c$ for each of the branches, only the revised values of λ_1 corresponding to the configurations with self contact that are shown in Figures 5.3, 5.4, 5.5, 5.6, and 5.7 are depicted in the diagram with dotted arrows pointing from the values that correspond to the contact-free configurations (with self-penetration) to the values (indicated

---

[8]In the sense in which the term is used in reference [37]

by '*') that correspond to equilibrium configurations with self contact.

As a result of the perfectness of the system $\mathcal{S}$ (for the molecule $\mathcal{H}300$) all the branches that are shown in Figure 5.1 are connected. The computation of a connected bifurcation diagram requires a starting equilibrium configuration at a given c. All other equilibria can then be calculated using the continuation methods described in Section 4.4 . For the present example the existence of equilibrium configuration with an approximately helical axial curve was assumed. The first equilibrium configuration was computed by constructing an intrinsically helical molecule with $_o\theta_3^n > 0$ and all other properties identical to those of $\mathcal{H}300$ such that, as oppose to the molecule $\mathcal{H}300$, the intrinsically helical molecule would be able to attain its intrinsic configuration without penetrating itself when stress free. Having such a hypothetical molecule in hand, one can set the initial guess at high value of c to be the molecule's intrinsic configuration and calculate equilibrium configurations along a branch of solutions (at constant c) with $_o\theta_3^n$ the varying parameter that is gradually decreased toward zero. Using an initial guess that was derived in that way helical equilibrium configurations in the branch labeled H were calculated and found to be the global minimizers of the total energy U. For values of c less than $1.25\,\text{M}$ the configurations on H have a nearly helical axial curve with a pitch greater than $20\,\text{Å}$, and hence in the range of c shown in Figure 5.1 these configurations do not have self contact. Seven helical configurations in a range of interest to experimenters [9] are shown in Figure 5.2. A significant increase in both the pitch and the radius of the helical configurations as the value of c is decreasing demonstrates the remarkable influence of salt concentration on the (globally) stable equilibrium configurations of $\mathcal{H}300$.

Each branch in the bifurcation diagrams shown in the present work is a two dimensional representation of a curve in $\mathbb{R}^{3N} \times \mathbb{R}$. Each point on that curve corresponds to a single solution $(^3\boldsymbol{\alpha},\ c)$. However, a point in the (two dimensional) bifurcation diagram shown in Figure 5.1 may represent 1, 2, or 4 solutions that correspond to different

---

[9]DNA is known to denature when c is less than $10^{-3}\,\text{M}$.
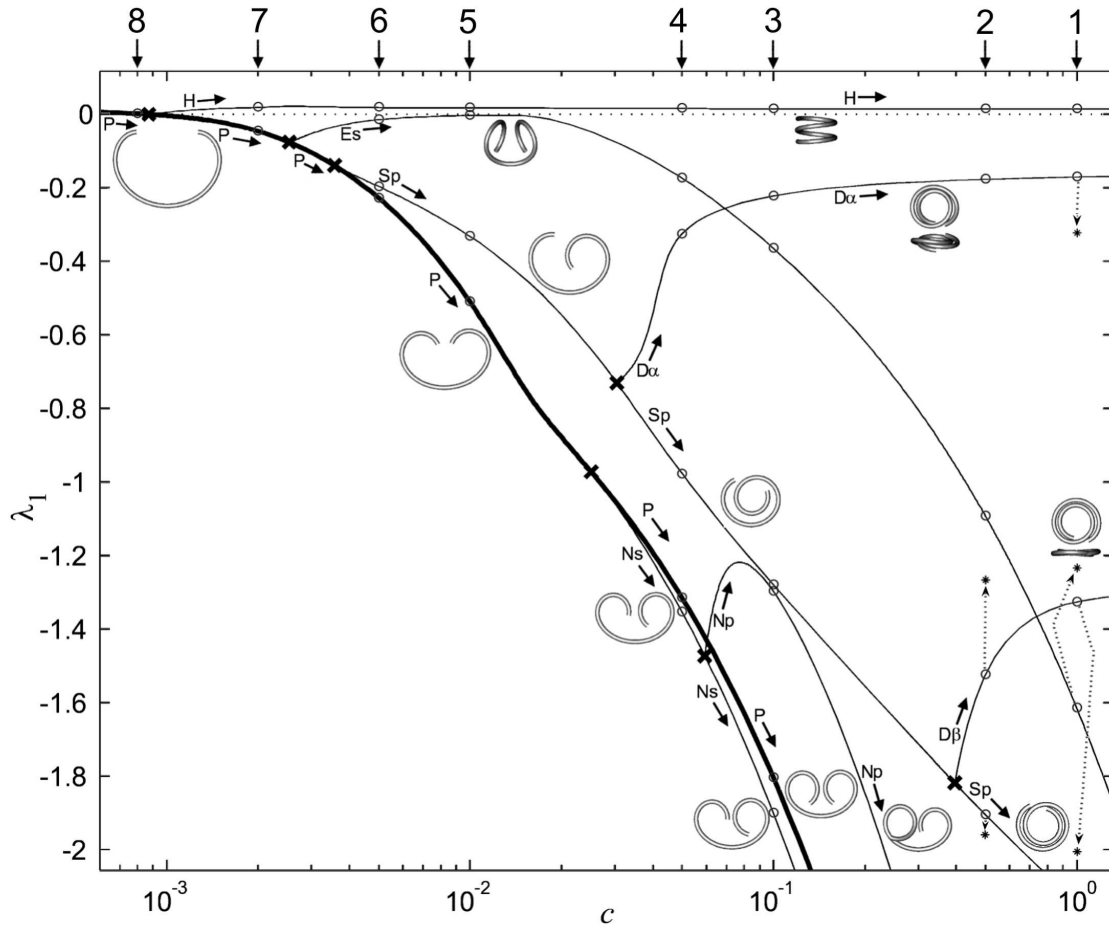
Figure 5.1: A bifurcation diagram for equilibrium configurations of the 300 base pair homogeneous DNA molecule labeled $\mathcal{H}300$. The diagram is presented as a graph of λ_1, the smallest proper number of the matrix $\mathbf{S}$ of equation (4.13), versus the salt concentration c. The configurations with $\lambda_1 > 0$, i.e., configurations along the primary branch H and configurations along the part of the branch P that is above the horizontal dotted line ($\lambda_1 = 0$) are (globally) stable. The symbol "✗" indicates a bifurcation point. The stem branch P is drawn in boldface, and all the other branches are drawn in lightface. Small circles denote configurations shown in Figures 5.2, 5.3, 5.4, 5.5, 5.6, and 5.7. These configurations are labeled by the lower case letters indicating their branch and by a number 1, 2, 3, 4, 5, 6, 7, or 8 pointing (with a vertical arrow) to the value of c at which the configuration was calculated, e.g., the helical equilibrium configurations on branch H at $c = 1$M and $c = 5 \times 10^{-1}$M are denoted by the small circles at the topmost right corner and are labeled "h1" and "h2". At least one configuration is depicted to illustrate the shape of configurations along the branch in its proximity. Arrows with dotted lines point to the values of λ_1 when contact forces are taken into account.
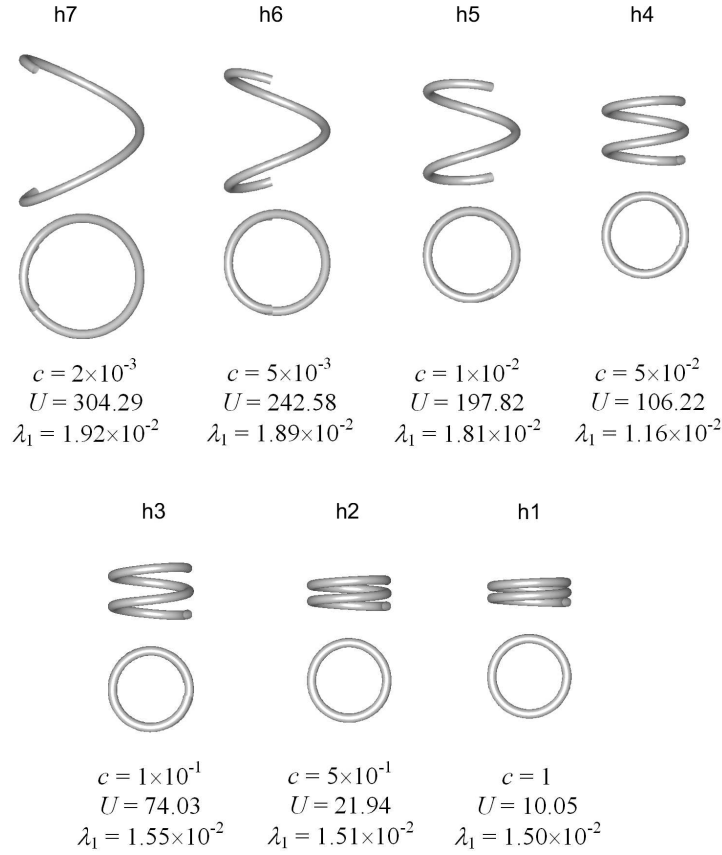
Figure 5.2: Seven helical equilibrium configurations of the 300 base pair homogeneous molecule $\mathcal{H}300$ that are in the branch H. Every configuration on H is a global minimizer of the total energy U. The line of view for the upper drawing is perpendicular to an axis of a cylinder that is optimally fitted, using a uniquely derived nonlinear least square scheme, to the 300 data points along the axial curve of the molecule. The line of view for the lower drawing is along that axis. The scale of length is the same for each case. The salt concentration, c, is expressed in moles per liter. The smallest proper number of $\mathbf{S}$, λ_1, and the total energy, U, are given in units of $k_B T$ with $T = 300K$.

points in $\mathbb{R}^{3N} \times \mathbb{R}$. Each point in the branch H of (nearly) helical equilibrium configurations represents two helical configurations with opposite chirality that are related by the transformation given in (5.12). On the other hand, when applied on a configuration in the branch H, the transformation (5.13) would map the configuration into itself. The point on the continuous curve of solutions $(^3\alpha, c)$ that connects the branch of right handed to the branch of left handed helical configurations is a bifurcation point that is represented by the point $(c = 8.69 \times 10^{-4}, \lambda_1 = 0)$ in the bifurcation diagram. As follows from (5.12), this bifurcation point corresponds to a planar configuration with

$\theta_1^n = \theta_3^n = 0$ for $n = 1, ..., 299$.[10] The branch H originates from this point at a pitch-fork bifurcation of a branch labeled P. Each point in P corresponds to a single planar equilibrium configuration, with zero excess tilt and zero excess twist. [11]

As for any value of $c \geq 0$ there exist a single equilibrium configuration in P, this branch is referred to as the *stem branch*. Each branch, such as the branch H, that originates from P is called a *primary branch*. A *secondary branch* is a branch that issues from a primary branch. Eight equilibrium configurations in the stem branch P are shown in Figure 5.3. For values of $c < 8.69 \times 10^{-4}$ the configurations in P are the global minimizers of U, and were found to be the only stable configurations in this range of c. As shown in the bifurcation diagram, the smallest proper number λ_1 associated with configurations in P is negative for $c > 8.69 \times 10^{-4}$, i.e., the configurations in this range of c are unstable, and the helical configurations in H are the only stable configurations.

The primary branch Es originates from a second bifurcation point, $(c = 2.55 \times 10^{-3}, \lambda_1 = -7.69 \times 10^{-2})$, in the branch P at which $\lambda_2 = 0$. For values of c greater than 2.55×10^{-3} M the proper number λ_2 for configurations in P is negative, while for configurations in Es λ_2 is positive. Six everted equilibrium configurations in the branch Es are shown in Figure 5.4. As c is increasing the equilibria in Es are such that the two (helical) subregions of the molecule approaches each other with a decreasing distance of closest approach. For values of c greater than $c_c = 5.1 \times 10^{-1}$ M the equilibrium configurations in Es posses self-contact. As illustrated in Figure 5.4 the two darkened base-pair steps in the configuration es1 are in contact.[12] Like the

---

[10]In general, it also follows that $\rho_2^n = 0$ but since for the molecule $\mathcal{H}300$ μ equals 3, the shift, slide and rise are fixed in their intrinsic values, and obey (5.2), that assertion holds for any configuration.

[11]Each planar equilibrium configuration of $\mathcal{H}300$ in P have symmetries implying that it is mapped into itself under both transformations (5.12) and (5.13).

[12]As oppose to a continuous rod with self contact in which a single point of contact occurs when two subsegments of the rod are approaching each other, it often happens that contact between two (very short) DNA subsegments involves multiple points of contact in a close proximity. In the discussion given in the present section such contact between two short subsegments is referred to as a contact point.
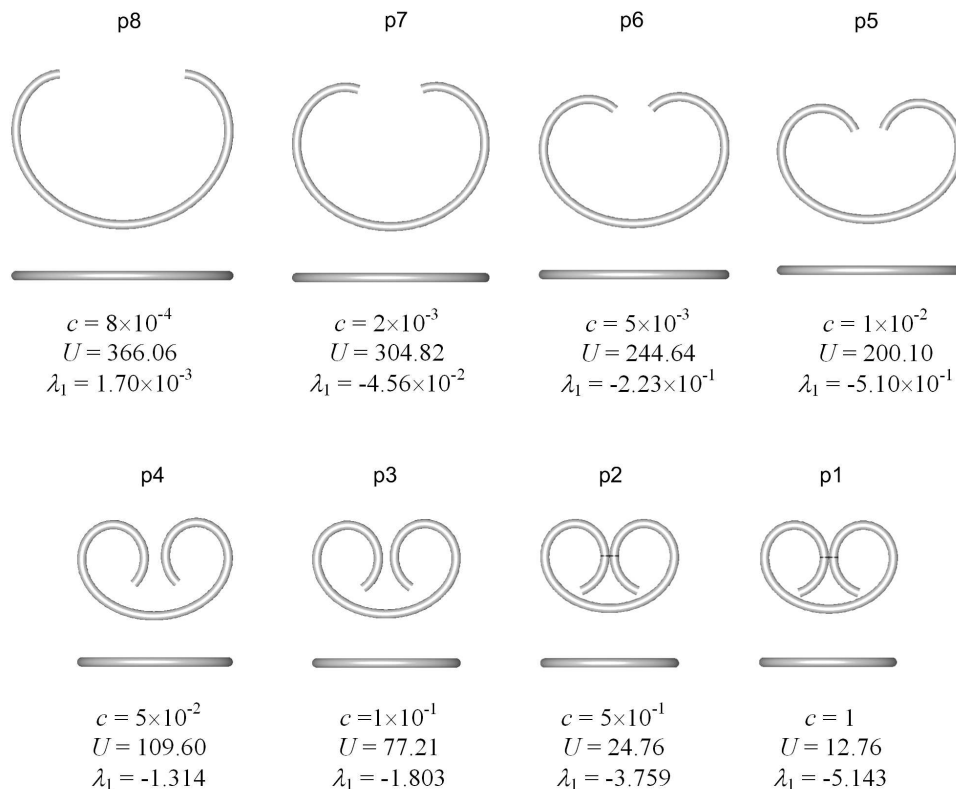
Figure 5.3: Eight equilibrium configurations of $\mathcal{H}300$ in the stem branch P. The configuration p8 is a global minimizer of U. The configurations p3, p4, p5, p6, and p7 are unstable. The configurations p1 and p2 have points of self contact, and the cylindrical surface that is associated with each of the base-pair steps that are in contact is darkened.

configurations in P, the configurations in Es are symmetric in the sense that the two halves of their axial curve are mirror images. These configurations are characterized by two approximately helical subregions of opposite handedness that are separated by a transition region. Configurations with similar geometry are often called "perversions". [13] In the present work configurations of that type are termed *everted helices* or everted configurations. As in any of the primary branches associated with the molecule $\mathcal{H}300$, each point in Es corresponds to two congruent equilibrium configurations. The symmetry of the configurations in Es implies that any of the transformations (5.12),

---

[13] In their study Domokos and Healy [38] have found such "perverted" equilibrium configurations of a (finite) homogenous intrinsically-curved elastic rod with zero intrinsic torsion that is subject to a tensile force acting along the line, ℓ, connecting the midpoints of its two ends. The two ends of the treated rod are clamped so that their cross sections are perpendicular to ℓ and are not permitted to rotate about ℓ.

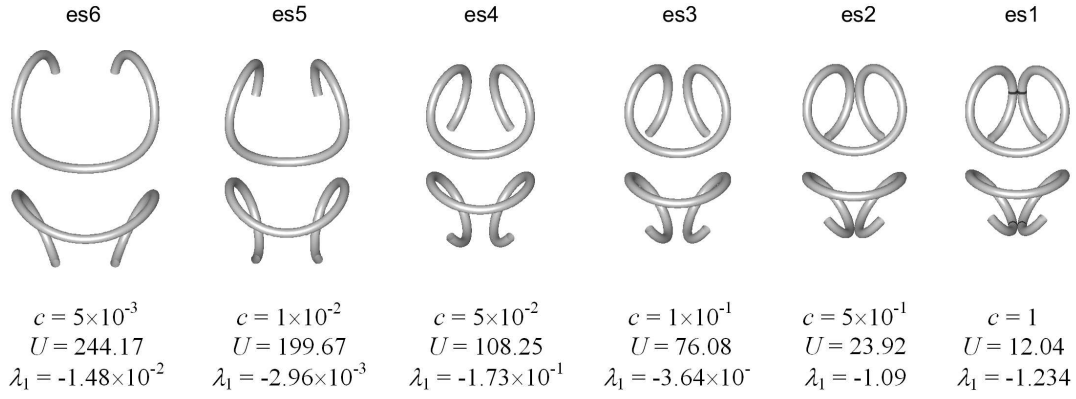| es6	es5	es4	es3	es2	es1
$c = 5 \times 10^{-3}$	$c = 1 \times 10^{-2}$	$c = 5 \times 10^{-2}$	$c = 1 \times 10^{-1}$	$c = 5 \times 10^{-1}$	$c = 1$
$U = 244.17$	$U = 199.67$	$U = 108.25$	$U = 76.08$	$U = 23.92$	$U = 12.04$
$\lambda_1 = -1.48 \times 10^{-2}$	$\lambda_1 = -2.96 \times 10^{-3}$	$\lambda_1 = -1.73 \times 10^{-1}$	$\lambda_1 = -3.64 \times 10^{-}$	$\lambda_1 = -1.09$	$\lambda_1 = -1.234$

Figure 5.4: Six equilibrium configurations of $\mathcal{H}300$ in the primary branch Es. All the configurations on this branch are unstable. The configuration es1 has a point of self contact.

and (5.13) would map an everted equilibrium configuration to its associated congruent configuration.[14] The bifurcation diagram in Figure 5.1 shows that, although all the points in Es lie in the region where λ_1 is negative, and hence the equilibrium configurations in Es are unstable, λ_1 as a function of c attains a maximum value that is very close to zero at $c = 1.23 \times 10^{-2}$ M. This behavior suggests that a minor change in the properties of the molecule may result a range of c in which stable everted equilibrium configurations exist. As discussed in the next section and in the study reported in [9], a DNA molecule with the same intrinsic and mechanical properties as $\mathcal{H}300$ but with 450 base pairs was found to have stable everted configurations.

As the value of c is increasing the branch P encounters a third bifurcation point, at $\left(c = 3.59 \times 10^{-3}, \lambda_1 = -1.41 \times 10^{-1}\right)$, that is a result of the vanishing of λ_3. The primary branch Sp (with $\lambda_3 > 0$) of spiral equilibrium configurations that are planar originates at this pitchfork bifurcation. Again, each point in the branch Sp corresponds to two congruent configurations. Each of the spiral configurations in Sp is mapped by the transformation (5.12) into itself , and by (5.13) to its congruent configuration. Six planar spiral configurations are shown in Figure 5.5 . For c greater than $c_c = 4.5 \times 10^{-1}$ M the spiral configurations have two points of contact: each of the molecule's ends is in

---

[14]A composite transformation of (5.12) and (5.13) would map an everted configuration into itself.

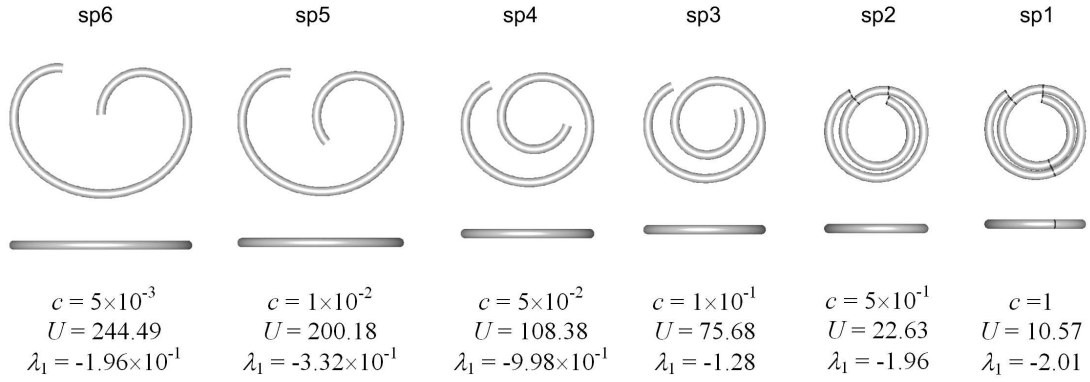| sp6	sp5	sp4	sp3	sp2	sp1
$c = 5\times10^{-3}$	$c = 1\times10^{-2}$	$c = 5\times10^{-2}$	$c = 1\times10^{-1}$	$c = 5\times10^{-1}$	$c = 1$
$U = 244.49$	$U = 200.18$	$U = 108.38$	$U = 75.68$	$U = 22.63$	$U = 10.57$
$\lambda_1 = -1.96\times10^{-1}$	$\lambda_1 = -3.32\times10^{-1}$	$\lambda_1 = -9.98\times10^{-1}$	$\lambda_1 = -1.28$	$\lambda_1 = -1.96$	$\lambda_1 = -2.01$

Figure 5.5: Six equilibrium configurations of $\mathcal{H}300$ in the primary branch Sp. All the configurations on this branch are unstable. The configurations sp1 and sp2 have points of contact.
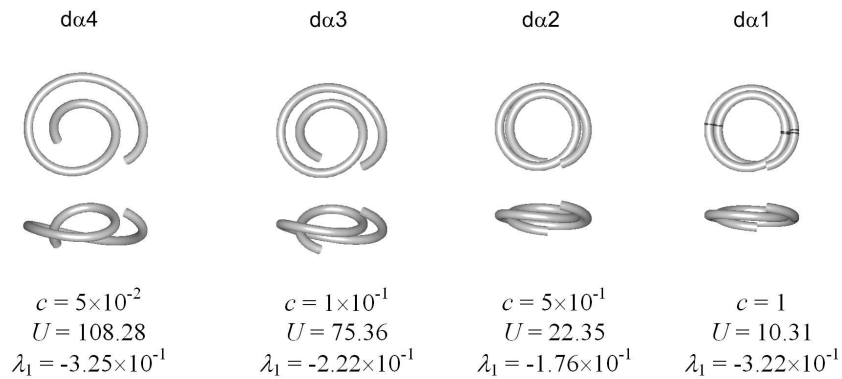

dα4	dα3	dα2	dα1
$c = 5\times10^{-2}$	$c = 1\times10^{-1}$	$c = 5\times10^{-1}$	$c = 1$
$U = 108.28$	$U = 75.36$	$U = 22.35$	$U = 10.31$
$\lambda_1 = -3.25\times10^{-1}$	$\lambda_1 = -2.22\times10^{-1}$	$\lambda_1 = -1.76\times10^{-1}$	$\lambda_1 = -3.22\times10^{-1}$

Figure 5.6: Four equilibrium configurations of $\mathcal{H}300$ in the secondary branch Dα. All the configurations on this branch are unstable. The configuration dα1 has points of contact.

contact with a base-pair steps in the intermediate region (see for example the configurations sp1 and sp2 shown in Figure 5.5). For values of c greater than $0.71\,\mathrm{M}$ the configurations on Sp have a third contact point.

As one moves along the branch Sp in the direction of increasing c one comes across a bifurcation point at $(c=3.05\times10^{-2}, \lambda_1=-7.30\times10^{-1})$, with $\lambda_3= 0$, that gives rise to the inception of a secondary branch, Dα, of distorted spiral configurations that are highly non-planar. An additional secondary branch, Dβ, of distorted spirals originates from a second bifurcation point, $(c=3.97\times10^{-1}, \lambda_1=-1.81)$ in Sp, in which $\lambda_4= 0$. The configurations in Dβ are similar to those in Dα but have a lower degree of non-planarity. As Dα and Dβ are secondary branches each point in them corresponds to four congruent equilibrium configurations that can be mapped into each other by the two transformations (5.12) and (5.13).

Four configurations in $D\alpha$ and two configurations in $D\beta$ are shown in Figures 5.6 and 5.7. The equilibrium configurations in $D\alpha$ have a single point of contact in the range of c between $c_c= 7.0\times10^{-1}$ M and 7.5×10^{-1}. For values of c greater than 7.5×10^{-1} M the configurations in $D\alpha$ have two points of contact. Such case is illustrated by the configuration $d\alpha1$ in Figure 5.6. The configurations in $D\beta$ have two points of contact for c greater than 7.1×10^{-1} M. It was found that when contact is taken into account, the branch $D\beta$ merges into the branch Sp for $c > 9.5\times10^{-1}$ M, and hence the configuration $d\beta1$ is identical to the configuration sp1.

A fourth (subcritical pitchfork) bifurcation point in the stem branch P was found at $(c=2.51\times10^{-2}, \lambda_1=-9.72\times10^{-1})$. At this bifurcation λ_3 that is negative in the range $3.59\times10^{-3}<c< 2.51\times10^{-2}$ vanishes towards a positive value in the range $c> 2.51\times10^{-2}$. The primary branch Ns of non-symmetric planar configurations originates at this bifurcation point, and as c is increasing the branch Ns encounters a pitchfork bifurcation point at $(c=5.94\times10^{-2}, \lambda_1=-1.47)$ from which the secondary branch Np of non-planar and non-symmetric configurations originates. Examples of configurations in the primary branch Ns and the secondary branch Np are shown in Figures 5.8 and 5.9.
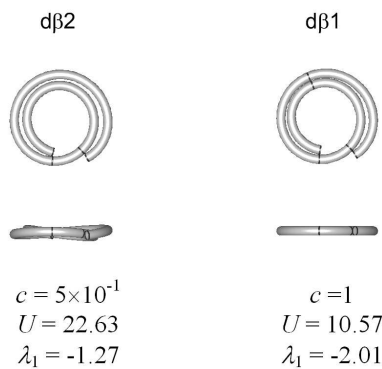

Figure 5.7: Two equilibrium configurations of $\mathcal{H}300$ in the secondary branch $D\beta$. All the configurations on this branch are unstable. The configurations $d\beta1$ and $d\beta2$ have points of contact. The configuration $d\beta2$ is identical to the configuration sp1 because, when self contact is taken into account, the two branches merge for $c > 9.50\times10^{-1}$ M.

ns4   ns3

$c = 5 \times 10^{-2}$ $c = 1 \times 10^{-1}$
$U = 109.68$ $U = 77.37$
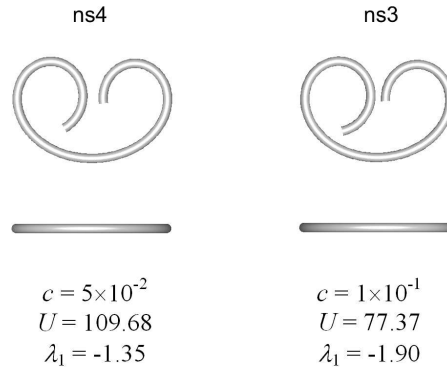$\lambda_1 = -1.35$ $\lambda_1 = -1.90$

Figure 5.8: Two equilibrium configurations of $\mathcal{H}300$ in the primary branch Ns. All the configurations on this branch are unstable.

np3

$c = 1 \times 10^{-1}$
$U = 77.32$
$\lambda_1 = -1.30$

Figure 5.9: An equilibrium configuration of $\mathcal{H}300$ in the secondary branch Np. All the configurations on this branch are unstable.

5.1.2 Equilibrium paths of the molecule $\mathcal{P}300$

As discussed in the beginning of the present section the qualitative differences (I) and (II) between the molecules $\mathcal{P}300$ and $\mathcal{H}300$ result an imperfect system $\mathcal{S}$ for the molecule $\mathcal{P}300$. The imperfect system has solutions that form smooth and continuous equilibrium paths in $\mathbb{R}^{6N} \times \mathbb{R}$ that are not connected to each other, and have subregions that correspond to equilibrium configurations of distinct character. A bifurcation diagram of the periodic molecule $\mathcal{P}300$ is shown in Figure 5.10. For the sake of comparison the bifurcation diagram for the homogenous molecule $\mathcal{H}300$ is also plotted in gray. Each equilibrium path is labeled by a script arabic numeral.

As the intrinsic configuration of the periodic molecule $\mathcal{P}300$ is not mapped into itself by the transformations (5.12) and (5.13), these transformations do not preserve
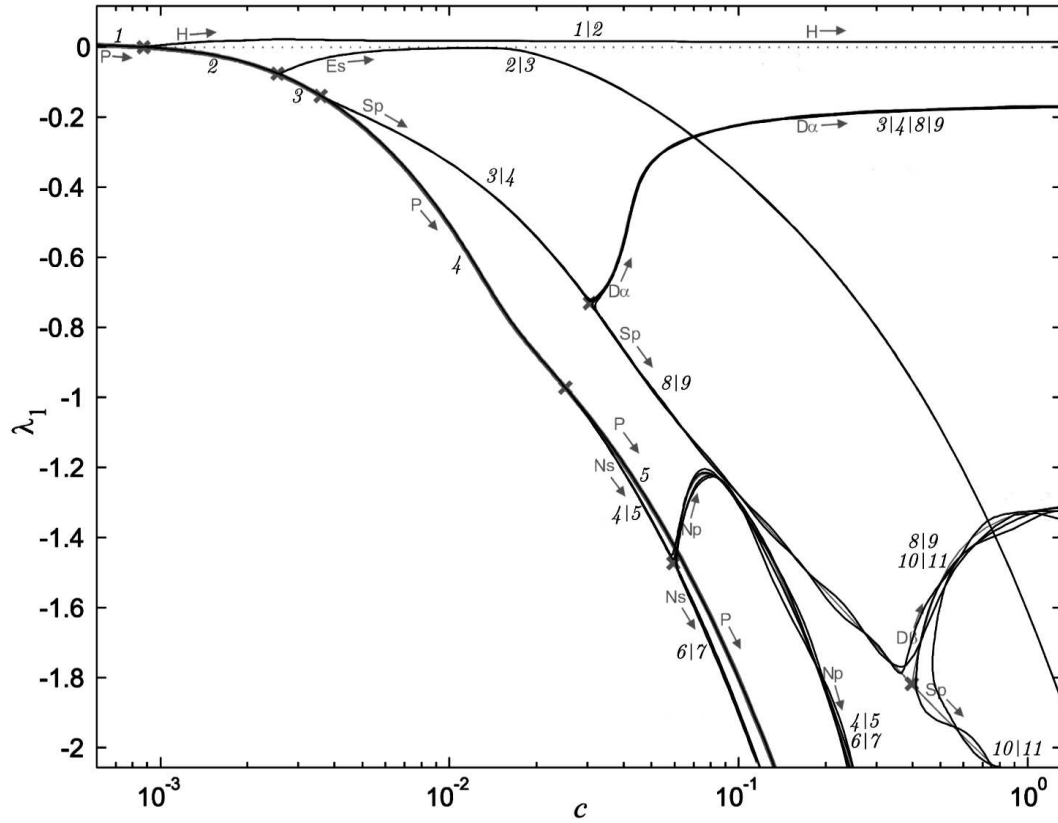
Figure 5.10: A bifurcation diagram for equilibrium configurations of the 300 base pair periodic DNA molecule labeled $\mathcal{P}300$. The diagram is presented as a graph of λ_1, the smallest proper number of the matrix $\mathbf{S}$ of equation (4.13), versus the salt concentration c. The bifurcation diagram of the homogenous DNA $\mathcal{H}300$ is drawn in gray to illustrate the differences and similarities between the perfect system induced by $\mathcal{H}300$ and the imperfect system induced by $\mathcal{P}300$. The script arabic numerals label the 11 equilibrium paths each of which is separated from the others. Two or four numerals separated by vertical lines indicate the existence of two or four equilibrium paths in a close proximity to primary or secondary branch of the perfect system.

the elastic energy of a configuration and hence do not yield several congruent solutions. The two (or four) configurations associated with each primary (or secondary) branch in the perfect system are replaced by a family of two (or four) configurations in different equilibrium paths such that, for a given c, their corresponding values of λ_1 and U are very close to each other (and to the value of the corresponding configuration of $\mathcal{H}300$) but not identical. Nevertheless, each configuration in such family has axial curve that is almost indistinguishable from one of the corresponding congruent configurations of $\mathcal{H}300$.
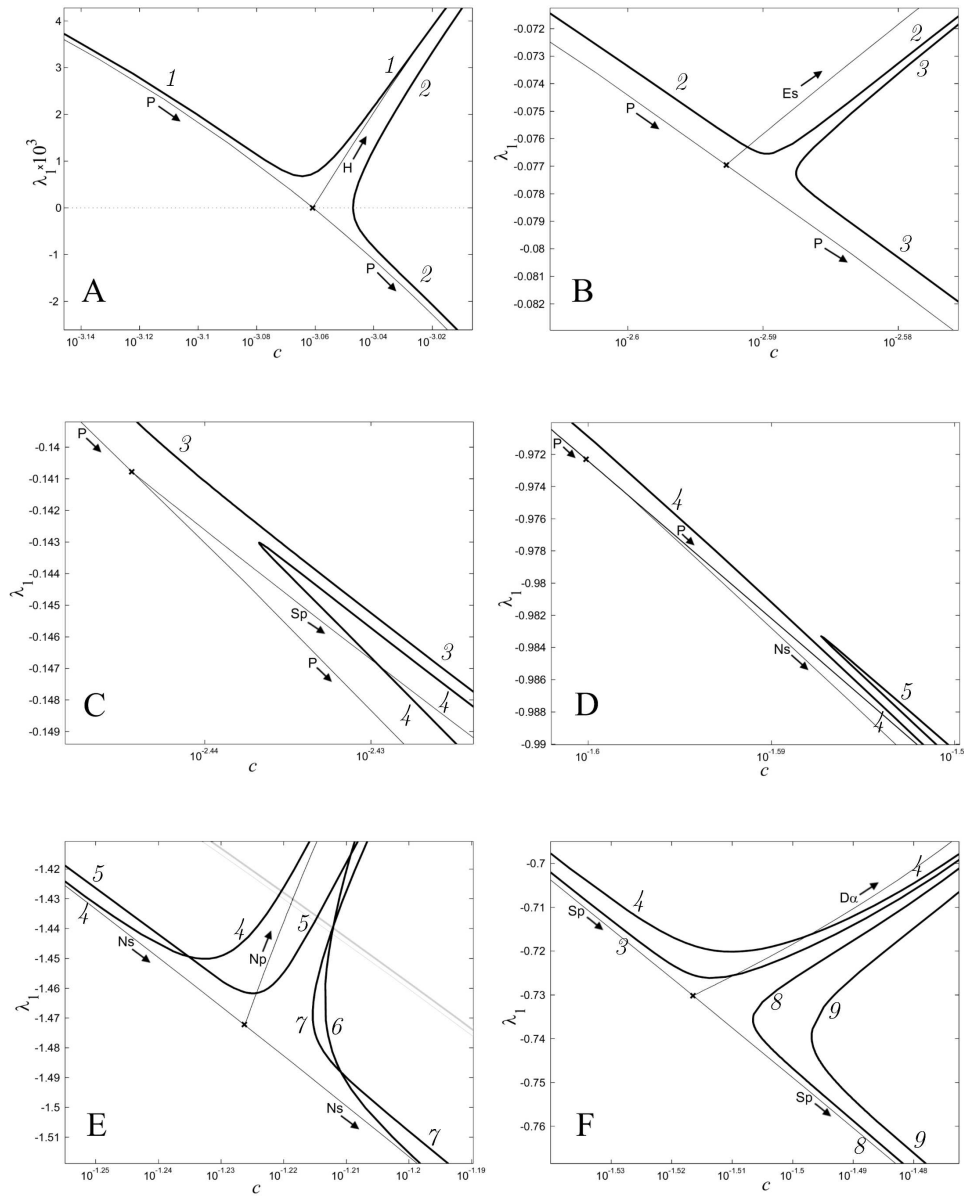
Figure 5.11: Enlargements of the areas including 6 of the bifurcation points shown in Figure (5.1) together with the equilibrium paths of the imperfect system that are shown in (5.10)). **A** An enlargement of the region including the bifurcation point ($c = 8.69 \times 10^{-4}$, $\lambda_1 = 0$) at which the primary branch H originates from the stem branch P. **B** An enlargement of the region including the bifurcation point ($c = 2.55 \times 10^{-3}$, $\lambda_1 = -7.69 \times 10^{-2}$) at which $\lambda_2 = 0$ and the primary branch Es originates from the stem branch P. **C** An enlargement of the region including the bifurcation point ($c = 3.59 \times 10^{-3}$, $\lambda_1 = -1.41 \times 10^{-1}$) at which $\lambda_3 = 0$ and the primary branch Sp originates from the stem branch P. **D** An enlargement of the region including the bifurcation point ($c = 2.51 \times 10^{-2}$, $\lambda_1 = -9.72 \times 10^{-1}$) at which $\lambda_3 = 0$ and the primary branch Ns originates from the stem branch P. **E** An enlargement of the region including the bifurcation point ($c = 5.94 \times 10^{-2}$, $\lambda_1 = -1.47$) at which $\lambda_4 = 0$ and the secondary branch Np originates from the primary branch Ns. **F** An enlargement of the region including the bifurcation point ($c = 3.05 \times 10^{-2}$, $\lambda_1 = -7.30 \times 10^{-1}$) at which $\lambda_3 = 0$ and the secondary branch Dα originates from the primary branch Sp.

Each pitchfork bifurcation point of the perfect system for $\mathcal{H}300$ is replaced by a fold and a subregion of equilibrium path that is free of singular points nearby. The turning point of such a fold connects subregion, with equilibrium configurations that are similar[15] to configurations in a primary (or secondary) branch of the perfect system, to subregions with configurations similar to those that were found in the stem (or primary) branch of the perfect system. This behavior can be observed in Figure 5.11 which shows a magnification of the equilibrium paths in the vicinity of 6 of the seven bifurcation points.

For the computation of bifurcation diagram of the imperfect system, a left and a right handed helical equilibrium configurations of the periodic molecule $\mathcal{P}300$ were calculated by employing the same technique that was used to find a starting configuration for the homogeneous molecule. [16] Each of the two helical configurations was used to explore the equilibrium path in which it resides by using the continuation methods described in Section 4.4. The results can be perceived by observing the magnification of the area in the vicinity of the bifurcation point ($c = 8.69 \times 10^{-4}, \lambda_1 = 0$) shown in Figure 5.11A. The branches of the perfect system are drawn in lightface with the branches labels nearby. The subregions of the two equilibrium paths of the imperfect system are plotted in boldface. As one moves along the equilibrium path 1 from right to left (i.e., in the direction of decreasing c) one sees that the corresponding equilibrium configurations are varying from configurations with approximately left handed helical axial curves to configurations with approximately planar axial curves. The minimum value of λ_1 lies in an intermediate transition subregion. On the other hand, the subregion above the turning point (in which $\lambda_1 = 0$) of the equilibrium path labeled 2 corresponds to configurations with right handed helical axial curves while the subregion below the turning point corresponds to approximately planar configurations. If one keeps following the equilibrium path 2 downward one arrives to the area shown in

---

[15]In the sense that their axial curves are almost indistinguishable.

[16]See the discussion given in the second paragraph of subsection 5.1.1.

Figure 5.11B. The configurations in the equilibrium path $\mathscr{2}$ are varying from planar to everted configurations as c is increasing in the range depicted in Figure 5.11B.

To find a starting configuration on the equilibrium path $\mathscr{3}$ the extrapolation method described in Section 4.4 was employed by using three configurations in the subregion of the equilibrium path $\mathscr{2}$ of approximately planar configurations together with a relatively large value of $\Delta\sigma$,[17] such that the predictor procedure would provide an initial configuration that is approximately planar and close enough to an equilibrium configuration at the extrapolated value of c that is in the subregion of planar configurations in the equilibrium path $\mathscr{3}$. With a configuration in the equilibrium path $\mathscr{3}$ in hand the full equilibrium path was explored. The equilibrium path $\mathscr{3}$ has a subregion with everted configurations above the turning point of the fold (shown in Figure 5.11B) across which λ_2 changes sign, a subregion with planar configurations below that turning point, and a subregion characterized by (planar) spiral configurations (with axial curves similar to one of the two congruent configurations in the branch Sp of the homogeneous molecule) that is smoothly connected to a subregion with distorted spiral configuration similar to one of the four congruent configurations associated with each point in $D\alpha$. The three transitions between the four subregions comprising the equilibrium path $\mathscr{3}$ can be seen in Figures 5.11B, 5.11C, and 5.11F.

A total number of 11 separated equilibrium paths was explored. A starting configuration in each of the equilibrium paths was found using the extrapolation scheme to "jump" from one equilibrium path to another. Enlargements of the area in the vicinity of six of the seven bifurcation points of the perfect system are shown in Figures 5.11A−F. As shown, the two congruent configurations of each primary branch of the perfect system, are replaced by subregions of two equilibrium paths, and the four congruent configurations of each secondary branch are replaced by subregions of four equilibrium paths. Three examples of the families of equilibrium configurations of $\mathcal{P}300$ at the physiological value $c= 1\times 10^{-1}\,\mathrm{M}$ in subregions that correspond to the

---

[17] See the discussion in the last paragraph of Section 4.4.

hr3 hl3

$c = 1 \times 10^{-1}$
$U = 74.37$
$\lambda_1 = 1.554 \times 10^{-2}$

$c = 1 \times 10^{-1}$
$U = 74.29$
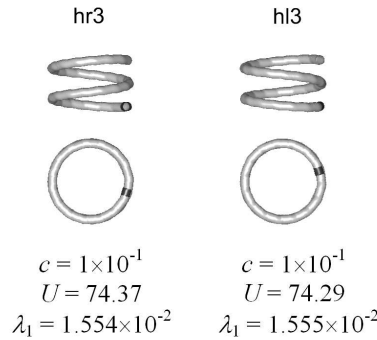$\lambda_1 = 1.555 \times 10^{-2}$

Figure 5.12: Two helical equilibrium configuration of $\mathcal{P}300$ at $c = 1 \times 10^{-1}$ M with opposite handedness. The five base-pair steps at the intrinsically straight end are darkened.

esr3 esl3

$c = 1 \times 10^{-1}$
$U = 76.34$
$\lambda_1 = -3.621 \times 10^{-1}$

$c = 1 \times 10^{-1}$
$U = 76.34$
$\lambda_1 = -3.618 \times 10^{-1}$

Figure 5.13: Two distinct everted equilibrium configurations of $\mathcal{P}300$ at $c = 1 \times 10^{-1}$ M. The five base-pair steps at the intrinsically straight end are darkened.

primary branches H and Es and to the secondary branch Dα are shown in Figures 5.12, 5.13, and 5.14. The figures show that the configurations hr3, esr3 (or esl3), and dαc3 (or dαd3) have axial curves that are very close to those of the configurations h3, es3, and dα3 shown in Figures 5.2, 5.4, and 5.6, respectively. This suggests, that a homogenous molecule of the type $\mathcal{H}300$ may be a good approximation to a real molecule that can be approximated by the periodic molecule $\mathcal{P}300$, in the sense that its equilibrium configurations have values of total energy that are remarkably close to the periodic molecule and with almost indistinguishable axial curves. In the concluding subsection of this section a bifurcation diagram of a homogenous molecule labeled $\mathcal{H}450$ of 450 base pairs with the same properties as the molecule $\mathcal{H}300$ is analyzed.

dαa3   dαb3   dαc3   dαd3

$c = 1 \times 10^{-1}$ $c = 1 \times 10^{-1}$ $c = 1 \times 10^{-1}$ $c = 1 \times 10^{-1}$
$U = 75.63$ $U = 75.63$ $U = 75.63$ $U = 75.63$
$\lambda_1 = -2.234 \times 10^{-1}$ $\lambda_1 = -2.240 \times 10^{-1}$ $\lambda_1 = -2.213 \times 10^{-1}$ $\lambda_1 = -2.237 \times 10^{-1}$

Figure 5.14: Four distinct distorted spiral equilibrium configurations of $\mathcal{P}300$ at $c = 1 \times 10^{-1}$ M. The five base-pair steps at the intrinsically straight end are darkened.

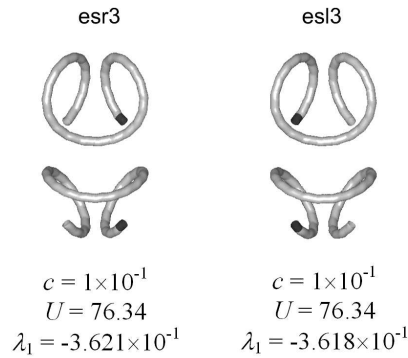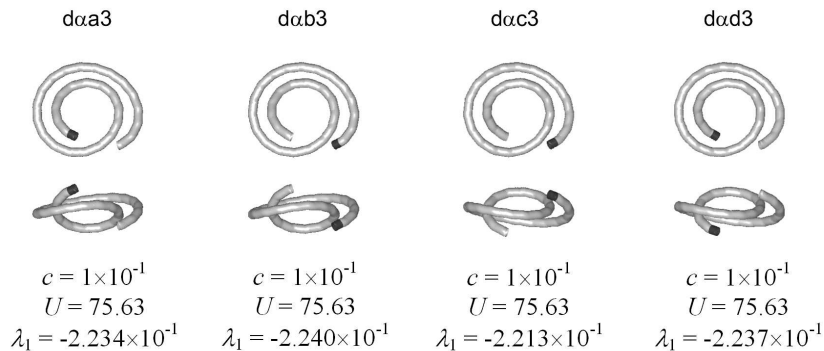## 5.2   Bifurcations of equilibria of the molecule $\mathcal{H}450$

To conclude this chapter a computation of equilibria of an open homogeneous molecule, $\mathcal{H}450$, with 450 base pairs and properties identical to the properties of the molecule $\mathcal{H}300$, i.e., for which (5.2), (5.3), (5.7), and (5.9) hold for $N = 449$, and the end conditions are given by (5.1), was performed and analyzed. As in the case of the shorter homogenous molecule, the translational parameters were assumed to be fixed, i.e., $\mu = 3$. A detailed discussion on the bifurcation diagram of this molecule is given in [9]. In the present subsection an emphasis is given to branches with equilibrium configurations that either do not exist in the bifurcation diagram of $\mathcal{H}300$ or exhibit a range with stable configurations.

As in the case of the homogeneous molecule, $\mathcal{H}300$, each calculated equilibrium configuration of $\mathcal{H}450$ is a representative of a group of 1,2, or 4 congruent equilibrium configurations that are related by the transformations (5.13), (5.12) or any composition of them. Because the overall effect of the repulsive electrostatic forces on equilibrium configurations of the 450 base-pair DNA molecule, $\mathcal{H}450$, is significantly higher than the effect on the 300 base-pair molecules, all the equilibrium configurations correspond to the domain reported in the bifurcation diagram shown in Figure 5.15 are free of self contact and self penetration.

As in the previously discussed examples the calculations showed the existence of
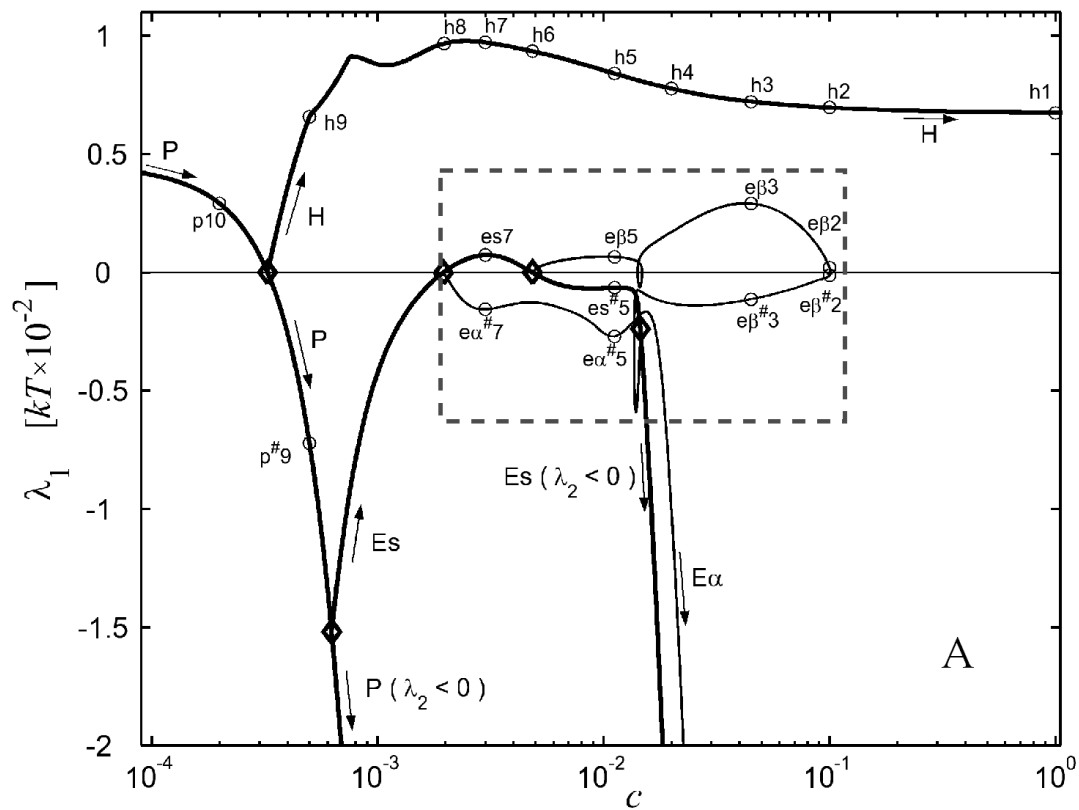
Figure 5.15: A bifurcation diagram for equilibrium configurations of $\mathcal{H}450$ presented as a graph of λ_1 versus the salt concentration c. Configurations with $\lambda_1 > 0$ are (locally) stable. Small circles denote configurations shown in Figures 5.16, 5.19, 5.18, 5.20, and 5.21. The labels of these configurations are shown next to the indicated circles. The symbol "◆" indicates a bifurcation point. The stem branch P and the primary branches H and Es are drawn in boldface; the secondary branches Eα and Eβ in lightface.

Figure 5.16: Four distinct helical configurations of $\mathcal{H}450$. The configurations on H are the global minimizers of the total energy U. For the molecule $\mathcal{H}450$ the values of λ_1 given here and in all other figures are in unit of $10^{-2} k_{\mathrm{B}} T$. The total energy is given in units of $k_{\mathrm{B}} T$. The perpendicular views of each configuration are derived in the same way explained in the caption of Figure 5.2. The scale of length in all the figures showing configuratio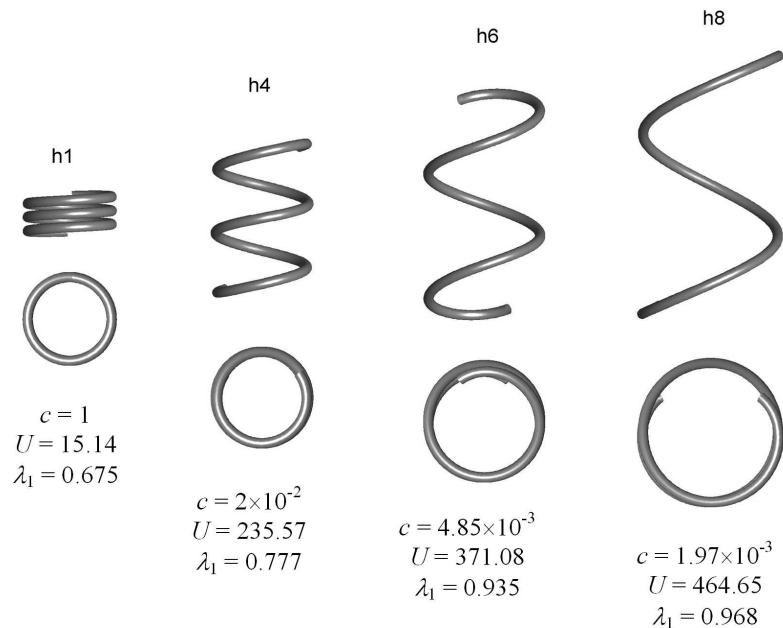ns of $\mathcal{H}450$ is the same as the scale in figures of configurations of $\mathcal{H}300$ and $\mathcal{P}300$. The numbers in the labels of the configurations do not correspond to the same values of c as in the 300 base pair molecules.

stable configurations with an approximately helical axial curve that are the global minimizers of the total energy U and, for values of c less than $1.4\,\mathrm{M}$, are free of self penetration. The helical configurations lie in the branch labeled H. To illustrate the sensitivity of the globally stable configurations to changes in c, four configurations in the branch H are shown in Figure 5.16. The primary branch H originates at the bifurcation point $\left(c{=}3.26{\times}10^{-4}, \lambda_1{=}0\right)$ of the stem branch P. The primary branch Es of symmetric everted configurations originates at the bifurcation point $\left(c{=}6.30{\times}10^{-4}, \lambda_1{=}{-}1.52\right)$ at which λ_2 vanishes. In contrast to the case of the short molecule, for values of c in the range $1.95{\times}10^{-3}{<}c{<}4.84{\times}10^{-3}$ the configurations on Es are stable. Secondary branches labeled Eα and Eβ originate at the bifurcation points, with $\lambda_1{=}0$, that bound this range.[18] The configurations in the secondary branches Eα and Eβ have axial curves

---

[18]There are no branches similar to Eα and Eβ for the shorter DNA molecule $\mathcal{H}300$ treated previously.
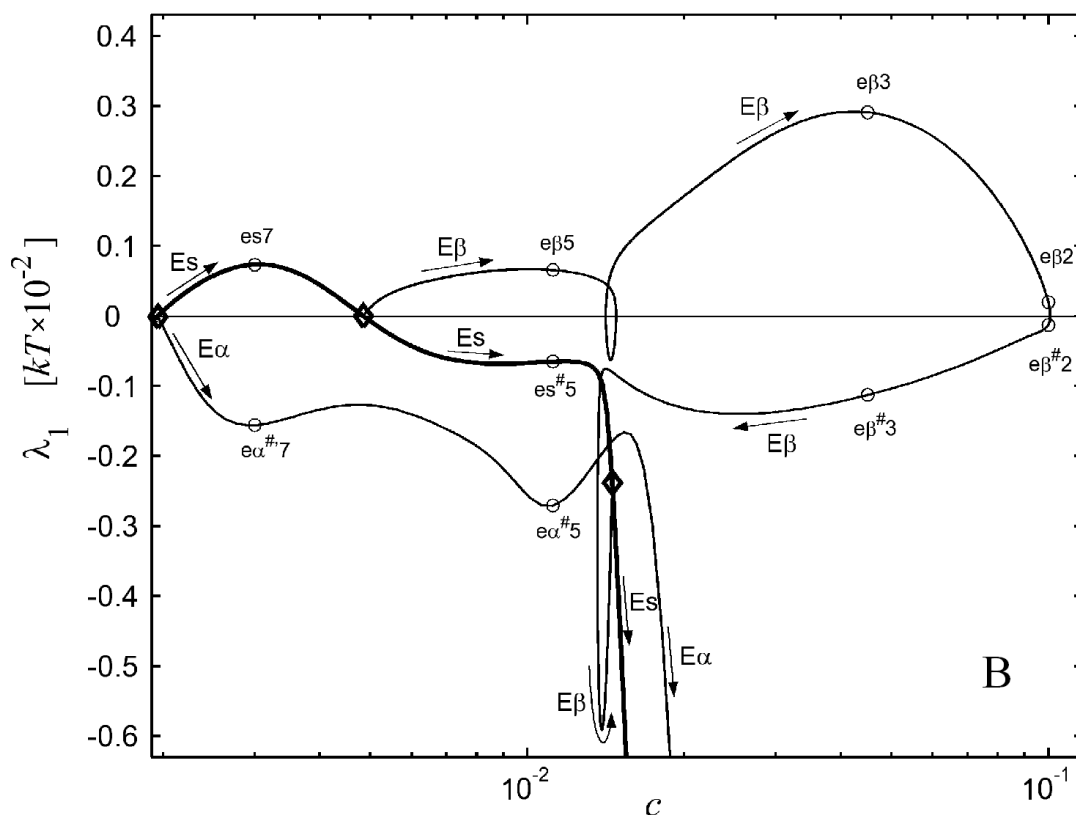
Figure 5.17: An enlargement of the rectangular region that is bounded by dashed lines in the bifurcation diagram shown in Figure 5.15.

that are closely related to the axial curves of the symmetric everted configurations, but they are not symmetric. The mid point of the intermediate transition region between the two approximately helical subregions of opposite handedness is positioned away of the middle base-pair step of the molecule, and, hence, yield helical subregions of different lengths. The stability of the configurations in these branches was found to be remarkably sensitive to the position of the transition region in the configurations. As shown in Figure 5.17 all the configurations in Eα were found to be unstable. The two configurations, e$\alpha^{\#}$5, and e$\alpha^{\#}$7 depicted in Figures 5.19 and 5.18, illustrate that the configurations in Eα are characterized by a transition region that is significantly off the middle base-pair step. On the other hand, the configurations in the

h7   es7   eα#7

$c = 3 \times 10^{-3}$
$U = 420.57$
$\lambda_1 = 0.972$

$c = 3 \times 10^{-3}$
$U = 421.86$
$\lambda_1 = 0.074$

$c = 3 \times 10^{-3}$
$U = 421.93$
$\lambda_1 = -0.156$

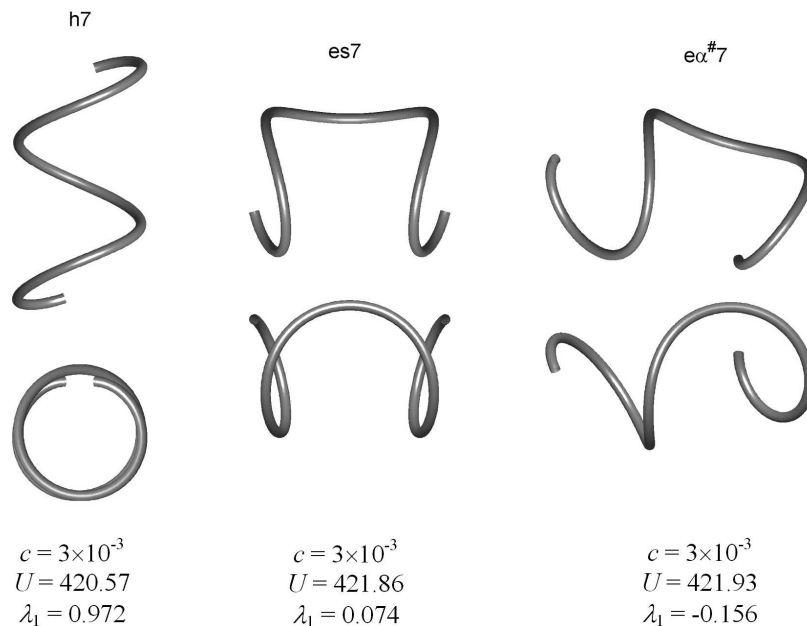Figure 5.18: Three distinct equilibrium configurations of $\mathcal{H}450$ at $c = 3 \times 10^{-3}$ M. The configuration eα#7 is unstable; es7 is locally stable; h7 is globally stable.

branch Eβ have at least one stable configuration at each value of c in the range between the bifurcation point $(c=4.84 \times 10^{-3}, \lambda_1=0)$ at which the branch Eβ originates and the turning point $(c=1.01 \times 10^{-1}, \lambda_1=0)$. If one starts at the bifurcation point $(c=4.84 \times 10^{-3}, \lambda_1=0)$ and follows the branch Eβ in the direction indicated by arrows on the enlarged region shown in Figure 5.17 one encounters three folds with turning points across which λ_1 changes sign followed by a fourth fold with a turning point at which $\lambda_2 = 0$. The branch Eβ merges back to the primary branch Es at the bifurcation point $(c=1.46 \times 10^{-2}, \lambda_1=-0.24)$ at which $\lambda_2 = 0$.

Thus, the bifurcation diagram for the molecule $\mathcal{H}450$ has regions in which several distinct equilibrium configurations with more than one of them stable occur at a single value of c. This is the case for c in the range of values appropriate to Figure 5.17. Shown in Figures 5.18, 5.19, and 5.20 are 3 equilibrium configurations that occur at $c=3 \times 10^{-3}$ M, 4 at $c=1.12 \times 10^{-2}$ M, and 3 at $c=4.52 \times 10^{-2}$ M; in each of these cases two of the distinct configurations are stable. In the small subrange $1.41 \times 10^{-2} < c < 1.48 \times 10^{-2}$ of the range shown in Figure 5.17, i.e., for values of c
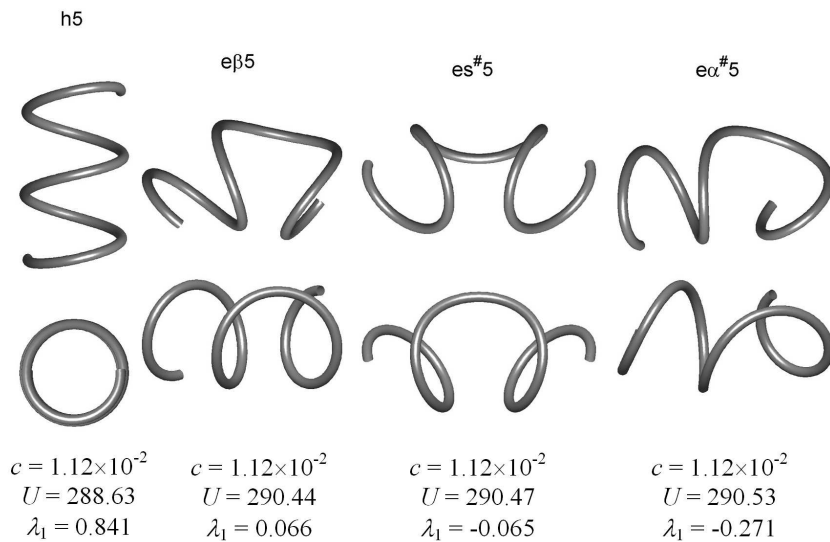
Figure 5.19: Four distinct equilibrium configurations of $\mathcal{H}450$ at $c=1.12\times10^{-2}$ M. The configurations $\text{es}^{\#}5$ and $\text{e}\alpha^{\#}5$ are unstable; $\text{e}\beta5$ is locally stable; h5 is globally stable.

between the first and second depicted folds in the branch $\text{E}\beta$, there are 3 distinct stable configurations, with 2 in the branch $\text{E}\beta$ and 1 in the branch H. For values of c greater than 1.01×10^{-1} M the configurations on H are the only stable configurations. Therefore a small increase in c from a value below to a value above 1.01×10^{-1} M will give rise to a transition from a locally stable configuration in the branch E to a globally stable configuration in the branch H. Shown in Figure 5.21 are 2 configurations in the branch $\text{E}\beta$ and a configuration in the branch H for $c= 1\times10^{-1}$ M.

$$c = 4.52{\times}10^{-2}$$
$$U = 168.33$$
$$\lambda_1 = 0.722$$

$$c = 4.52{\times}10^{-2}$$
$$U = 169.38$$
$$\lambda_1 = 0.291$$

$$c = 4.52{\times}10^{-2}$$
$$U = 169.39$$
$$\lambda_1 = -0.113$$
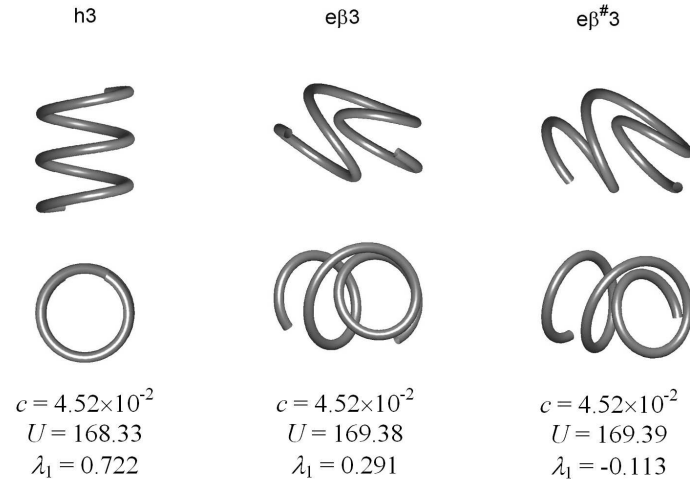
Figure 5.20: Three distinct equilibrium configurations of $\mathcal{H}450$ at $c{=}4.52{\times}10^{-2}$ M. The configuration e$\beta^{\#}3$ is unstable; e$\beta 3$ is locally stable; h3 is globally stable.

$$c = 0.1$$
$$U = 111.61$$
$$\lambda_1 = 0.675$$

$$c = 0.1$$
$$U = 112.24$$
$$\lambda_1 = 2.000{\times}10^{-2}$$

$$c = 0.1$$
$$U = 112.24$$
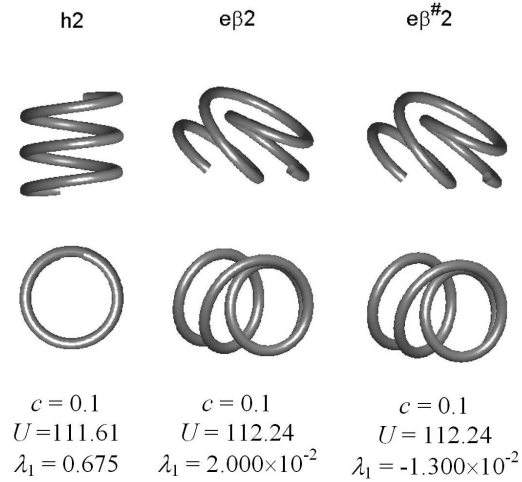$$\lambda_1 = -1.300{\times}10^{-2}$$

Figure 5.21: Three distinct equilibrium configurations of $\mathcal{H}450$ at $c{=}\,1{\times}10^{-1}$ M, a value of c less than but very close to the critical value $c{=}\,1.01{\times}10^{-1}$ M. The configuration e$\beta^{\#}2$ is unstable; e$\beta 2$ is locally stable; h2 is globally stable.

Chapter 6

Analysis of equilibrium configurations of closed DNA molecules

In this chapter computational results of examples of closed DNA molecules are reported. The first section gives an introduction to the end conditions and the topology of closed DNA molecules. Several examples including homogeneous and strictly non-homogeneous DNA molecules are described in the following sections. The reported calculations are more likely to be accessible to experimental verification than the cases of open molecules discussed in the previous chapter. Even when a closed molecule is assumed to be free of self contact a solution, $^{\mu}\underline{\alpha}$, of the system $\mathcal{S}$ of the equilibrium equations (3.7) includes not only the equilibrium configuration $^{\mu}\alpha$ but also the six number $(\tau_1, \tau_2, \tau_3, P_1, P_2, P_3)$ characterizing the force and moment that the $(N{+}1)$-th base pair exerts on the 1-st. As stated in (3.8), when self contact is present a solution includes also the list of Lagrange multipliers characterizing the contact forces.

6.1 End conditions and topology of closed DNA molecules

A transition from an open (linear) DNA molecule to a closed (circular) molecule may occur when each of the two strands of the DNA is covalently attached to a single nucleotide, such that each end of the molecule contains a single base, and the two bases (in the two ends) are complementary to each other. When in such a molecule the two ends are in a close proximity and are appropriately oriented, the two complementary bases would adhere to each other through the formation of hydrogen bonds to constitute a single base pair in a closed molecule. In the present work a closed DNA molecule

with N base pairs is treated as a molecule with $N+1$ base pairs, such that, its 1-st and $(N+1)$-th base pairs coincide, and with no electrical charge associated with the $(N+1)$-th base pair. Accordingly, a closed molecule obeys the following kinematical end conditions:

$$\zeta_i = 0, \quad i = 1, 2, 3, \tag{6.1a}$$

$$\ell_k = 0, \quad k = 1, 2, 3, \tag{6.1b}$$

where the angles ζ_i determining the relative orientation between the base pairs in the two ends of the molecule are defined by the relation (2.15), and the components of the end-to-end vector, $\boldsymbol{\ell}$, are as in equation (2.29). [1]

The end conditions (6.1) are satisfied for any integral value of the molecule's linking number, L_k. The linking number can be changed by nicking one strand (or cleaving both strands) of the molecule and twisting[2] the base pair in one side of the cleavage through an integral numbers of turns while holding the base pair in the other side fixed. In living cells such changes in the topology of a DNA molecule are preformed with the aid of enzymes called topoisomerases.

In the present model the intermediate process of raising or lowering L_k was performed by gradually changing the (end-to-end) twist, ζ_3, between the two ends of the molecule. When the value of ζ_3 is controlled, and all other end conditions are as in (6.1), the two base pairs in the ends of the molecule lie in the same plane (with $\mathbf{d}_3^1$ normal to that plane and in coincident with $\mathbf{d}_3^{N+1}$) and their barycenters coincide. The angle ζ_3 under these conditions is the angle that $\mathbf{d}_1^{N+1}$ makes with $\mathbf{d}_1^1$.

The (integral valued) linking number L_k is related to the writhe, W_r, and the *total*

---

[1]A DNA molecule obeying (6.1) is often referred to as a circular DNA, see e.g., the book by A.V. Vologodskii [39]. A relatively short DNA molecule with N in the order of several hundreds is called miniplasmid or minicircle.

[2]In the case of nicked DNA, i.e., a molecule in which one of the sugar-phosphate chains is nicked while the other is closed, the twist is performed with the sugar-phosphate chain of the closed strand as a pivot.

twist, T_{w}, of a closed configuration by the equation,

$$L_{\mathrm{k}} = W_{\mathrm{r}} + T_{\mathrm{w}}. \tag{6.2}$$

The total twist $T_{\mathrm{w}} = \tilde{T}_{\mathrm{w}}(\mathcal{C}, \mathcal{C}_{\mathrm{sp}})$ is the number of times one of the DNA sugar-phosphate chains is wound around the axial curve $\mathcal{C}$ of the molecule; when a DNA configuration is planar and circular (with no self-crossing) $T_{\mathrm{w}} = L_{\mathrm{k}}$. In the present model the closed curve, $\mathcal{C}_{\mathrm{sp}}$, that represents the spatial course of one of the two sugar-phosphate chains is taken to be the piecewise-linear curve that connects the points $\{\mathbf{x}^n + \frac{1}{2}\mathcal{D}_{\mathrm{o}}\, \mathbf{d}_2^n\,\}$, $n = 1, ..., N+1$. It was found that, when (as here) the local twist θ_3^n is in accord with the definition of El Hassan and Calladine [8], the value of T_{w} is well approximated by

$$T_{\mathrm{w}} \approx \frac{1}{2\pi} \sum_{n=1}^{N} \theta_3^n. \tag{6.3}$$

An equilibrium configuration $^6\boldsymbol{\alpha}$ for which ζ_3 is preassigned, and for which the end conditions

$$\zeta_1 = 0, \qquad \zeta_2 = 0, \qquad \boldsymbol{\ell} = \mathbf{0}, \tag{6.4}$$

are obeyed, has a curve $\mathcal{C}_{\mathrm{sp}}(^6\boldsymbol{\alpha})$ that is closed if and only if $\zeta_3/2\pi$ is an integer. Given such a configuration, one can construct a closed piecewise linear curve, $\mathcal{C}_{\mathrm{sp}}^*(^6\boldsymbol{\alpha}, \zeta_3)$, that connects the points
$\{\mathbf{x}^n + \frac{1}{2}\mathcal{D}_{\mathrm{o}}\, \mathbf{d}_*^n\,\}$, $n = 1, ..., N+1$, where

$$\mathbf{d}_*^n = \mathbf{d}_2^n \cos\left(\zeta_3 \frac{n-1}{N}\right) + \mathbf{d}_1^n \sin\left(\zeta_3 \frac{n-1}{N}\right). \tag{6.5}$$

With $\mathcal{C}_{\mathrm{sp}}^*$ constructed that way, the linking number of the closed curves $\mathcal{C}_{\mathrm{sp}}^*$ and $\mathcal{C}$ is independent of ζ_3. With this in mind, one can define the *excess link* of the configuration $^6\boldsymbol{\alpha}$ to be

$$\Delta L_{\mathrm{k}} = W_{\mathrm{r}} + \tilde{T}_{\mathrm{w}}(\mathcal{C}, \mathcal{C}_{\mathrm{sp}}^*) - {}_{\mathrm{o}}T_{\mathrm{w}}^*, \tag{6.6}$$

where

$$_{\mathrm{o}}T_{\mathrm{w}}^* = {}_{\mathrm{o}}T_{\mathrm{w}} - \frac{\zeta_3}{2\pi}. \tag{6.7}$$

The quantity $_{\mathrm{o}}T_{\mathrm{w}}$ is the total twist of a reference configuration that is planar but not necessarily closed and not necessarily stress-free. When such a reference configuration is constrained to remain planar with end-to-end twist equals to $-\zeta_3$ its total twist is equal to $_{\mathrm{o}}T_{\mathrm{w}}^{*}$. The excess link is commonly varying as a result of a change in the total twist of the reference configuration and not as a result of a change in the end-to-end twist. However, equation (6.6) suggests that a change in the end-to-end twist ζ_3 together with the end conditions (6.4) can be expressed in terms of an opposite change in the total twist of the reference configuration. If for a homogeneous, transversely isotropic, intrinsically planar DNA molecule the intrinsic configuration is taken to be the reference configuration then a change $-\zeta_3/2\pi$ in the total twist of the reference configuration is equivalent to a change in the end-to-end twist ζ_3, in the sense that the associated equilibrium configurations have equal values of the total energy and identical axial curves.

6.2   Examples of intrinsically curved 549 base pair molecules

In the study reported in this section the dependence on c of equilibrium configurations of a circularized DNA molecule, labeled $\mathcal{H}550$ was investigated. The 549 base pair molecule ($N+1 = 550$) has an intrinsic curvature such that each 220 base pair sub-segment has the shape of a (perfectly) circular ring when in its stress free state. [3] The molecule can be closed to forms a perfectly circular ring that is taken to be the reference configuration. The linking number is set equal to that of the reference configuration with $\zeta_3 = 0$, i.e., $L_{\mathrm{k}} = {}_{\mathrm{o}}T_{\mathrm{w}}$, and $\Delta L_{\mathrm{k}} = 0$.

As was discussed in the previous chapter a molecule, as $\mathcal{H}550$, that obeys (5.2), (5.3), and (5.6) has solutions with mechanical response and axial curve that are indifferent to the choice of L_{k}, and the simplest choice, $L_{\mathrm{k}} = 0$ was made. Thus, the intrinsic parameters of $\mathcal{H}550$ are given by (5.7) with $N_{\mathrm{o}} = 220$, and the elastic moduli of $\mathcal{H}550$

---

[3]The highly curved sequences found in the kinetoplast DNA of Trypanosmamatidae are believed to have intrinsic curvature of that order [40], [41], [42], [43].

are as in (5.3) and (5.9). For all the examples in this section $\mu= 3$ i.e., the shift, slide, and rise in each of the base-pair steps are fixed at their intrinsic values.

To investigate the influence of the intrinsic curvature, and the ratio F_{33}^n/F_{11}^n on equilibrium configurations, three different molecules labeled $\mathcal{H}550_{270}$, $\mathcal{H}550_{1.4}$, and $\mathcal{H}550_{0.7}$, were also studied. Each one of the molecules differs from $\mathcal{H}550$ by only one property. The molecule $\mathcal{H}550_{270}$ has intrinsic curvature such that each 270 base pair subsegment of it forms a circular ring when stress free, i.e., $N_{\text{o}}= 270$. For the molecules $\mathcal{H}550_{1.4}$ and $\mathcal{H}550_{0.7}$ the ratio F_{33}^n/F_{11}^n was taken to be 1.4 and 0.7 respectively. In the last subsection of this section results from a calculation of equilibria of the molecule $\mathcal{H}550$ that is closed such that $\Delta L_{\text{k}}= -1$ are reported.

6.2.1 Bifurcations of equilibria of $\mathcal{H}550$ with $\Delta L_{\text{k}}= 0$

A planar, intrinsically curved, transversely isotropic, and homogenous molecule (such as $\mathcal{H}550$) that is closed to form a ring with zero excess link has a trivial perfectly planar equilibrium configuration. In the case for which $\mu= 3$, this trivial ring configuration is independent of the salt concentration as a result of the inextensibility of the molecule. If such a closed molecule obeys (5.2), (5.7), and (5.3), has N base pairs (or base-pair steps), its trivial (ring) equilibrium configuration is given by,

$$\theta_1^n = 0, \quad \theta_2^n = \frac{2\pi}{N}, \quad \theta_3^n = 0, \qquad n = 1, ...,N, \tag{6.8}$$

and of course (5.2). [4] It can be shown that a ring configuration (of a molecule with the above mentioned characteristics) that obeys (6.8) is a solution of the equations of equilibrium (2.43) if the external force vector $\mathbf{P}=\tilde{\mathbf{P}}(c)$ obeys the relation [5]

$$\mathbf{P} = \frac{g_{\text{o}}}{2}(\mathbf{d}_1^1 - \cot(\pi/N)\mathbf{d}_3^1), \tag{6.9}$$

---

[4] A highly unstable "everted ring" configuration that is an equilibrium configuration for all values of c can be obtained by changing the sign of θ_2^n. A thorough investigation revealed that, for the DNA molecule $\mathcal{H}550$, none of the branches that are connected to this additional stem branch contain stable configurations.

[5] The external force and moment $\mathbf{P}$ and $\mathbf{T}$ are as in equations (2.42) and (2.43); their components are determined by the 6 Lagrange multipliers associated with the kinematical end conditions.
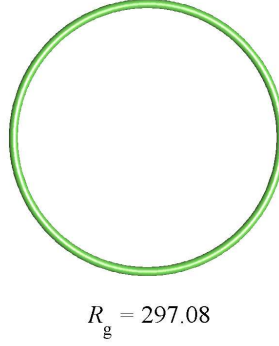
$$R_{\mathrm{g}} = 297.08$$

Figure 6.1: The Ring configuration of $\mathcal{H}550$. The ring is an equilibrium configuration for all values of c. The radius of gyration here and in all the following figures is given in Å (angstroms).

where g_{o} is the magnitude (that is independent of n) of the electrostatic force $\mathbf{g}^n$ acting on each of the base pairs in the ring configuration, and the external moment $\mathbf{T}$ in the ring configuration is given by

$$\mathbf{T} = F_{22}^n (2\pi/N_{\mathrm{o}} - 2\pi/N)\mathbf{d}_2^1. \tag{6.10}$$

In the above solution the symmetry of the ring configuration implies that the moment $\mathbf{m}^n$ is independent of n, and thus, by (2.43c) $\mathbf{T} = -\mathbf{m}^n$. The ring configuration is shown in Figure 6.1 in the same scale of length as in all the figures showing configurations.

The energy of a homogenous closed molecule such as $\mathcal{H}550$ was found to be practically indifferent to slithering motions for any value of c when the distance of closest approach $\mathcal{D}_{\mathrm{ca}}$ is equal or greater than $\mathcal{D}_{\mathrm{o}}$. [6] This observation implies that for each non perfectly circular configuration there is an identically zero proper number that corresponds to a neutral variation in addition to the zero proper numbers of $\bar{\mathbf{S}}$ that are associated with the rigid body rotation and the active constraints. The ring configuration is an exceptional case of equilibrium configuration that is not associated with such

---

[6]In a closed continuous rod a slithering motion is a motion in which each cross section of the rod is transported along the axial curve of the rod in such a way that the axial curve is unchanged and each of the cross sections traveled the same distance along the axial curve. Similarly, in the naturally discrete model used in the present work, a slithering motion is a motion in which each of the base pairs travels along an imaginary smooth curve (closely related to, but different from, the axial curve) such that, if the motion is long enough, each of the base pairs would reach the original position and orientation of its adjacent neighbor simultaneously. A slithering mode is an infinitesimally short motion of that kind.

additional neutral variation. This exception is a result of the fact that the smooth curve (see the last footnote) associated with slithering in a ring configuration is the circle circumscribed around its polygonal axial curve, and hence a slithering motion of a ring keeps the kinematical variables unchanged.

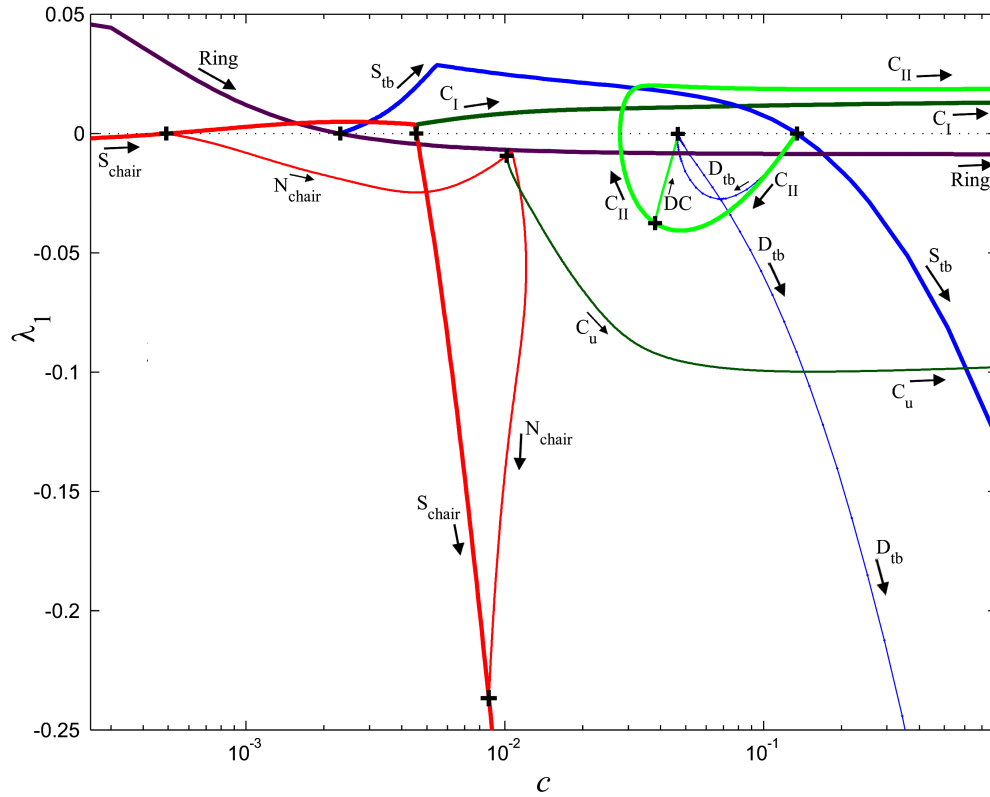A bifurcation diagram of λ_1 versus c is shown in Figure 6.2. The stem branch, la-

Figure 6.2: Bifurcation diagram of λ_1 versus c for equilibrium configurations of the closed 549 base pair DNA molecule $\mathcal{H}550$. Bifurcation points are indicated by the symbol "+".

beled "Ring" contains only the trivial equilibrium configuration, $^3\alpha_{\text{ring}}$, that is given by (6.8) with $N = 549$. The ring configuration is stable for values of c less than $c_{\text{b}} = 2.32 \times 10^{-3}$ M. At the bifurcation point $(c_{\text{b}}, \lambda_1 = 0)$ two proper numbers of $\bar{\mathbf{S}}$ vanish. A primary branch labeled S_{tb} originates from that point. The configurations in S_{tb} have a form of a symmetrically buckled ring. The axial curve of the buckled rings has a shape similar to that of the curve dividing the surface of a tennis ball to two identical pieces with two perpendicular mirror symmetry planes. Six equilibrium
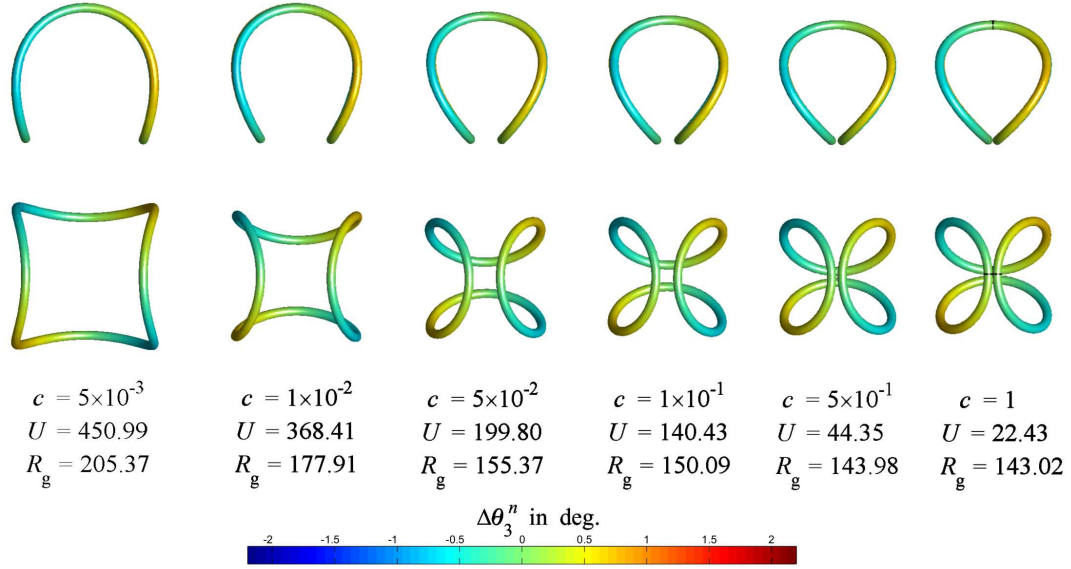
Figure 6.3: Six symmetrically buckled ring ("tennis ball") configurations of $\mathcal{H}550$ in the branch S_{tb}. The equilibrium configuration at $c = 1\,M$ have two points of self contact. Here and in all the figures showing configurations in the present section the values of the excess twist, $\Delta\theta_3^n$, are represented by assigning a color to each subsection of the tube associated with a base-pair steps. The numeric value of each color is indicated in the color-bar shown in the bottom.

configurations in the branch S_{tb} are shown in Figure 6.3.

Each of the buckled ring configurations in S_{tb} has 4 evenly spaced sites[7] in which the excess twist $\Delta\theta_3^n$ vanishes (or changes its sign). The position of the sites along the axial curve can be changed with no energy cost by a slithering motion. In the vicinity of the bifurcation point, a slithering variation of the buckled ring can be described by adding to the ring configuration, ${}^3\boldsymbol{\alpha}_{\text{ring}}$, vectors that are linear combinations of the two vectors, ${}^3\mathbf{V}\,\mathbf{y}_1$ and ${}^3\mathbf{V}\,\mathbf{y}_2$, where $\mathbf{y}_1$ and $\mathbf{y}_2$ are the normalized proper vectors associated with the vanishing proper numbers of $\bar{\mathbf{S}}$. More precisely, the one parameter family of vectors in $\mathbb{R}^{3N}$,

$$ {}^3\boldsymbol{\alpha}_{\text{ring}} + \varepsilon\left({}^3\mathbf{V}\,u\mathbf{y}_1 + {}^3\mathbf{V}\,\sqrt{1-u^2}\,\mathbf{y}_2\right), \qquad 0 \le u \le 1, \qquad (6.11) $$

with $\varepsilon \ll 1$, characterizes a slithering motion that is expressed by continuously varying the parameter u. In the inception and through all the range of the branch S_{tb} one of the two proper numbers that vanished at the bifurcation point remains in its zero value;

---

[7]In the sense that the distances between adjacent sites along the axial curve are equal.

the proper number associated with it corresponds to a neutral slithering variation.

The additional identically zero proper number of $\bar{\mathbf{S}}$ is pertained to a rank deficit of the jacobian matrix $\mathbf{J}$. Such singularity of $\mathbf{J}$ was numerically overcome by the introduction of a (slack) constraint in which one of the kinematical variables in the 1-st base-pair step is constraint to have a preassigned value. In such a way, a single choice of the infinitely many equilibrium configurations of equal energy is made, and, as a result, the Lagrange multiplier associated with such constraint must be zero.

The existence of the trivial solution ${}^3\boldsymbol{\alpha}_{\mathrm{ring}}$ of the system $\mathcal{S}$ of equations (3.7) for all values of c makes it possible to analyze the dependence on c of the following two quantities. The first quantity is the normalized radius of gyration, $R_{\mathrm{g}}/R_{\mathrm{ring}}$, that is the ratio between the radius of gyration of a configuration to the radius of the ring configuration, R_{ring}. The radius of gyration of a closed DNA molecule is here defined as,

$$R_{\mathrm{g}} = \left(\frac{1}{N} \sum_{n=1}^{N} (\mathbf{x}^n - \bar{\mathbf{x}}) \cdot (\mathbf{x}^n - \bar{\mathbf{x}}) \right)^{1/2}, \quad \bar{\mathbf{x}} = \frac{1}{N} \sum_{n=1}^{N} \mathbf{x}^n. \tag{6.12}$$

The second quantity is the difference between the total energy, U, of a configuration and the total energy, U_{ring}, of the ring configuration, where both energies are calculated at the same salt concentration c. Two bifurcation diagrams showing the dependence of $R_{\mathrm{g}}/R_{\mathrm{ring}}$ and $U - U_{\mathrm{ring}}$ on c are shown in Figures 6.4 and 6.5. In Figure 6.4 several representative equilibrium configurations are drawn near the corresponding branches.

Figure 6.5 shows that for values of c less than $2.32 \times 10^{-3}\,\mathrm{M}$ the ring configurations are the global minimizers of the total energy and for values of c in the range $2.32 \times 10^{-3} < c < 3.48 \times 10^{-2}\,\mathrm{M}$ the buckled ring configurations in $\mathrm{S_{tb}}$ are the global minimizers of U.

In the range $2.32 \times 10^{-3} < c < 1.34 \times 10^{-1}\,\mathrm{M}$ the configurations in the branch $\mathrm{S_{tb}}$ are stable, while in the range $c > 1.34 \times 10^{-1}\,\mathrm{M}$ they are unstable. At the bifurcation point $(c = 1.34 \times 10^{-1}, \lambda_1 = 0)$ two proper numbers of $\bar{\mathbf{S}}$ vanish and give rise to two secondary branches that issue from it. The proper vectors associated with the two vanishing proper numbers characterize two different variations that break the symmetry
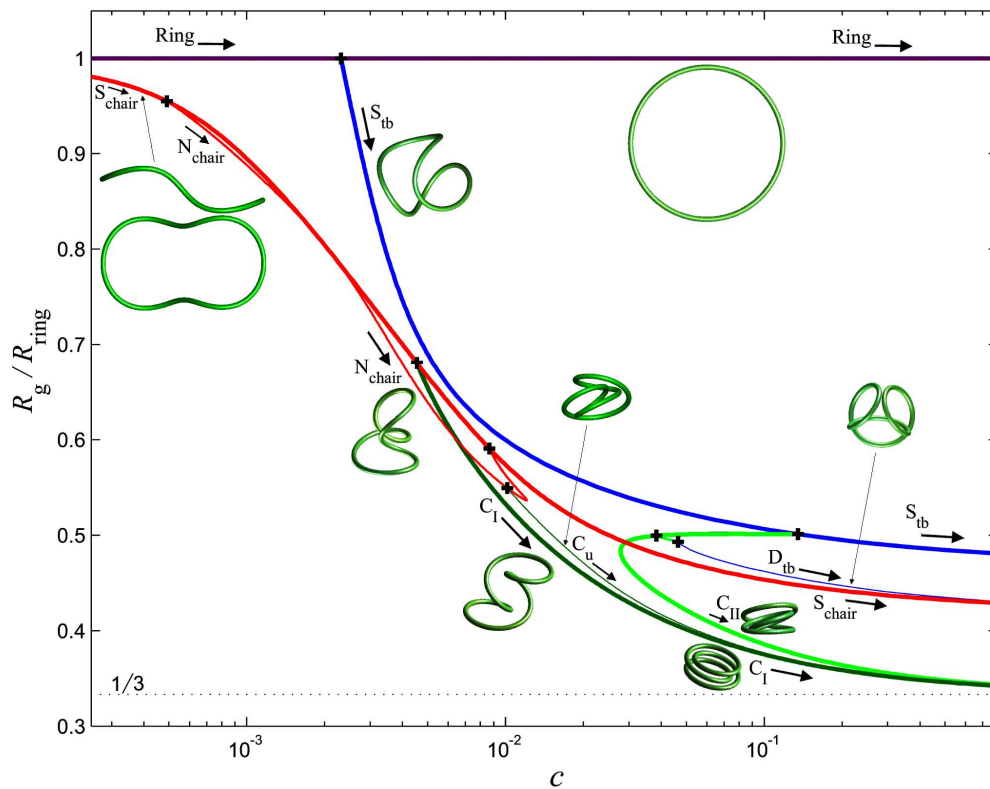
Figure 6.4: Bifurcation diagram showing $R_\mathrm{g}/R_\mathrm{ring}$ versus c of the closed 549 base pair DNA molecule $\mathcal{H}550$. Bifurcation points are indicated by the symbol "$+$".

of the buckled ring configuration. In the first case the variation is such that, when the configuration is viewed in a direction that is perpendicular to one of the mirror symmetry planes (as in the top views of the configurations shown in Figure 6.3), the two points of closest approach (i.e., the two lowest points seen in such view,) are moving vertically in opposite directions, and, as a result, the equilibrium configurations lose one of the two planes (of reflection) symmetry. In the second case, when the configuration is viewed in the same way, the two points of closest approach are moving in parallel to the line of view, but in opposite directions. The two secondary branches that originate at the bifurcation point are labeled D_tb and C_II. The configurations in the branch D_tb have a single mirror symmetry plane, and they are unstable through almost all the range of c in which they are exist. In the small range between the turning point $(c=4.63 \times 10^{-2},\ \lambda_1 = 0)$ and the bifurcation point $(c=4.66 \times 10^{-2},\ \lambda_1 = 0)$ the
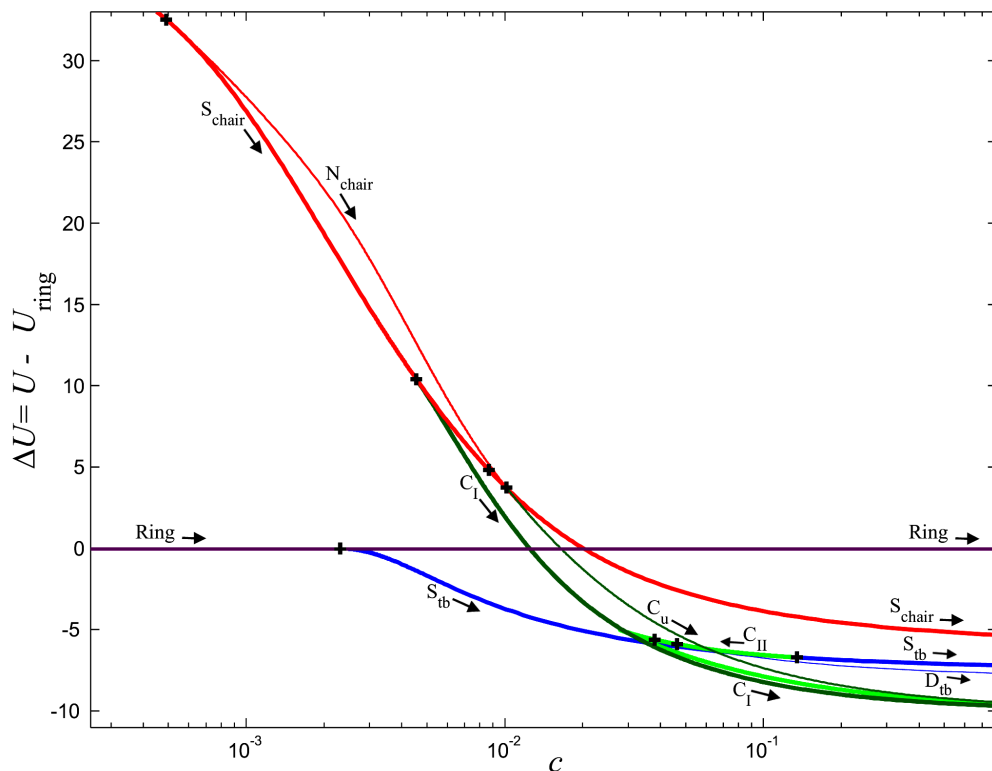
Figure 6.5: Bifurcation diagram showing $\Delta U = U - U_{\text{ring}}$ versus c of the closed 549 base pair DNA molecule $\mathcal{H}550$. Bifurcation points are indicated by the symbol "$+$".

configurations in D_{tb} are stable. Five configurations in this branch are shown in Figure 6.6.

The configurations in the branch C_{II} have a "hidden" symmetry. [8] The axial curves of these configurations have a two-fold (proper) rotation symmetry. If one follows the secondary branch C_{II} from the bifurcation point $(c=1.34 \times 10^{-1}, \lambda_1 = 0)$ in the direction indicated by the arrows in Figure 6.2 one encounters first the bifurcation point $(c=3.80 \times 10^{-2}, \lambda_1 = -3.74 \times 10^{-2})$ at which $\lambda_2 = 0$ and then the turning point $(c=2.78 \times 10^{-2}, \lambda_1 = 0)$ across which the configurations in C_{II} are stable. As can be observed from Figure 6.4 and the six equilibrium configurations in Figure 6.7, the stable configurations are collapsing to a shape of triply wound configurations with radii

---

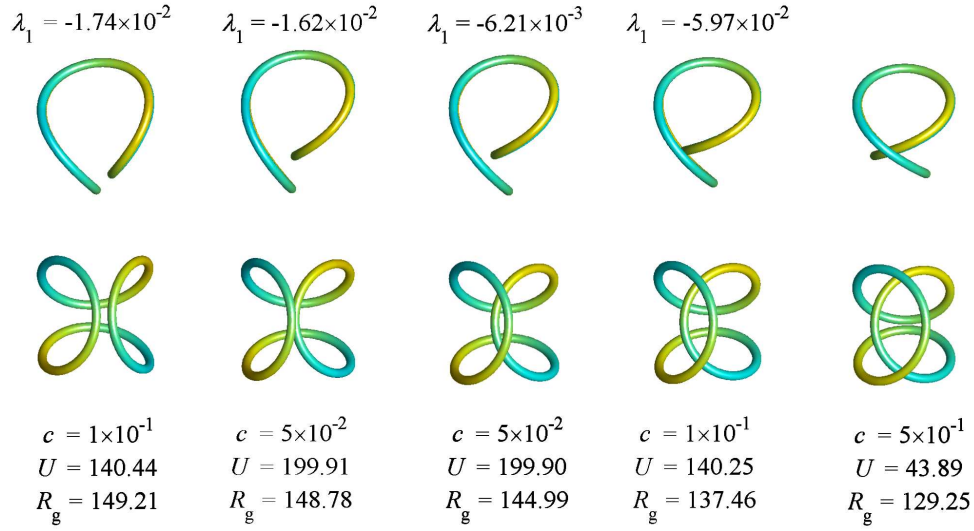[8]In the sense in which the term is used in reference [44].

Figure 6.6: Five configurations of $\mathcal{H}550$ in the branch D_{tb}. The values of λ_1 are indicated in cases in which two distinct equilibrium configurations occur at the same value of c.

of gyration that are approaching to almost one third of R_{ring} as c is increasing.

The branch labeled DC connects the bifurcation point $(c{=}4.66 \times 10^{-2},\ \lambda_1{=}\ 0)$ in the secondary branch D_{tb} to the bifurcation point $(c{=}3.80 \times 10^{-2},\ \lambda_1{=}{-}3.74 \times 10^{-2})$ in the secondary branch C_{II}. A configuration in an intermediate value of c in the range of that branch is shown in Figure 6.8.

Through experimenting with a closed elastic ring it is easy to see that by applying a (twist) torque on one side of the ring while anchoring the opposite side one can get an equilibrium configuration that has a shape of a chair. Charitat and Fourcade [45] treated symmetric[9] chair configurations of an o-ring and analyzed their stability as function of the ratio between the twist modulus and the bending modulus. Symmetric chair configurations of a homogeneous, transversely isotropic, 150 base pair DNA o-ring were calculated, without taking the electrostatic energy into account, in reference [1]. In their study Coleman, Olson, and Swigon [1] has found that the (symmetric) chair configurations are stable when the ratio F^n_{33}/F^n_{11} is less than 1. These observations led

---

[9]In the sense that the configurations have not only an axis of two-fold proper rotation symmetry and an axis of two-fold improper rotation symmetry but also have a mirror symmetry plane.
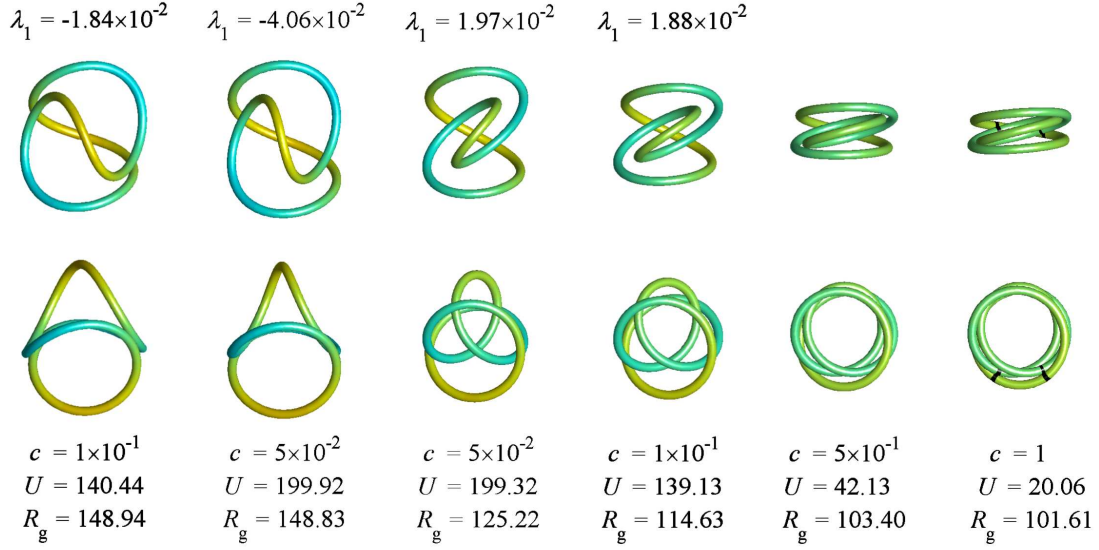
$\lambda_1 = -1.84 \times 10^{-2}$ $\lambda_1 = -4.06 \times 10^{-2}$ $\lambda_1 = 1.97 \times 10^{-2}$ $\lambda_1 = 1.88 \times 10^{-2}$

$c = 1 \times 10^{-1}$	$c = 5 \times 10^{-2}$	$c = 5 \times 10^{-2}$	$c = 1 \times 10^{-1}$	$c = 5 \times 10^{-1}$	$c = 1$
$U = 140.44$	$U = 199.92$	$U = 199.32$	$U = 139.13$	$U = 42.13$	$U = 20.06$
$R_g = 148.94$	$R_g = 148.83$	$R_g = 125.22$	$R_g = 114.63$	$R_g = 103.40$	$R_g = 101.61$

Figure 6.7: Six configurations of $\mathcal{H}550$ in the branch C_{II}. The values of λ_1 are indicated in cases in which two distinct equilibrium configurations occur at the same value of c. The two lines of view are perpendicular. The configurations in the upper row are viewed along the axis of (two-fold)rotation symmetry. The equilibrium configuration at $c = 1\,\mathrm{M}$ has points of self contact; each of the 4 darkened subsegments in that configuration contains two adjacent base pairs that have points of contact.

to a search for an equilibrium chair configuration of the molecule $\mathcal{H}550$.

The calculation of an initial chair configuration from which one can explore a set of connected branches was performed by starting with a ring configuration at a low enough salt concentration, say $c = 1 \times 10^{-2}\,\mathrm{M}$, and varying the end-to-end twist ζ_3 as the bifurcation parameter while c is fixed. This calculation was performed up to the point in which $\zeta_3/2\pi$ attained the value of -1. The corresponding equilibrium configuration has a form of a doubly wound ring and for it $\Delta L_k = -1$. At this step the following transformation was applied on that configuration,

$$
\begin{aligned}
\theta_i^n &\mapsto \theta_i^{n+m} & \text{for } n = 1, ..., N-m; \\
\theta_i^n &\mapsto \theta_i^{n-(N-m)} & \text{for } n = (N-m+1), ..., N+1,
\end{aligned}
\tag{6.13}
$$

with $i = 1, 2, 3$ and $m = 275$. The transformation (6.13) introduces a change in the choice of the 1-st and $(N+1)$-th base pairs and, since $\mathcal{H}550$ is homogenous and $\mu = 3$, the transformed configuration is an equilibrium configuration. Finally, the end-to-end
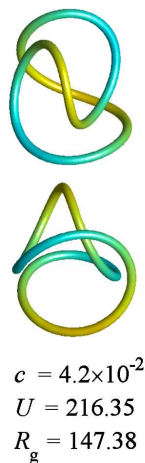
$c = 4.2 \times 10^{-2}$
$U = 216.35$
$R_g = 147.38$

Figure 6.8: A selected configuration of $\mathcal{H}550$ in the branch DC.

twist ζ_3 was gradually varied from -2π back to 0 to yield a symmetric chair equilibrium configuration with zero excess link. In a case of a continuous elastic rod the process just described is similar to the process resulted by the following steps: (1) Cut the closed rod, hold one end fixed and (positively) twist the other end by a full turn. (2) Reseal the ends and cut the rod in the cross section that originally was in the opposite side of the ring configuration. (3) While holding one end apply a negative twist of a full turn to the other end such that the excess link of the resulted configuration is zero.

Starting with a symmetric chair configuration in the branch, labeled $\mathrm{S_{chair}}$, containing symmetric chair configurations was explored for all range of values of c. The branch $\mathrm{S_{chair}}$ is not connected to the stem branch Ring (or to any of the branches that are connected to the stem branch) in a bifurcation diagram in which c is the bifurcation parameter. But as the two branches $\mathrm{S_{chair}}$ and Ring are connected in a bifurcation diagram in which ζ_3 is the bifurcation parameter the branch $\mathrm{S_{chair}}$ can be considered as a primary branch. For the molecule $\mathcal{H}550$ the symmetric chair configurations are stable only for values of c less than $4.54 \times 10^{-3}\,\mathrm{M}$. Six symmetric chair configurations are shown in Figure 6.9.

The secondary branch $\mathrm{C_I}$ originates at the bifurcation point $(c = 4.54 \times 10^{-3},\ \lambda_1 = 0)$. The configurations in $\mathrm{C_I}$ have a two-fold improper reflection symmetry (with no mirror
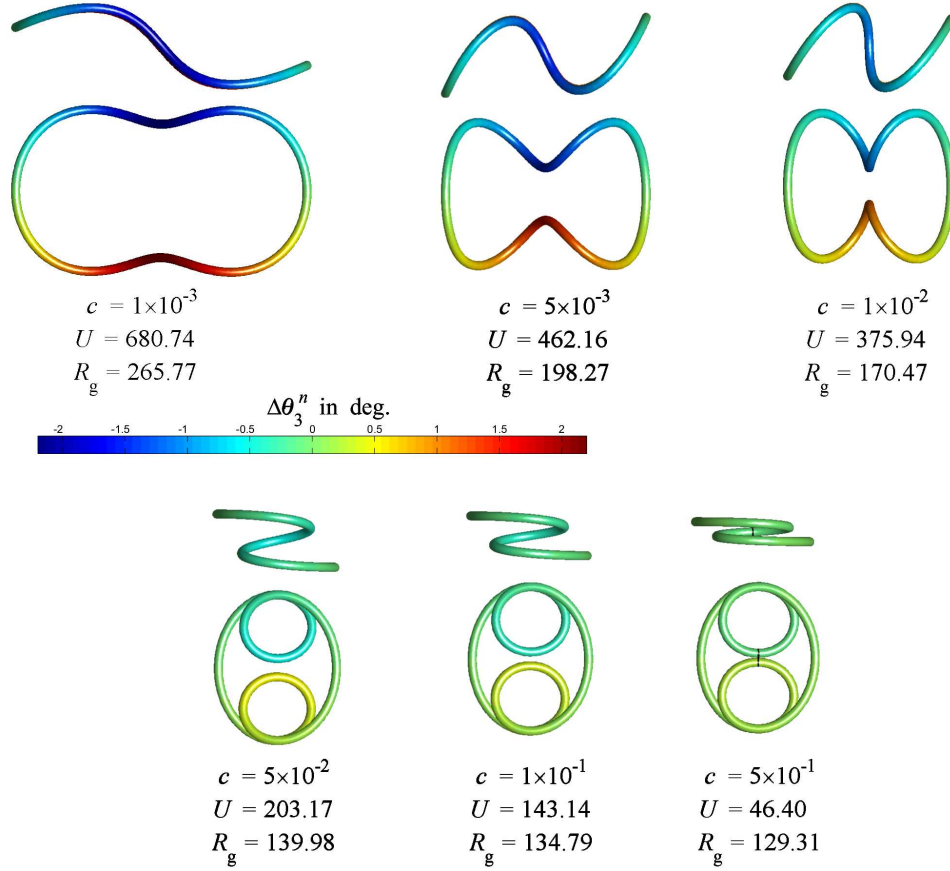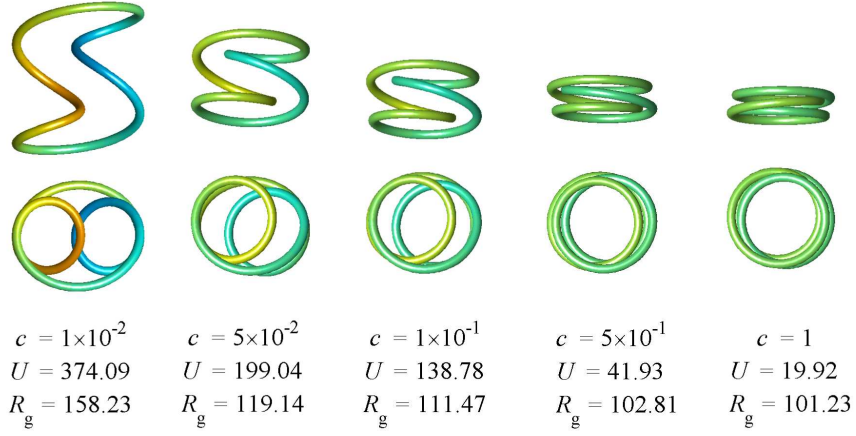
Figure 6.9: Six symmetric "chair" configurations of $\mathcal{H}550$ in the branch $\mathrm{S_{chair}}$. The numeric value of the excess twist in each base-pair step, that is indicated by assigning a color to each value of $\Delta\theta_3^n$ can be deduced from the color-bar.

symmetry plane), and they are always stable. As c is increasing the equilibrium configuration in $\mathrm{C_I}$ have axial curves of the form of a triply wound collapsed ring made of two approximately helical regions of opposite handedness. As can be seen in Figure 6.5 the configurations in $\mathrm{C_I}$ are the global minimizers of U only for values of c greater than $c_\mathrm{J}{=}3.48 \times 10^{-2}\,\mathrm{M}$. This implies (see Figure 6.4) that a small change in c from a value slightly below to a value above c_J may result an abrupt reduction of 21.4% in R_g due to a transition from a buckled ring configuration in $\mathrm{S_{tb}}$ to a collapsed triply wound configuration in $\mathrm{C_I}$. Four globally stable configurations and one locally stable configuration in the branch $\mathrm{C_I}$ are shown in Figure 6.10.

A secondary branch labeled $\mathrm{N_{chair}}$ connects the two additional bifurcation points $(c{=}4.92 \times 10^{-4},\ \lambda_1{=}\ 0)$ and $(c{=}8.67 \times 10^{-3},\ \lambda_1{=}{-}2.37 \times 10^{-1})$ in the primary branch

$$c = 1 \times 10^{-2} \qquad c = 5 \times 10^{-2} \qquad c = 1 \times 10^{-1} \qquad c = 5 \times 10^{-1} \qquad c = 1$$
$$U = 374.09 \qquad U = 199.04 \qquad U = 138.78 \qquad U = 41.93 \qquad U = 19.92$$
$$R_g = 158.23 \qquad R_g = 119.14 \qquad R_g = 111.47 \qquad R_g = 102.81 \qquad R_g = 101.23$$

Figure 6.10: Five stable configurations of $\mathcal{H}550$ in the branch C_I. With the exception of the configuration on the left hand side, for which $c = 1 \times 10^{-2}$ M, all other four configurations are global minimizers of U.

S_{chair}. All the configurations in N_{chair} are unstable. Four configurations in N_{chair} are shown in Figure 6.11. The bifurcation point $(c=1.01 \times 10^{-2}, \lambda_1 = -9.30 \times 10^{-3})$ in the branch N_{chair} gives rise to the inception of the tertiary branch labeled C_u of unstable, triply-wound, collapsed-ring configurations. Three configurations in the branch C_u are shown in Figure 6.12.
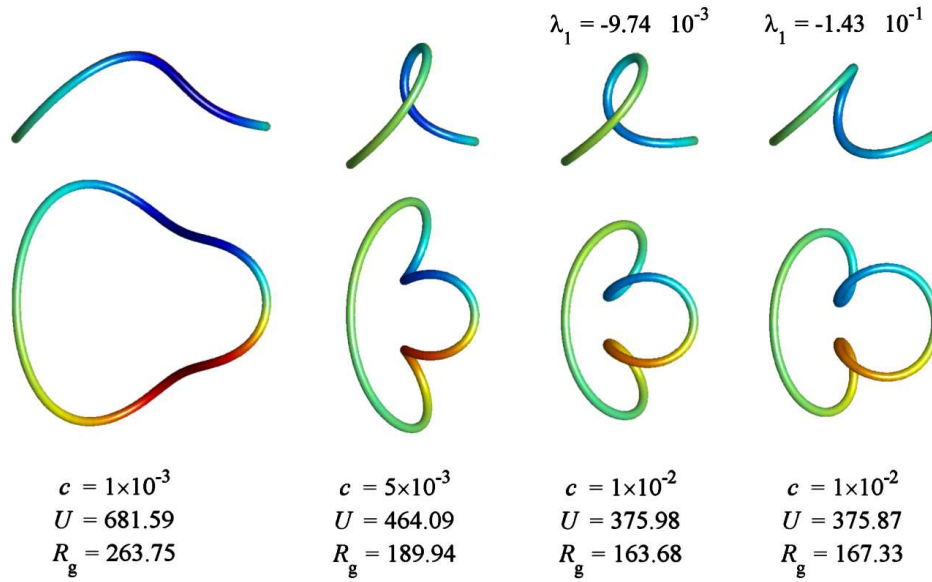
$\lambda_1 = -9.74 \ 10^{-3}$ $\lambda_1 = -1.43 \ 10^{-1}$

$c = 1\times10^{-3}$
$U = 681.59$
$R_g = 263.75$

$c = 5\times10^{-3}$
$U = 464.09$
$R_g = 189.94$

$c = 1\times10^{-2}$
$U = 375.98$
$R_g = 163.68$

$c = 1\times10^{-2}$
$U = 375.87$
$R_g = 167.33$

Figure 6.11: Four configurations of $\mathcal{H}550$ in the branch N_{chair}. The values of λ_1 are indicated for the two configurations on the right hand side that correspond to points on the bifurcation diagram in Figure 6.2 above and below the turning point of the fold.
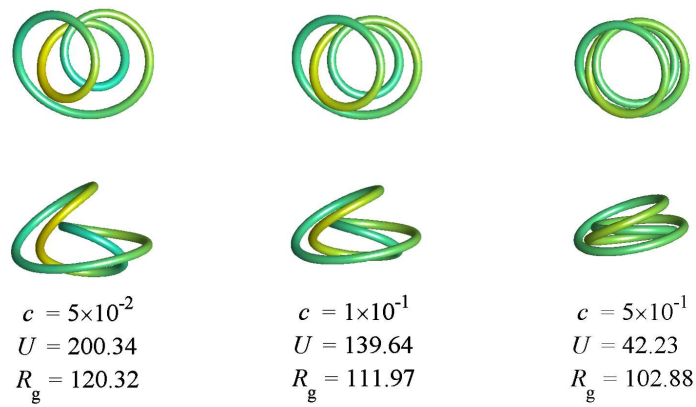

$c = 5\times10^{-2}$
$U = 200.34$
$R_g = 120.32$

$c = 1\times10^{-1}$
$U = 139.64$
$R_g = 111.97$

$c = 5\times10^{-1}$
$U = 42.23$
$R_g = 102.88$

Figure 6.12: Three unstable collapsed configurations of $\mathcal{H}550$ in the branch C_u.

6.2.2 The influence of changes in the intrinsic curvature and the ratio F_{33}^n/F_{11}^n on equilibrium configurations

In this subsection results from calculations of bifurcation diagrams of the molecules labeled $\mathcal{H}550_{270}$, $\mathcal{H}550_{0.7}$ and partial results of equilibrium configurations of the molecule $\mathcal{H}550_{1.4}$ are reported. As in the previous subsection all the calculations assume the 549 base pair molecules are confined to a zero excess link.

A bifurcation diagram of the molecule $\mathcal{H}550_{0.7}$ in which λ_1 is the dependent parameter and c is the bifurcation parameter is drawn (solid lines) next to the bifurcation diagram of $\mathcal{H}550$ (dashed lines) in Figure 6.13. As can be seen, a change in F_{33}^n/F_{11}^n
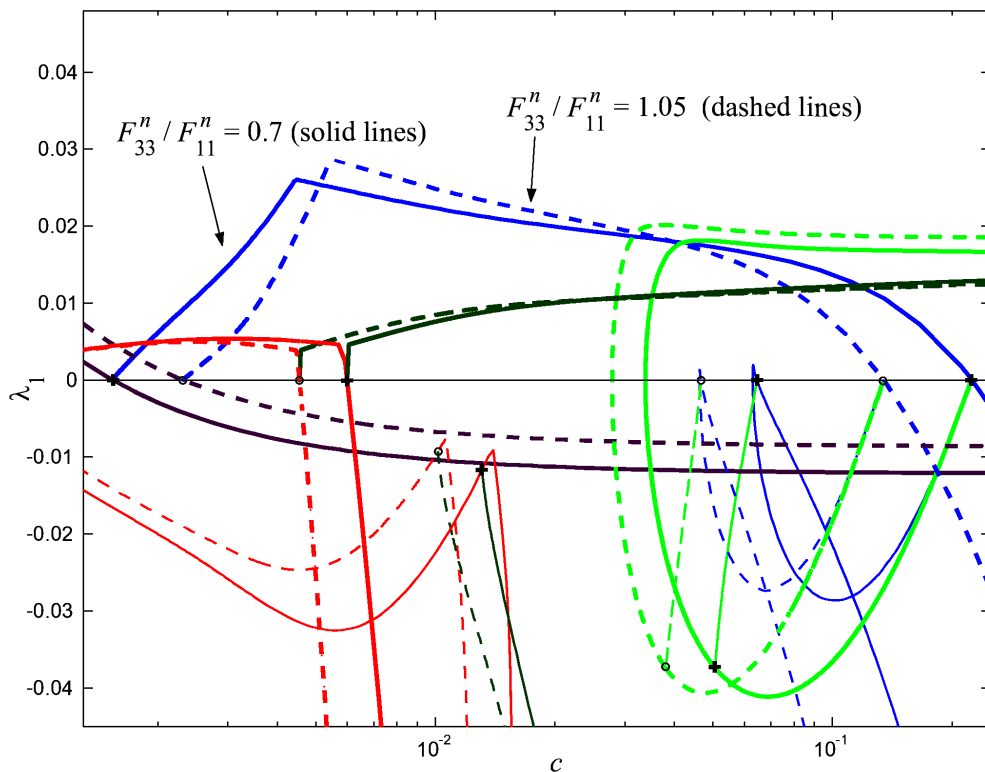

Figure 6.13: A bifurcation diagrams of λ_1 versus c of the molecules $\mathcal{H}550$ (dash lines) and $\mathcal{H}550_{0.7}$ (solid lines) showing the influence of the ratio F_{33}^n/F_{11}^n on the results. The different branches are drawn with the same colors as in Figure 6.2. Bifurcation points are indicated by the symbol "+" for the molecule $\mathcal{H}550_{0.7}$ and by the symbol "o" for $\mathcal{H}550$.

yields no difference in the topology of the diagram. However, because the cost of twisting energy is reduced when F_{33}^n/F_{11}^n is decreased one can expect, as was found here,

a shift towards lower value of c of the bifurcation point, from which the branch $\mathrm{S_{tb}}$ of buckled ring configurations originates. Furthermore, as the buckled ring configurations have regions with higher magnitude of excess twist than the collapsed configurations in the branch $\mathrm{C_{II}}$, the bifurcation point in $\mathrm{S_{tb}}$ from which the branch $\mathrm{C_{II}}$ originates is shifted towards higher values of c as F_{33}^n/F_{11}^n is decreasing. Similarly, as F_{33}^n/F_{11}^n is decreased a shift of the bifurcation point towards higher value of c, from which the branch $\mathrm{C_I}$ of triply wound collapsed configurations (that are characterized by a lower magnitude of twisting energy than the symmetric chair configurations in $\mathrm{S_{chair}}$) was found. For the molecules $\mathcal{H}550_{1.4}$, $\mathcal{H}550$ and $\mathcal{H}550_{0.7}$ the bifurcation points from which the branch $\mathrm{C_I}$ originates are $(c{=}3.89 \times 10^{-3},\ \lambda_1{=}0)$, $(c{=}4.54 \times 10^{-3},\ \lambda_1{=}0)$, and $(c{=}5.99 \times 10^{-3},\ \lambda_1{=}0)$ respectively.

Two bifurcation diagrams exhibiting the dependence of $R_\mathrm{g}/R_\mathrm{ring}$ and ΔU on c of the molecule $\mathcal{H}550_{0.7}$ are shown in Figures 6.14 and 6.15. The two diagrams, when compared to the diagrams shown in Figures 6.4 and 6.5, reveal that a change in F_{33}^n/F_{11}^n yields no qualitative difference in the results. The minimum energy configurations vary with c from the ring configurations for low values of c to the buckled ring configurations (in the branch $\mathrm{S_{tb}}$) for values in an intermediate range of c and to the triply wound collapsed configurations in the branch $\mathrm{C_I}$.

To demonstrate the effects of a change in the intrinsic curvature the molecule $\mathcal{H}550_{270}$ was thoroughly studied. Each 270 base pair subsegment of $\mathcal{H}550_{270}$ forms a perfectly circular ring when stress free. Two bifurcation diagrams of that molecule depicting $R_\mathrm{g}/R_\mathrm{ring}$ and ΔU versus c are shown in Figures 6.16 and 6.17. The pitchfork bifurcation of equilibria of the molecule $\mathcal{H}550$ from the branch of ring configurations to the branch $\mathrm{S_{tb}}$ turns into a subcritical pitchfork when equilibria of the molecule $\mathcal{H}550_{270}$ are considered. This change suggests that a slight increase from a value less than $c{=}1.09{\times}10^{-1}\,\mathrm{M}$ to a value above it may result a significant reduction of circa 48% in the radius of gyration. However, as can be seen in Figure 6.17 the energy difference between the ring configuration and the buckled ring configuration at
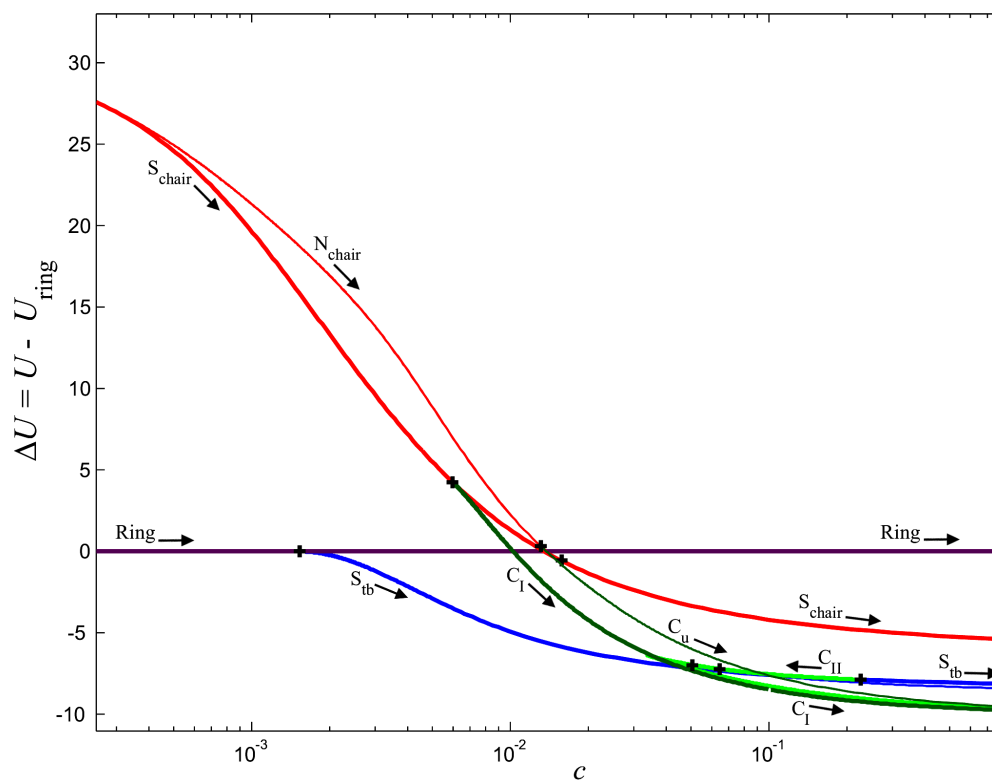
Figure 6.14: A bifurcation diagram showing $R_{\mathrm{g}}/R_{\mathrm{ring}}$ versus c of the molecule labeled $\mathcal{H}550_{0.7}$.

$c = 1.09 \times 10^{-1}\,\mathrm{M}$ is less than $0.2\,k_{\mathrm{B}}\,T$. Thus, in a thermal equilibrium an ensemble of molecules obeying the Boltzmann distribution would have an almost equal distribution of the configurations that are closely related to the ring configuration and the configurations with a shape similar to the collapsed rings.

To conclude this subsection five equilibrium configurations, including the (presumably) minimum energy configurations of the molecules $\mathcal{H}550_{0.7}$, $\mathcal{H}550_{1.4}$ and $\mathcal{H}550_{270}$ at $c = 1 \times 10^{-1}\,\mathrm{M}$, are shown in Figure 6.18. The resemblance between the minimum energy configuration of the molecules $\mathcal{H}550_{0.7}$ and $\mathcal{H}550_{1.4}$ may explain why an experimental determination of the average value of F_{33}^{n}/F_{11}^{n} is still a complicated task that often yield values ranging from 0.7 to 1.6. [10]

---

[10]See the remark made in footnote 48 of reference [1].

Figure 6.15: Bifurcation diagram showing $\Delta U = U - U_{\text{ring}}$ versus c of the molecule labeled $\mathcal{H}550_{0.7}$.
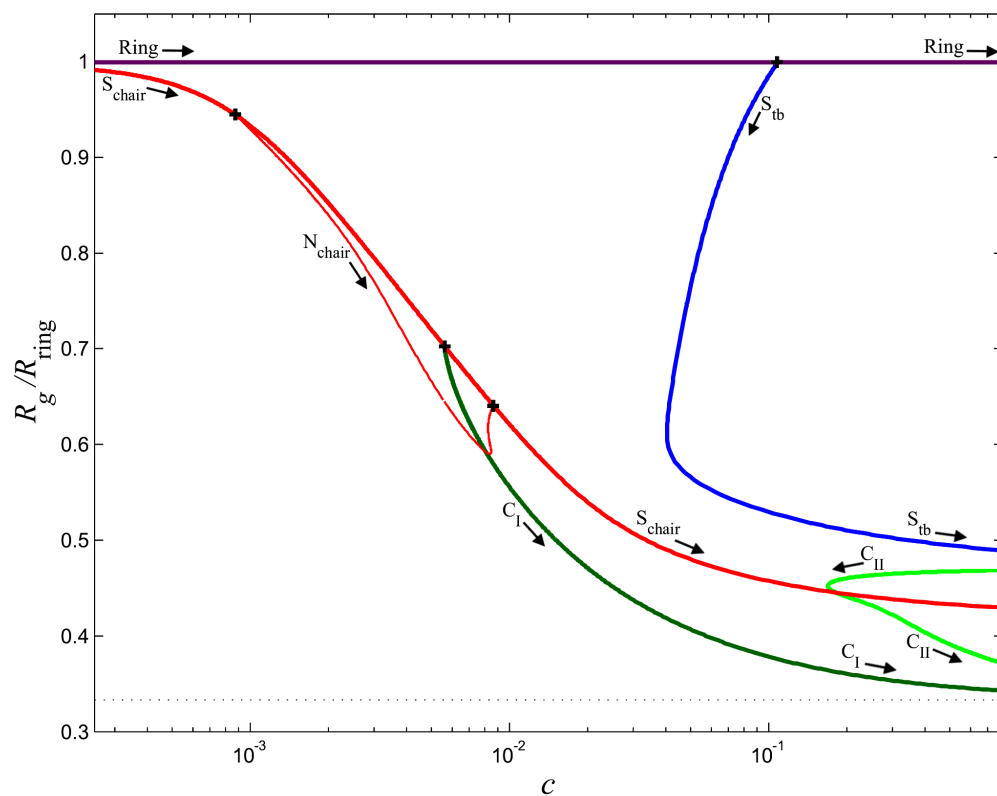
Figure 6.16: A bifurcation diagram showing R_g/R_ring versus c of the molecule labeled $\mathcal{H}550_{270}$.
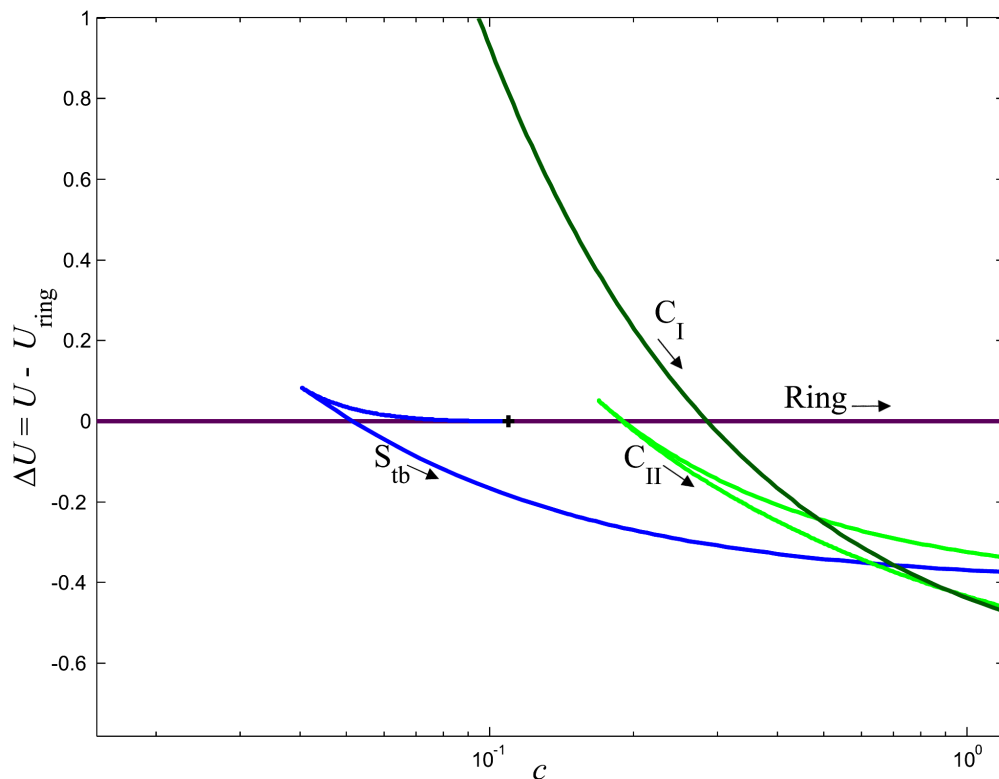
Figure 6.17: A bifurcation diagram showing $\Delta U = U - U_{\text{ring}}$ versus c of the molecule labeled $\mathcal{H}550_{270}$.
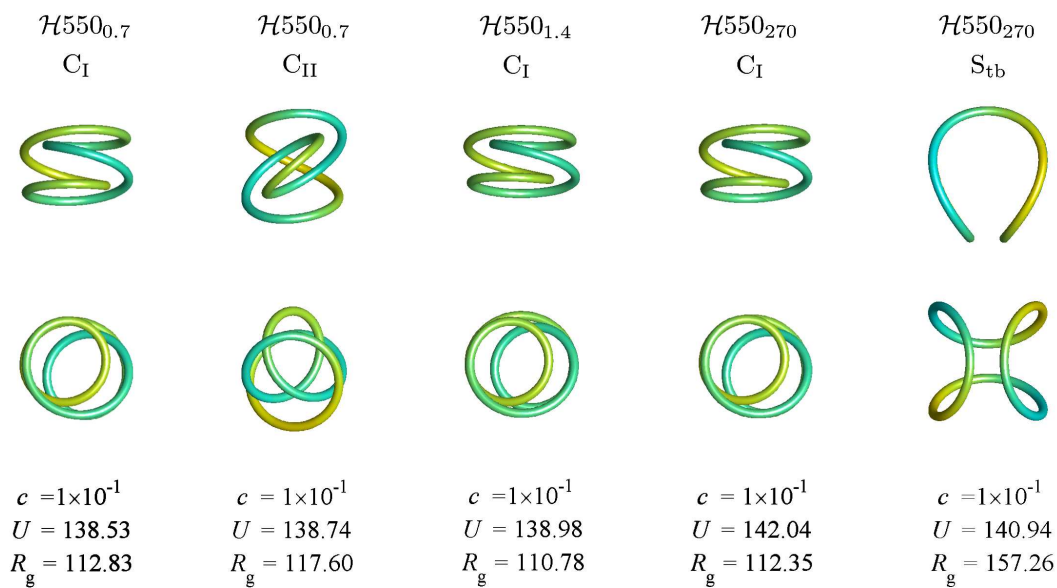

Figure 6.18: Five stable configurations of the molecules $\mathcal{H}550_{0.7}$, $\mathcal{H}550_{1.4}$, and $\mathcal{H}550_{270}$ at $c = 1 \times 10^{-1}$ M. The labels of the molecule and the branch type are indicated above the two perpendicular views showing each of the configurations.

6.2.3 Bifurcations of equilibria of $\mathcal{H}550$ with $\Delta L_{\mathrm{k}} = -1$

To investigate the dependence of equilibrium configurations of the closed molecule $\mathcal{H}550$, that is confined to $\Delta L_{\mathrm{k}} = -1$, several pre-calculated closed equilibrium configurations of zero excess link were chosen to be the initial configurations in explorations of branches of equilibria in which the end-to-end twist angle, ζ_3, is the bifurcation parameter and c is fixed. In such branches the configurations with $\zeta_3/2\pi = -1$, i.e., $\Delta L_{\mathrm{k}} = -1$, were used as initial configurations for the calculation of branches of equilibria in which c is the bifurcation parameter. When one varies ζ_3 one can set the choice of the base pairs for which $n = 1$ and $n = N+1$ by applying the transformation 6.13 with m in the range $1, ..., N-1$.

The branch of minimum energy configurations of $\mathcal{H}550$ with $\Delta L_{\mathrm{k}} = -1$ was found by starting with the ring configuration for which $\Delta L_{\mathrm{k}} = 0$, fixing c and calculating, using the continuation methods described in section 4.4, a branch of equilibria in which ζ_3 is the bifurcation parameter. As was discussed in subsection 6.2.1 an initial configuration in this branch can also be calculated by starting with a symmetric chair configuration, setting the base pair for which $n = 1$ to be one of the two adjacent base pairs that form the base-pair step with maximum value of excess twist, and appropriately varying ζ_3. As indicated in the bifurcation diagram of λ_1 versus c shown in Figure 6.19 the stem branch of minimum energy configurations (drawn in solid blue) is above the zero for all values of c which implies that no other branches are connected to it. The configurations in the stem branch are characterized by an internal loop with an approximate form of a left handed helix and an external loop of opposite handedness. As c is increasing the configurations in this branch acquire compact forms of doubly wound rings with radius of gyration that approaches $0.5 R_{\mathrm{ring}}$. This effect is depicted in Figure 6.20 in which a bifurcation diagram of $R_{\mathrm{g}}/R_{\mathrm{ring}}$ versus c is shown with four stable configurations, two of which are doubly wound rings, that correspond to the points indicated by arrows.

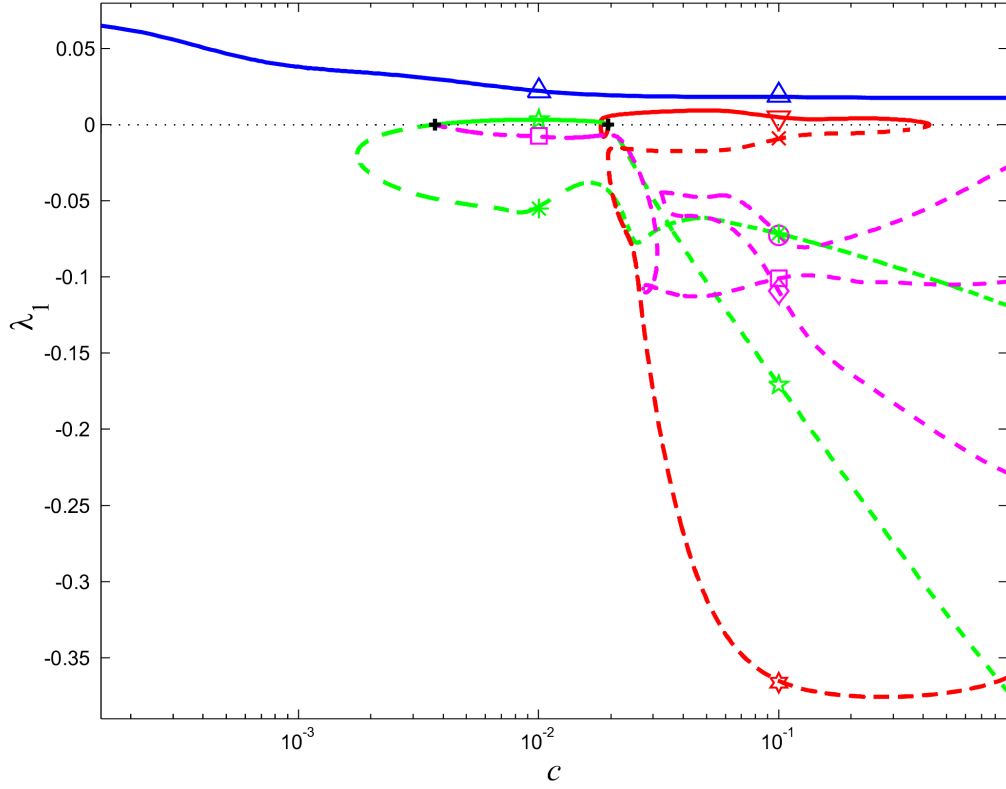An initial configuration in a separate system of connected branches was found in

Figure 6.19: A bifurcation diagram of λ_1 versus c for equilibrium configurations of $\mathcal{H}550$ with $\Delta L_{\mathrm k} = -1$. The symbol "**+**" indicates a bifurcation point. All other symbols indicate configurations that are shown in figures 6.21 and 6.22. Regions of branches with $\lambda_1 > 0$, (which correspond to stable configurations) are drawn with solid lines, while regions with $\lambda_1 < 0$ are drawn with dashed lines.

the same way by starting with a collapsed ring configuration of $\mathcal{H}550$ with $\Delta L_{\mathrm k} = 0$ and appropriately varying ζ_3. A branch, drawn in green in Figures 6.19 and 6.20, with configurations like the middle configuration shown in the upper half of Figure 6.20 (the one next to the origin of an arrow pointing to a point at which $c = 1 \times 10^{-2}\,\mathrm{M}$), was found to have a range of c with stable configurations between the two bifurcation points $(c = 3.67 \times 10^{-3}, \lambda_1 = 0)$ and $(c = 1.95 \times 10^{-2}, \lambda_1 = 0)$. The configurations in this branch have a two-fold (proper) rotation symmetry. The bifurcation point, $(c = 3.67 \times 10^{-3}, \lambda_1 = 0)$, gives rise to the inception of a branch, drawn in purple in Figures 6.19 and 6.20, that contains only unstable configurations. An additional branch, originating at the second bifurcation point $(c = 1.95 \times 10^{-2}, \lambda_1 = 0)$, is drawn
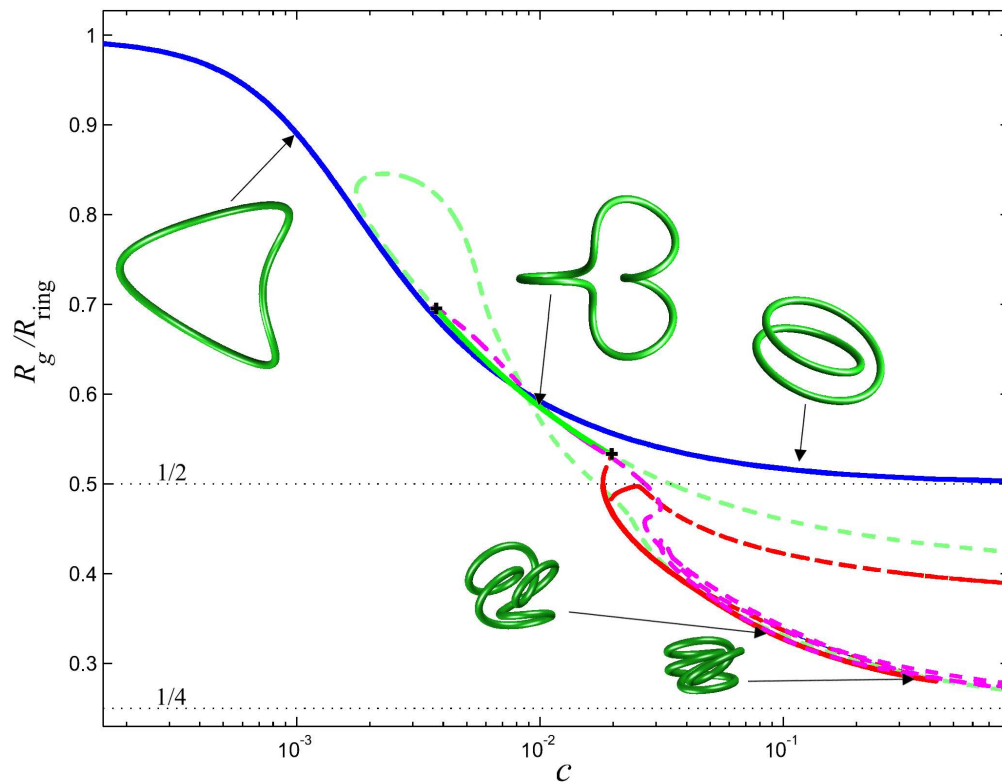
Figure 6.20: A bifurcation diagram showing R_g/R_{ring} versus c of $\mathcal{H}550$ with $\Delta L_k = -1$. The symbol "**+**" indicates a bifurcation point. Regions of branches with points that correspond to stable configurations are drawn as solid lines. Dashed lines indicate regions with unstable configurations. The colors of the branches are in accord with figure 6.19. The drawn equilibrium configurations are stable and their corresponding points are indicated by the arrows.

in red in Figures 6.19 and 6.20. It contains stable configurations in the range of c between the turning points ($c=1.80 \times 10^{-2}$, $\lambda_1 = 0$) and ($c=4.24 \times 10^{-1}$, $\lambda_1 = 0$). As can be observed in Figure 6.20 the three connected branches contain subregions with highly compact configurations. As c is increasing (above 2×10^{-2} M) the configurations in these subregions acquire shapes of quadruply wound configurations that, for high values of c, their radii of gyration approach $0.25 R_{ring}$. All the distinct equilibrium configurations at $c = 1 \times 10^{-1}$ M and $c = 1 \times 10^{-2}$ M are shown in Figures 6.21 and 6.22.
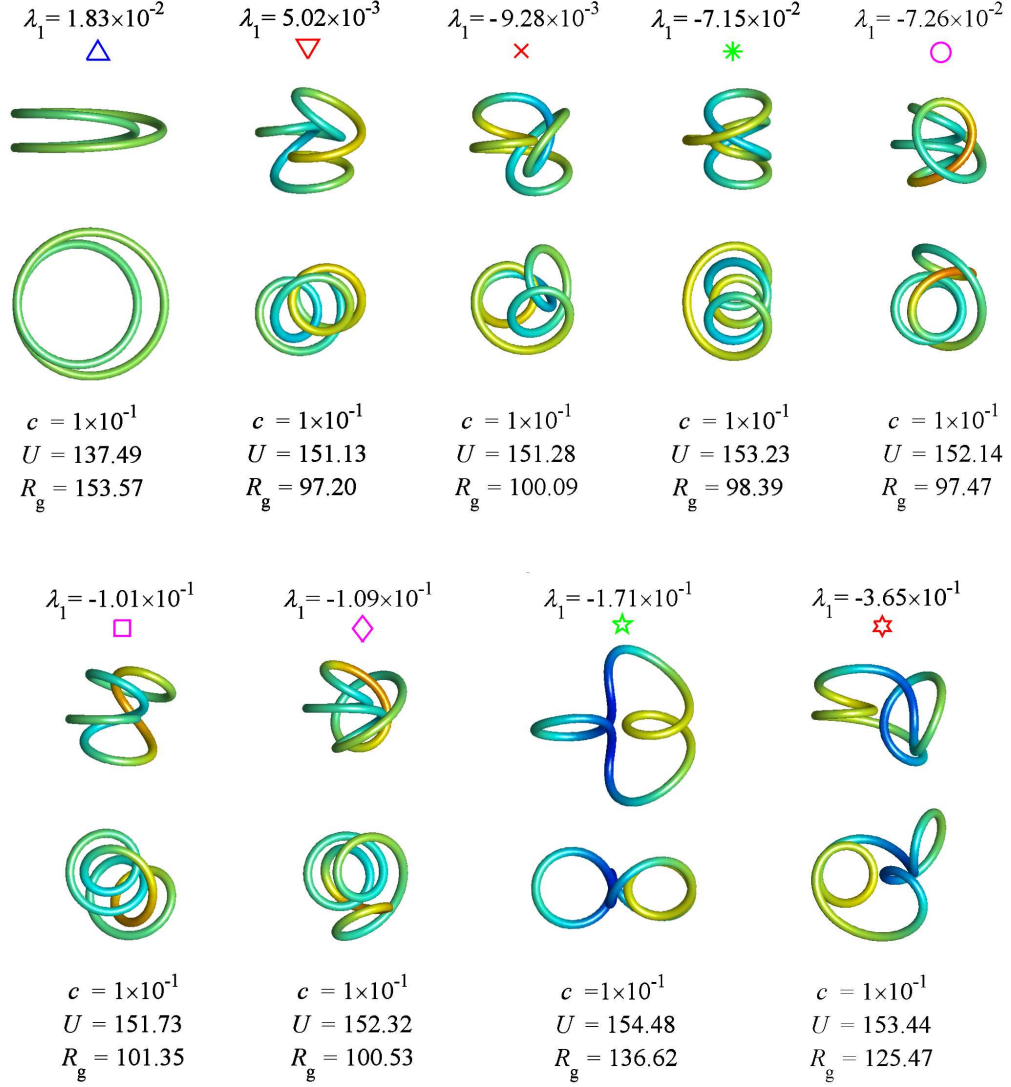
Figure 6.21: Nine configurations of $\mathcal{H}550$ with $\Delta L_k = -1$ at $c = 1 \times 10^{-1}$ M. Each configuration is drawn in two perpendicular views. The color of the cylindrical tube indicates the local excess twist in accord with the color-bar shown in figure 6.9. The color symbols (markers) indicate the location of the corresponding points in the bifurcation diagram 6.19. The doubly wound configuration on the upper left corner (blue triangle pointing upward) is the global minimizer of the total energy.
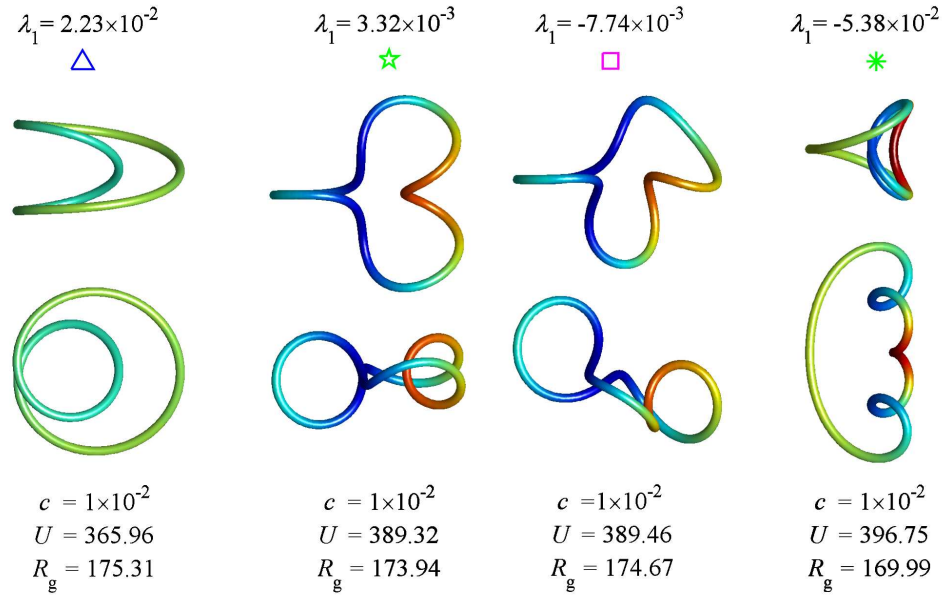
Figure 6.22: Four configurations of $\mathcal{H}550$ with $\Delta L_k = -1$ at $c = 1 \times 10^{-2}$ M. The color symbols (markers) indicate the location of the corresponding points in the bifurcation diagram 6.19. The doubly wound configuration on the upper left corner (blue triangle pointing upward) is the global minimizer of the total energy.

6.3 Equilibria of a nonhomogeneous 339 base pair minicircle DNA

In their recent research Fogg, Kolmakova, Rees, Magonov, Hansma, Perona, and Zechiedrich [20] were able to generate and isolate large quantities of several distinct topoisomers,[11] of a closed 339 base pair DNA molecule. The treated molecule, here labeled $\mathcal{Z}339$, has the following sequence:

```
TTTATACTAACTTGAGCGAAACGGGAAGGGTTTTCACCGATATCACCGAA
ACGCGCGAGGCAGCTGTATGGCGAAATGAAAGAGTTCTTCCCGGAAAACG
CGGTGGAATATTTCGTTTCCTACTACGACTACTATCAGCCGGAAGCCTAT
GTACCGAGTTCCGACACTTTCATTGAGAAAGATGCCTCAGCTCTGTTACA
GGTCACTAATACCATCTAAGTAGTTGATTCATAGTGACTGCATATGTTGT
GTTTTACAGTATTATGTAGTCTGTTTTTTATGCAAAATCTAATTTAATAT
ATTGATATTTATATCATTTTACGTTTCTCGTTCAGCTTT
```

---

[11] DNA topoisomers are molecules with identical sequence that differ only in their linking number.

in which the first and the last base pairs form a base-pair step. The topoisomers obtained in their experiments were examined using gel electrophoresis and atomic force microscopy (AFM). The results suggested the existence of topoisomers with linking numbers varying from $L_k = 32$ down to highly supercoiled minicircles with $L_k = 26$.

Thus, to conclude the present chapter, a calculation of equilibrium configurations of the molecule treated in [20], for several values of L_k and with $\mu = 6$ was performed. All the results in this example were calculated at $c = 1 \times 10^{-1}$ M. The values of the intrinsic parameters and elastic moduli associated with each of 10 unique base-pair steps are in accord with the database in the web-site [12]

`http://dnaserver.rutgers.edu/%7Eghzheng/db/search.php`

The values of the parameters were derived by statistical analysis of X-ray structure data [35] [46].

Starting with (kinematical) end conditions that are close enough to those of the intrinsic configuration, a series of equilibrium configurations of open molecules was calculated by successively varying the end conditions such that the final calculated configuration in the series is closed, i.e., obeys equations (6.1). With a closed equilibrium configuration in hand, the end-to-end twist angle ζ_3 was varied (as a bifurcation parameter) using the continuation methods described in section 4.4 to explore a single equilibrium path. In such equilibrium path, the value of $\zeta_3/2\pi$ may attain integral values that correspond to different values of L_k. The dependence of the total energy, U, on $\zeta_3/2\pi$ along the equilibrium path, that, based on a thorough study, is believed to contain the minimum energy configurations for each value of $\zeta_3/2\pi$, is shown in Figure 6.23.[13] The graph shows that, as was suggested in [20], $L_k = 32$ for the "most relaxed" closed configuration of $\mathcal{Z}339$.

The (presumably) minimum energy configurations of $\mathcal{Z}339$ with seven linking numbers varying from 29 to 35 are shown in Figure 6.24. The configurations with

---

[12]The web-site was constructed by Guohui Zheng from W.K. Olson's group at Rutgers University.

[13]The shown equilibrium path contains at least one stable configuration for each value of $\zeta_3/2\pi$.

$L_k = 29$ and $L_k = 35$ have points of self contact associated with base-pair steps that are represented by darkened cylindrical regions. As oppose to the previous examples in which the treated molecules were assumed homogenous and therefore the values of the total energy of their equilibrium configurations are practically indifferent to slithering modes, for the present example, the equilibrium configurations are highly sensitive to such modes. As a result, the proximity and relative orientation of sequentially remote sites (that might be in contact) is highly sequence-dependent. For the topoisomer with $L_k = 29$ there are two points of contact. The contact shown on the right hand side is of case IV. [14] It is located between the central base-pair steps in the subsequences TTTCACCG and TAGTGACT that are 139 base pairs apart. The second point of contact is of case III and located between the central base-pair step in the subsequence GAGGCAGC and the base pair in the center of the subsequence AATACCA that is 151 base pairs apart. For the topoisomer with $L_k = 35$ there is a single point of contact of case IV. It is located between the central base-pair steps in the subsequences TCACCGAT and TGCCTCAG that are 149 base pairs apart.
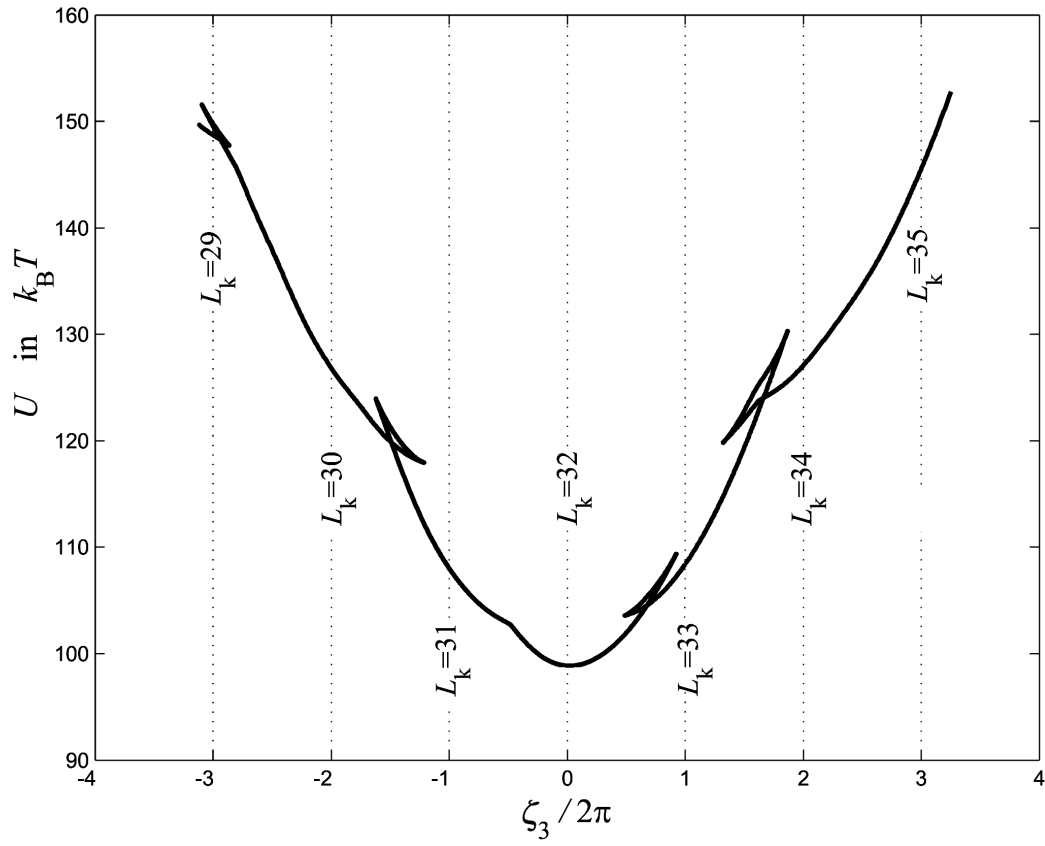
---

[14]See Figure 2.3.

Figure 6.23: The total energy U of the minicircle $\mathcal{Z}339$ at $c = 1 \times 10^{-1}$ M as a function of $\zeta_3/2\pi$.
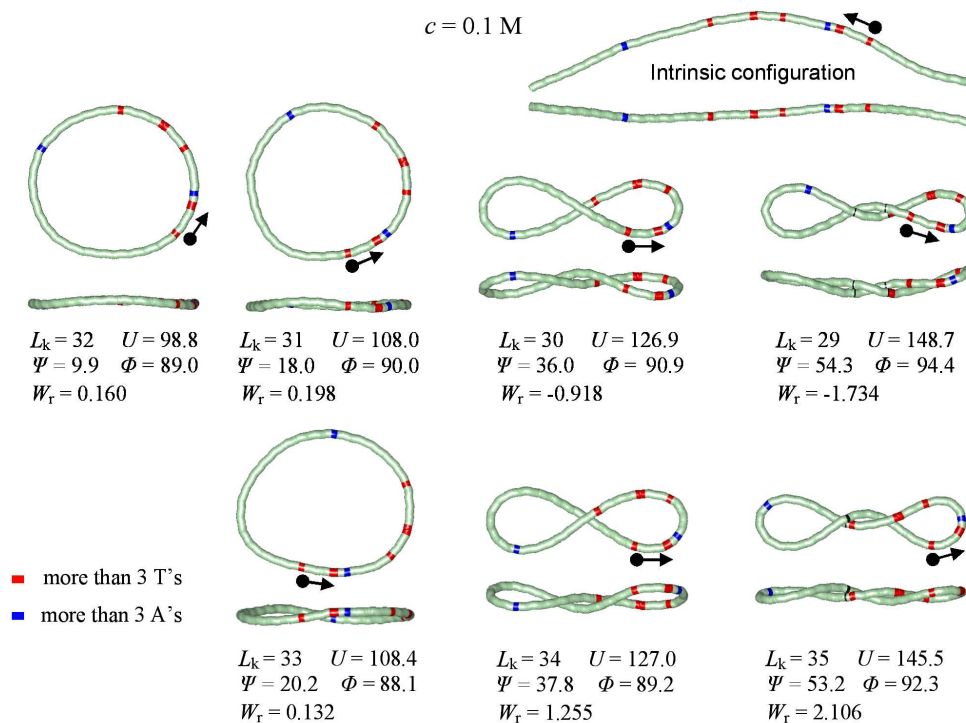
Figure 6.24: Equilibrium configurations at $c = 1 \times 10^{-1}$ M of seven topoisomers of $\mathcal{Z}339$ with linking numbers $L_k = 29, 30, ..., 35$. Two perpendicular views of the intrinsic configuration are shown in the upper right corner of the figure. Each equilibrium configuration is drawn in two perpendicular views. Sequences of more than three adjacent A's (Adenine) and T's (Thymine) are drawn in blue and red. The arrows indicate the position and direction of an arbitrarily chosen subsequence of the DNA molecule. A lengthy search of other equilibrium configurations suggests that the shown configurations are the minimum energy configurations of $\mathcal{Z}339$ confined to the indicated linking numbers.

Chapter 7

Conclusions and future study

The calculations reported in chapters 5 and 6 predict that the dependence of equilibrium DNA configurations on salt concentration is much stronger than might have been conjectured previously. The knowledge gained from the long calculations and the wide range of possible future calculations, based on the mathematical theory and numerical schemes that were presented, should encourage experimenters to investigate cases of DNA molecules that exhibit a significant change in their radius of gyration as a result of a small change in the ionic strength of the aqueous media.

For example, it is conceivable that an experimenter may attempt an electron cryo-microscopy study of a molecule similar to the 549 base pair DNA molecule $\mathcal{H}550$ treated here using a recently developed apparatus that is expected to be able to freeze samples rapidly to obtain images at well defined values of c. For each value of c the images obtained in such an experiment should correspond to configurations from a canonical (Boltzmann) distribution with configurations of maximum likelihood that are close to the minimum energy configuration. Such studies, when combined with the present theory and numerical schemes, may lead to a direct measurement of intrinsic parameters and elastic modulii. However, a prediction of the canonical distribution is necessary for more accurate and reliable results.

In a current study a Metroplis Monte Carlo method [47] in which each randomly generated configuration is closed with a preassigned value of ΔL_{k} is being developed. The method takes into account the sequence-dependence of the elastic energy, the intramolecular electrostatic interaction, and the impenetrability of the DNA molecule.

With such a method one will be able to sample a canonical ensemble and to calculate the free energy differences between DNA minicircles in different conditions or topologies, e.g., between two topoisomers with distinct values of ΔL_k or DNA molecules in aqueous solution with different salt concentrations.

Appendix A

In this appendix the El Hassan and Calladine's procedure [8] for constructing their relation between the six kinematical variables θ_1^n, θ_2^n, θ_3^n, ρ_1^n, ρ_2^n, ρ_3^n and the numbers $D_{ij}^n = \mathbf{d}_i^n \cdot \mathbf{d}_j^{n+1} = \tilde{D}_{ij}(\theta_1^n, \theta_2^n, \theta_3^n)$ and $r_i^n = \mathbf{r}^n \cdot \mathbf{d}_i^n$ is discussed. With the derived forms of the functions $\tilde{D}_{ij}$ in hand the functions $\tilde{\Gamma}_{ij}$ are expressed by following the relations (**??**) and (2.14).

Let $(\mathbf{d}_1^n, \mathbf{d}_2^n, \mathbf{d}_3^n)$ and θ_1^n, θ_2^n, θ_3^n be given, and let the angles ξ^n and ω^n and a unit vector $\mathbf{d}_\omega^n$ (called the "hinge vector"), in the plane of $\mathbf{d}_1^n$ and $\mathbf{d}_2^n$, be defined by the relations [1]

$$\xi^n = \sqrt{(\theta_1^n)^2 + (\theta_2^n)^2}, \qquad \theta_1^n = \xi^n \sin(\omega^n), \qquad \theta_2^n = \xi^n \cos(\omega^n), \qquad \text{(A.1)}$$

$$\mathbf{d}_\omega^n = -\mathbf{d}_1^n \sin\left(\frac{\theta_3^n}{2} - \omega^n\right) + \mathbf{d}_2^n \cos\left(\frac{\theta_3^n}{2} - \omega^n\right). \qquad \text{(A.2)}$$

By applying to $(\mathbf{d}_1^n, \mathbf{d}_2^n, \mathbf{d}_3^n)$ a positive rotation about $\mathbf{d}_\omega^n$ of magnitude $\xi^n/2$ one obtains an orthonormal triad $(\mathbf{d}_1^{n'}, \mathbf{d}_2^{n'}, \mathbf{d}_3^{n'})$ which one then rotates about $\mathbf{d}_3^{n'}$ through the angle $\theta_3^n/2$ to obtain another orthonormal triad, $(\mathbf{d}_1^{n+\frac{1}{2}}, \mathbf{d}_2^{n+\frac{1}{2}}, \mathbf{d}_3^{n+\frac{1}{2}})$, which in reference [8] is called the "mid-step triad". Here, as in [8], the displacement variables are, by definition, the components of $\mathbf{r}^n$ with respect to the elements of the mid step triad:

$$\rho_i^n = \mathbf{r}^n \cdot \mathbf{d}_i^{n+\frac{1}{2}}. \qquad \text{(A.3)}$$

This last equation can be written in the form (2.1) with the numbers R_{ji}^n the components of the vectors $(\mathbf{d}_1^{n+\frac{1}{2}}, \mathbf{d}_2^{n+\frac{1}{2}}, \mathbf{d}_3^{n+\frac{1}{2}})$, with respect to the basis $(\mathbf{d}_1^n, \mathbf{d}_2^n, \mathbf{d}_3^n)$:

$$R_{ji}^n = \mathbf{d}_i^n \cdot \mathbf{d}_j^{n+\frac{1}{2}} = \tilde{R}_{ji}(\theta_1^n, \theta_2^n, \theta_3^n). \qquad \text{(A.4)}$$

---

[1]Equations (A.1) are the same as equations (5.4).

The procedure just described yields explicit expressions [8] for the functions $\tilde{R}_{ji}(\theta_1^n, \theta_2^n, \theta_3^n)$ in (2.1), namely,

$$R_{ji}^n = \tilde{R}_{ji}(\theta_1^n, \theta_2^n, \theta_3^n) = Z_{ik}\left(\frac{\theta_3^n}{2} - \omega^n\right) Y_{kl}\left(\frac{\xi^n}{2}\right) Z_{lj}(\omega^n), \qquad \text{(A.5)}$$

where $Y_{ij}(\varsigma)$ and $Z_{ij}(\varsigma)$ are, for each ς, elements of the following rotation matrices:

$$[Y_{ij}(\varsigma)] = \begin{bmatrix} \cos(\varsigma) & 0 & \sin(\varsigma) \\ 0 & 1 & 0 \\ -\sin(\varsigma) & 0 & \cos(\varsigma) \end{bmatrix}, \quad [Z_{ij}(\varsigma)] = \begin{bmatrix} \cos(\varsigma) & -\sin(\varsigma) & 0 \\ \sin(\varsigma) & \cos(\varsigma) & 0 \\ 0 & 0 & 1 \end{bmatrix}. \quad \text{(A.6)}$$

The (fixed in space) hinge vector $\mathbf{d}_\omega^n$ in equation (A.2) can be expressed in terms of its components with respect to the mid-step triad as

$$\mathbf{d}_\omega^n = \mathbf{d}_1^{n+\frac{1}{2}} \sin(\omega^n) + \mathbf{d}_2^{n+\frac{1}{2}} \cos(\omega^n). \qquad \text{(A.7)}$$

The triad $(\mathbf{d}_1^{n+1}, \mathbf{d}_2^{n+1}, \mathbf{d}_3^{n+1})$, can be obtained by applying to $(\mathbf{d}_1^{n+\frac{1}{2}}, \mathbf{d}_2^{n+\frac{1}{2}}, \mathbf{d}_3^{n+\frac{1}{2}})$, first a rotation through an angle $\theta_3^n/2$ about $\mathbf{d}_3^{n+\frac{1}{2}}$ and then a rotation of magnitude $\xi^n/2$ about the hinge vector $\mathbf{d}_\omega^n$. As the second rotation brings the original triad into coincidence with $(\mathbf{d}_1^{n+1}, \mathbf{d}_2^{n+1}, \mathbf{d}_3^{n+1})$, the components of $\mathbf{d}_j^{n+1}$ with respect to $\mathbf{d}_i^{n+\frac{1}{2}}$ are given by

$$\mathbf{d}_i^{n+\frac{1}{2}} \cdot \mathbf{d}_j^{n+1} = Z_{ik}(-\omega^n) Y_{kl}\left(\frac{\xi^n}{2}\right) Z_{lj}\left(\frac{\theta_3^n}{2} + \omega^n\right), \qquad \text{(A.8)}$$

and as

$$D_{ij}^n = \mathbf{d}_i^n \cdot \mathbf{d}_j^{n+1} = \left(\mathbf{d}_i^n \cdot \mathbf{d}_k^{n+\frac{1}{2}}\right)\left(\mathbf{d}_k^{n+\frac{1}{2}} \cdot \mathbf{d}_j^{n+1}\right), \qquad \text{(A.9)}$$

in view of (A.4) and (A.8) the functions $\tilde{D}_{ij}$ can be expressed in the form [8],

$$D_{ij}^n = \tilde{D}_{ij}(\theta_1^n, \theta_2^n, \theta_3^n) = Z_{ik}\left(\frac{\theta_3^n}{2} - \omega^n\right) Y_{kl}(\xi^n) Z_{lj}\left(\frac{\theta_3^n}{2} + \omega^n\right). \qquad \text{(A.10)}$$

It follows from equations (2.12), (A.6), and (A.10) that the components Γ_{ij}^n in equation (2.13) are related to $\theta_1^n, \theta_2^n, \theta_3^n$ by [1],

$$[\Gamma_{ij}^n] = \begin{bmatrix} -\dfrac{\theta_1^n}{\xi^n}s^n + \dfrac{\theta_2^n t^n}{2\tan(\xi^n/2)} & -\dfrac{\theta_2^n}{\xi^n}s^n - \dfrac{\theta_1^n t^n}{2\tan(\xi^n/2)} & \tan(\xi^n/2)t^n \\[2ex] \dfrac{\theta_1^n}{\xi^n}t^n + \dfrac{\theta_2^n s^n}{2\tan(\xi^n/2)} & \dfrac{\theta_2^n}{\xi^n}t^n - \dfrac{\theta_1^n s^n}{2\tan(\xi^n/2)} & \tan(\xi^n/2)s^n \\[2ex] -\theta_2^n/2 & \theta_1^n/2 & 1 \end{bmatrix}, \quad \text{(A.11)}$$

where

$$t^n = \cos\left(\frac{\theta_3^n}{2} - \omega^n\right), \quad s^n = \sin\left(\frac{\theta_3^n}{2} - \omega^n\right). \tag{A.12}$$

References

[1] Coleman, B., Olson, W. & Swigon, D. Theory of sequence-dependent DNA elasticity. *J. Chem. Phys.* **118**, 7127–7140 (2003).

[2] Goriely, A. & Tabor, M. Spontaneous helix-hand reversal and tendril perversion in climbing plants. *Phys. Rev. Lett.* **80**, 1564–1568 (1998).

[3] Zandi, R., Golestanian, R. & Rudnick, J. Electromechanical stiffening of rods and tubes. *Appl. Phys. Lett.* **84**, 5467–5469 (2004).

[4] Watson, J. & Crick, F. A structure for deoxyribose nucleic acid. *Nature* **171**, 737–738 (1953).

[5] Calladine, C., Drew, H., Luisi, B. & Travers, A. *Understanding DNA* (Elsevier Academic Pres, 2004), 3rd edn.

[6] Zhurkin, V., Lysov, Y. & Ivanov, V. Anisotropic flexibility of DNA and the nucleosomal structure. *Nucleic Acids Res.* **6**, 1081–1096 (1979).

[7] Dickerson, R. E. DNA bending: The prevalence of kinkiness and the virtues of normality. *Nucl. Acids Res.* **26**, 1906–1926 (1998).

[8] El Hassan, M. & Calladine, C. The assessment of the geometry of dinucleotide steps in double-helical DNA: a new local calculation scheme. *J. Mol. Biol.* **251**, 648–664 (1995).

[9] Biton, Y., Coleman, B. & Swigon, D. On bifurcation of equilibria of intrinsically curved, electrically charged, rod-like structures that model DNA molecule in a solution. *J. Elasticity* **87**, 187–210 (2007).

[10] Dickerson, R. E. *et al.* Definitions and nomenclature of nucleic acid structure parameters. *European Molecular Biology Organization* **8**, 1–4 (1989).

[11] Westcott, T., Tobias, I. & Olson, W. Modeling self-contact forces in the elastic theory of DNA supercoiling. *J. Chem. Phys.* **107**, 3967–3980 (1997).

[12] Love, A. *A Treatise on the mathematical theory of elasticity* (Dover Publications, Inc., New York, 1927).

[13] Dill, E. Kirchhoff's theory of rods. *Arch. Hist. Exact Sci.* **44**, 1–23 (1992).

[14] Coleman, B., Tobias, I. & Olson, W. The dependence of DNA tertiary structure on end conditions: Theory and implications for topological transitions. *J. Chem. Phys.* **101**, 10990–10996 (1994).

[15] Coleman, B., Tobias, I. & Swigon, D. Theory of the influence of end conditions on self-contact in DNA loops. *J. Chem. Phys.* **103**, 9101–9109 (1995).

[16] Swigon, D., Coleman, B. & Tobias, I. The elastic rod model for DNA and its application to the tertiary structure of DNA minicircles in mononucleosomes. *Biophys. J.* **74**, 2515–2530 (1998).

[17] Ray, J. & Manning, G. An attractive force between two rodlike polyions mediated by the sharing of condensed counterions. *J. Am. Chem. Soc.* **10**, 2450–2461 (1994).

[18] Grønbech-Jensen, N., Mashl, R., Bruinsma, R. & Gelbart, W. Counterion-induced attraction between rigid polyelectrolytes. *Phys. Rev. Lett.* **78**, 2477–2480 (1997).

[19] Lee, K., Borukhov, I., Gelbart, W., Liu, A. & Stevens, M. Effect of mono- and multivalent salts on angle-dependent attractions between charged rods. *Phys. Rev. Lett.* **93**, 128101/1–128101/4 (2004).

[20] Fogg, J. *et al.* Exploring writhe in supercoiled minicircle DNA. *J. Phys.: Condens. Matter* **18**, S145–S159 (2006).

[21] Tobias, I., Swigon, D. & Coleman, B. Elastic stability of DNA configurations: I. general theory. *Phys. Rev. E* **61**, 747–758 (2000).

[22] Coleman, B., Swigon, D. & Tobias, I. Elastic stability of DNA configurations: II. supercoiled plasmids with self-contact. *Phys. Rev. E* **61**, 759–770 (2000).

[23] Coleman, B. & Swigon, D. Theory of supercoiled elastic rings with self-contact and its application to DNA plasmids. *J. Elasticity* **60**, 173–221 (2000).

[24] Simmons, D. *Nonlinear programming for operations research* (Prentice-Hall, New Jersey, 1976).

[25] Pike, R. *Optimization for engineering systems* (Van Nostrand Reinhold Company Inc., New York, New York, 1986).

[26] Kuhn, H. & Tucker, A. Nonlinear programming. In Neyman, J. (ed.) *Proceedings of the second Berkeley Symposium on Mathematical Statistics and Probability*, 481–492 (University of California Press, Berkley, 1951).

[27] Olson, W., Swigon, D. & Coleman, B. Implications of the dependence of the elastic properties of DNA on nucleotide sequence. *Phil. Trans. Roy. Soc.* **362**, 1403–1422 (2004).

[28] Manning, G. Limiting laws and counterion condensation in polyelectrolyte solutions: I. colligative properties. *J. Chem. Phys.* **51**, 924–933 (1969).

[29] Fenley, M., Manning, G. & Olson, W. Approach to the limit of counterion condensation. *Biopolymers* **30**, 1191–1203 (1990).

[30] Mittelmann, H. A pseudo-arclength continuation method for nonlinear eigenvalue problems. *SIAM J. Numer. Anal.* **23**, 1007–1016 (1986).

[31] Golub, G. & Van Loan, C. *Matrix Computations* (The Johns Hopkins University Press, Baltimor, 1996).

[32] Moore, G. & Spence, A. The calculation of turning points of nonlinear equations. *SIAM J. Numer. Anal.* **17**, 567–576 (1986).

[33] Waterman, M. (ed.). *Mathematical methods for DNA Sequences* (CRC, Boca Raton, Florida, 1989).

[34] White, J. Self-linking and the gauss integral in higher dimensions. *Am. J. Math.* **91**, 693–728 (1969).

[35] Olson, W., Gorin, A., Lu, X.-J., Hock, L. & Zhurkin, V. DNA sequence-dependent deformability deduced from protein-DNA crystal complexes. *Proc. Natl. Acad. Sci. USA* **95**, 11163–11168 (1998).

[36] Fuller, F. The writing number of a space curve. *Proc. Natl. Acad. Sci. USA* **68**, 815–819 (1971).

[37] Thompson, J. & Hunt, G. *A general theory of elastic stability* (John Wiley Sons, London, 1973).

[38] Domokos, G. & Healey, T. Multiple helical perversions of finite intrinsically curved rods. *Int. J. Bifurcation and Chaos.* **15**, 871–890 (2005).

[39] Vologodskii, A. *Topology and physics of circular DNA* (CRC Press, Boca Raton, 1992).

[40] Marini, J., Levene, S., Crothers, D. & Englund, P. Bent helical structure in kinetoplast DNA. *Proc. Natl. Acad. Sci., USA* **79**, 7664–7668 (1982).

[41] Diekmann, S. & Wang, J. On the sequence determinants and exibility of the kinetoplast DNA fragment with abnormal gel electrophoretic mobilities. *J. Mol. Biol.* **186**, 1–11 (1985).

[42] Haran, T., Kahn, J. & Crothers, D. Sequence elements responsible for DNA curvature. *J. Mol. Biol.* **244**, 135–144 (1994).

[43] Griffith, J., Bleyman, M., Rauch, C., Kitchin, P. & Englund, P. Visualization of the bent helix in kinetoplast DNA by electron microscopy. *Cell* **46**, 717–724 (1986).

[44] Domokos, G. & Healey, T. Hidden symmetry of global solutions in twisted elastic rings. *J. Nonlinear Science.* **11**, 47–67 (2001).

[45] Charitat, T. & Fourcade, B. Metastability of a circular o-ring due to intrinsic curvature. *European Phys. J. B* **1**, 333–336 (1998).

[46] Colasanti, A. *Conformational states of double helical DNA*. Ph.D. thesis, Rutgers University (2006).

[47] Metropolis, N., Rosenbluth, A., Rosenbluth, M., Teller, A. & Teller, E. Equation of state calculations by fast computing machines. *J. Chem. Phys.* **21**, 1087–1092 (1953).

Vita

Yoav Yaakov Biton

2002	M. Sc. in Mechanical engineering, Ben Gurion University of the Negev, Beer-Sheva, Israel
1997	B. Sc. in Mechanical Engineering, Ben Gurion University of the Negev, Beer-Sheva, Israel
1989	Graduated from Shoshana Sapir high school, Yeruham, Israel.
2002-2007	Graduate assistant, Mechanics, Rutgers University
2001-2002	Teaching assistant, Biomedical Engineering, Rutgers University
2000-2001	Excellence fellowship, Mechanics, Rutgers University
1997-1999	Teaching assistant, Mechanical Engineering, Ben Gurion University of the Negev, Beer-Sheva, Israel